DANIEL MEIER

THERMALLY GENERATED SPIN AND CHARGE TRANSPORT IN MAGNETIC MATERIALS

UNIVERSITÄT BIELEFELD
FAKULTÄT FÜR PHYSIK

Thermally generated spin and charge transport in magnetic materials

Thermally generated spin and charge transport in magnetic materials

Thesis by Daniel Meier

UNIVERSITÄT BIELEFELD
FAKULTÄT FÜR PHYSIK

Dissertation zur Erlangung des Doktorgrades

Diese Dissertation wurde von mir persönlich verfasst. Einige Textpassagen sind in veränderter Form aus Publikationen, deren Autor ich war, übernommen. Ich versichere weiterhin, dass ich, abgesehen von den ausdrücklich bezeichneten Hilfsmitteln, die Dissertation selbstständig und ohne unerlaubte Hilfe angefertigt habe.

Gutachter:
Prof. Dr. Günter Reiss
Prof. Dr. Jürgen Schnack

Juli 2015

There is no authority who decides what is a good idea.
Richard P. Feynman

Contents

Introduction

Information technology is one of the biggest and most rising industries in the world. We all use information technology every day and almost all day, e.g., computers at work and at home, smartphones and tablets. On all these devices we use applications like social networks, databases like search engines and cloud computing for access to all our personal data anywhere, anytime. This leads to an enormous increase of data we have to store.[1] For this reason we need huge data centers with lots of servers with more and more advanced data storage technology. Our requirements for sophisticated data storage include high density of information per space unit, low access times and preferably low need of energy.

[1] M. Gu et al. Light: Science & Applications **3** (2014) e177

However, the largest portion of energy needed in a data center is used for cooling. The gigantic production of wasted heat is one of the biggest issues in data processing. Information technology, for instance, is dominated by semiconductor electronics. The electron is the dominant information carrier and with it its charge. Electron collisions produce heat. This calls for a new method of information transport and for a meaningful use of wasted heat to reduce further energy consumption.

The first stage for that was set by spintronics. In spintronics the spin, i.e., the angular momentum of the electron, a property to be understood in terms of quantum mechanics is used. The spin is connected with a magnetic moment and can be manipulated by magnetic fields. Research of materials for applications and devices which use the spin is rising at the same rate as information technology. Currently, the most common spintronic application can be found in reading heads for hard discs where the *giant magnetoresistance effect* (GMR)[2] was used as a spin valve. This led to a drastic increase of data storage. Meanwhile, it has been replaced by the more sophisticated *tunnel magnetoresistance effect* (TMR)[3]. It is another purpose of further spintronic research to use the TMR to develop the so-called *magnetoresistive random access*

[2] G. Binasch et al. Physical Review B **39** (1989) 4828; M. N. Baibich et al. Physical Review Letters **61** (1988) 2472

[3] M. Julliere. Physics Letters A **54** (1975) 225

memory (MRAM)[4], a non-volatile memory with fast reading times. These devices are available but not yet profitable. New aspects are, e.g., the racetrack memory in nanowires[5], or optical storage arrays[6] which should replace hard drives completely.

In further basic research it is not the spin combined with a charge current that is of broad interest but the generation of a pure spin current accompanied by a significant reduction of wasted heat. Pure spin currents are mostly provoked by spin waves and their quanta, the magnon. This opens a new branch in spintronics which is called magnonics.

Material science is crucial for progress in advanced spintronic devices. However, basic research is important to explore new ways and methods of the advantages of the spin. Furthermore, heat is the most frequent form of energy which arises almost everywhere. A logical step is to combine the utilization of the spin in information technology with manipulation by heat. This combination is now known as the branch of spincaloritronics (or spin calorics).

This thesis

What this thesis is about focuses on one of the key effects promoting this branch of research, i.e., the *Spin Seebeck Effect* (SSE). It provides a detailed investigation of the SSE and all related transport phenomena in a broad range of different magnetic materials. Magnetic means, in the context of this thesis, that a collective magnetization is present which is known as ferromagnetism. In this work we also use ferrimagnetic materials, but for the sake of simplicity we will include this type when we talk about ferromagnetic materials.

In the next chapter we will give an introduction and detailed description of all relevant thermoelectric, spintronic and spin caloric transport phenomena of which we need to discuss all presented data. Understanding the symmetry of the described effects is important in order to understand the origin of the results. Our investigations include a combination of different contributions we have to disentangle carefully. The almost established spintronic effects we will present have to be examined in order to determine whether their origin, behaviour and appearance can be adapted to their thermal counterparts.

In the following three chapters we are going to present our data obtained in three different magnetic systems such as metallic, insulating and semiconducting material. One chapter will

[4] J. M. Slaughter. Annual Review of Materials Research **39** (2009) 277; K. Ando et al. Journal of Applied Physics **115** (2014) 172607

[5] S. Parkin and S.-H. Yang. Nature Nanotechnology **10** (2015) 195

[6] M. Gu et al. Light: Science & Applications **3** (2014) e177

be devoted to each of these materials. We started with the investigation of permalloy thin films, which were used in the first SSE reports in the literature. This helped us to get a first understanding of most of the unintended transport phenomena in SSE experiments. Furthermore, we were able to improve the measurement techniques for our further investigations. After that, we proceeded with the SSE investigation on a material system with semiconducting properties like $NiFe_2O_4$ and on an insulator like $Y_3Fe_5O_{12}$ to gradually cancel all unintended transport phenomena which occurred as side effects. Finally, we found that adjusting the measurement conditions presented us with further opportunities to disentangle all side effects from the intended SSE. We will give a detailed explanation of how these side effects can be separated and what transport phenomena are the dominant ones in the given material classes and measurement configurations.

Since the focus of this thesis is on transport measurement, we will not present methods or data for sample characterization. The samples used here were already characterized regarding their structural properties, which was mostly reported in previous publications which we will refer to. We will point out the sample properties whenever they are important for the origin and disentanglement of the observed transport phenomena.

Most of the results presented in this thesis have already been published in peer-reviewed journals or presented in open access reports. We will refer to these articles and reports in the relevant sections.

Theoretical background

The aim of this chapter is to provide the theoretical background about all important transport phenomena. Most of phenomena we are dealing with are present in transport measurements which were realized in the course of our work. The driving forces are almost potential differences to generate a charge current or a temperature gradient. Various effects can be observed with and without external magnetic fields. Here, we are going to introduce all relevant (thermo) electric and spin (calori)tronic effects related in this thesis. This will help the reader to understand the results presented in later chapters.

General relations of transport phenomena

In the linear response regime all transport phenomena can be described by reciprocal relations as presented by Lars Onsager in 1931 for irreversible processes like thermoelectric phenomena.[7] These *Onsager reciprocity relations* can be generally expressed as currents $\vec{J}^i$ and forces $\vec{X}^j$ related by a linear response matrix L^{ij} to

$$\vec{J}^i = L^{ij}\vec{X}^j \quad (i,j = 1,2,3,...,n). \tag{1}$$

[7] L. Onsager. Physical Review **37** (1931) 405

For $i = j$ the currents generated are associated with their driving forces, whereas for $i \neq j$ the different currents and forces are connected to each other. The main theorem of Onsager's reciprocity relations is the symmetry relation

$$L^{ij} = L^{ji}. \tag{2}$$

In this thesis, the main interest lies in the conduction of heat, charge and spin accompanied with the relation between them. Therefore, we can rewrite Eq. 1 into[8]

$$\begin{pmatrix} \vec{J}^c \\ \vec{J}^s \\ \vec{J}^q \end{pmatrix} = \begin{pmatrix} \tilde{\sigma}^{cc} & \tilde{\sigma}^{cs} & \tilde{\sigma}^{cq} \\ \tilde{\sigma}^{sc} & \tilde{\sigma}^{ss} & \tilde{\sigma}^{sq} \\ \tilde{\sigma}^{qc} & \tilde{\sigma}^{qs} & \tilde{\sigma}^{qq} \end{pmatrix} \cdot \begin{pmatrix} \vec{E} \\ \nabla\mu_s \\ -\nabla T \end{pmatrix} \tag{3}$$

[8] G. E. W. Bauer et al. Nature Materials **11** (2012) 391

with the charge current density $\vec{J}^c$, the spin current density $\vec{J}^s$, the heat flow $\vec{J}^q$, the electric field $\vec{E}$, a fictitious field $\nabla\mu_s$, which is connected to the spin density, and the temperature gradient ∇T. The matrix elements are the linear responses between the currents and the forces and, furthermore, they are tensors to satisfy the condition that all transport phenomena can be anisotropic. Eq. 3 is all we need to express the most relevant transport equations for this thesis.

Hall effects

The first term of Eq. 3 where the charge current density $\vec{J}^c$ is connected to the electric field $\vec{E}$ is known as *Ohm's law* in the form $\vec{J}^c = \tilde{\sigma}^{cc}\vec{E}$. The matrix $\tilde{\sigma}^{cc}$ is the conductivity tensor. We can write Ohm's law in the following component notation:

$$\begin{pmatrix} J_x^c \\ J_y^c \\ J_z^c \end{pmatrix} = \begin{pmatrix} \sigma_{xx} & \sigma_{xy} & \sigma_{xz} \\ \sigma_{yx} & \sigma_{yy} & \sigma_{yz} \\ \sigma_{zx} & \sigma_{zy} & \sigma_{zz} \end{pmatrix} \cdot \begin{pmatrix} E_x \\ E_y \\ E_z \end{pmatrix} \tag{4}$$

When an external magnetic field is applied perpendicular to a charge current, a transverse motion of the charge carriers is observed due to the Lorentz force.[9,10] This is well known as the *Hall effect* (Fig. 1). In Hall effect investigations the charge current $\vec{J}$ is the applied parameter and the electric field $\vec{E}$ is the measured quantity in form of a voltage V for an open circuit condition. Therefore, Ohm's law can be converted in the form $\vec{E} = \tilde{\rho}^{cc}\vec{J}$ with the resistivity tensor $\tilde{\rho}^{cc}$. We consider a ferromagnetic conductor with a magnetization in z-direction. Then we can write the resistivity tensor in the form[11]

$$\tilde{\rho}^{cc} = \begin{pmatrix} \rho_\perp & \rho_H & 0 \\ -\rho_H & \rho_\perp & 0 \\ 0 & 0 & \rho_\parallel \end{pmatrix} \tag{5}$$

with the Hall resistivity ρ_H and the resistivities $\rho_\perp$ and $\rho_\parallel$ perpendicular and parallel to the magnetization $\vec{M}$, respectively. For the Hall effect we obtain $E_y = -\rho_H J_x$ with the magnetization in z-direction. In general, the Hall effect can also be observed in non-magnetic conductors and the electric field $\vec{E}$ is a cross product given by

$$\vec{E} = -\mu_0 R_H \vec{J} \times \vec{H} \tag{6}$$

with the magnetic field $\vec{H}$, the magnetic permeability μ_0 and the Hall coefficient R_H. The free charge carriers are deflected due to

[9] E. H. Hall. American Journal of Mathematics **2** (1879) 287

[10] E. H. Hall. The London, Edinburgh, and Dublin Philosophical Magazine and Journal of Science **10** (1880) 301

[11] J. E. Wegrowe et al. Physical Review B **89** (2014) 094409

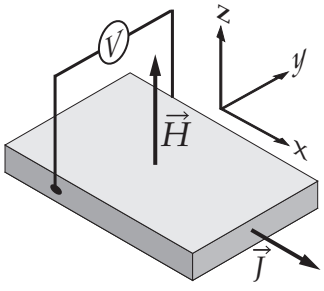

Figure 1: Measurement configuration of the Hall effect. A charge current density $\vec{J}$ is applied along a sample with an out-of-plane magnetic field $\vec{H}$. The voltage V is measured in the transverse direction.

the Lorentz force. The voltage V is proportional and, therefore, antisymmetric with respect to the magnetic field H (Fig. 2). In what follows, we will call this effect the ordinary Hall effect (OHE). In ferromagnetic conductors a second term of the Hall effect can be defined which is proportional to the magnetization vector $\vec{M}$ of the material. This effect is called the *anomalous Hall effect* (AHE) and is much larger than the OHE. The AHE is given by

$$\vec{E} = R_S \vec{J} \times \vec{M} \tag{7}$$

with a material dependent anomalous Hall coefficient R_S. In ferromagnetic materials the observed voltage V describes a hysteretic curve which is antisymmetric with respect to H. Furthermore, V reaches saturation for large enough magnetic fields (Fig. 3). In general, the OHE and AHE are entangled when the voltage is measured in the configuration of Fig. 1. The result is a superposition of two contributions with an increasing voltage V due to the OHE (Fig. 4). The origin of the AHE is divided into extrinsic and intrinsic effects. The extrinsic mechanisms are the side jump[12] and screw scattering[13] and caused by scattering on impurities or disorder of the material accompanied by spin-orbit coupling which promotes these scattering effects.[14] The intrinsic effect is described by a Berry phase of the Berry curvature which can be described as a *magnetic field in k-space*.[15] This occurs even in perfect crystals without disorder or impurities and is produced by the electronic band structure.[16]

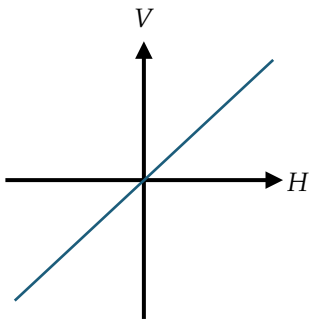

Figure 2: The ordinary Hall effect in all conducting materials. The voltage V is proportional to the magnetic field H.

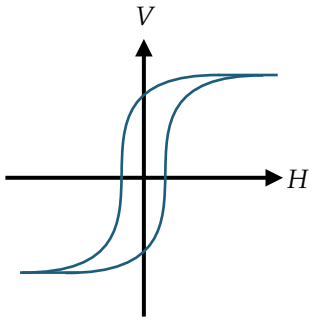

Figure 3: The anomalous Hall effect in ferromagnetic conductors. The voltage V as a function of the magnetic field H shows a hysteretic curve which is antisymmetric with respect to H.

Anisotropic magnetoresistance

The next effect introduced is produced by the difference of the resistivity parallel and perpendicular to the magnetization direction in a ferromagnetic conductor. This effect is called *anisotropic magnetoresistance* (AMR). The origin of the difference in resistivities can be explained in different scattering cross-sections of the conduction electrons. The atom orbitals in ferromagnetic materials are not spherically symmetric due to spin-orbit interaction. Hence, the atom orbitals overlap in the direction perpendicular to the magnetization. This leads to a smaller resistivity perpendicular to the magnetization.

Now, we consider a sample with a magnetization $\vec{M}$ in the x-y-plane with an angle θ relative to the current density $\vec{J}$ and electric field $\vec{E}$ which are also in the same plane. We can divide these quantities into $J_\parallel$ and $E_\parallel$ parallel and $J_\perp$ and $E_\perp$ perpendicular

[12] L. Berger. Physical Review B **2** (1970) 4559

[13] J. Smit. Physica **24** (1958) 39

[14] N. Nagaosa et al. Reviews of Modern Physics **82** (2010) 1539

[15] S. Murakami. arXiv.org (2004). arXiv: 0405003v1

[16] T. Jungwirth et al. Physical Review Letters (2001) 207208; J. Sinova et al. Physical Review Letters **92** (2004) 126603

[17] D. A. Thompson et al. Magnetics, IEEE Transactions on **11** (1975) 1039

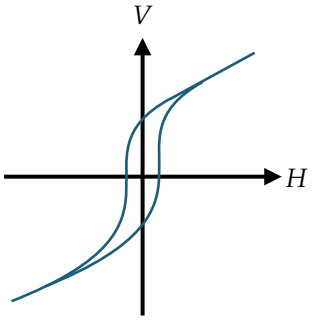

Figure 4: The sum of the ordinary and anomalous Hall effect in a ferromagnetic conductor. The voltage V describes a hysteretic curve which is antisymmetric with respect to H, but with no saturated value. The voltage V increases proportionally with H.

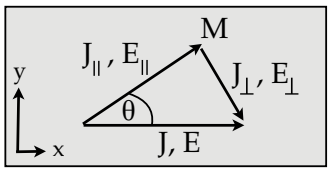

Figure 5: The magnetization M, the current density J and the electric field E lie in the same plane. J and E can be divided into a parallel and a perpendicular part with respect to M.

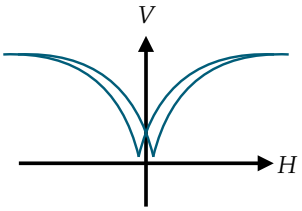

Figure 6: The voltage V as a function of the magnetic field H in an AMR and PHE configuration. V is symmetric with respect to H.

to $\vec{M}$ (Fig. 5). We use the derivation from Thompson et al.[17] to get expressions for E_x and E_y when a charge current J_x is applied. Then with $E_\parallel = \rho_\parallel J_\parallel$ and $E_\perp = \rho_\perp J_\perp$ we get

$$E_x = E_\parallel \cos(\theta) + E_\perp \sin(\theta)$$
$$E_y = E_\parallel \sin(\theta) - E_\perp \cos(\theta)$$

$$E_x = \rho_\parallel J_\parallel \cos(\theta) + \rho_\perp J_\perp \sin(\theta)$$
$$E_y = \rho_\parallel \sin(\theta) J_x \cos(\theta) - \rho_\perp \cos(\theta) J_x \sin(\theta)$$

$$E_x = J_x (\rho_\parallel \cos^2(\theta) + \rho_\perp \sin^2(\theta)) \quad (8)$$
$$E_y = J_x (\rho_\parallel - \rho_\perp) \sin(\theta)\cos(\theta). \quad (9)$$

For the longitudinal electric field E_x we can use the equation $\sin^2(\theta) + \cos^2(\theta) = 1$ which gives us

$$E_x = J_x[\rho_\perp + (\rho_\parallel - \rho_\perp)\cos^2(\theta)]. \quad (10)$$

The AMR occurs in a longitudinal resistivity measurement along the charge current density when the angle θ changes during a magnetic field loop. This is the case when magnetic anisotropies are present. Furthermore, the AMR varies in a $\cos^2(\theta)$ shape when an external magnetic field large enough to saturate the sample is rotated in the plane given by $\vec{J}$ and $\vec{M}$.

The transverse component E_y (Eq. 9) is called *planar Hall effect* (PHE). *Planar* means that all vectors lie in the same plane. The remarkable behaviour of the PHE is that the effect disappears when $\vec{M}$ is parallel or perpendicular to $\vec{J}$ and it shows its maximum at an angle $\theta = 45°$.

The AMR and the PHE show no change of sign in the voltage when the polarity of the magnetization is changed. Therefore, the polarity of the electric field $\vec{E}$, or the experimentally more convenient unit of voltage V, is symmetric with respect to the external magnetic field $\vec{H}$ shown in Fig. 6. The product $\sin(\theta)\cdot\cos(\theta)$ can be expressed as $\frac{1}{2}\sin(2\theta)$ which also shows the symmetry of this effect. The curve shape of Fig. 6 is a typical behaviour for a sample with an in-plane magnetic anisotropy. The voltage V changes when the angle θ between the current density J_x and the direction of the magnetization $\vec{M}$ changes. When the external magnetic field H is applied in a direction different from the easy axis a variation in V can be observed when H decreases. The magnetization vector $\vec{M}$ changes its direction from parallel to

H into the easy axis. A special case occurs when H is applied in the direction of this easy axis. The magnetization $\vec{M}$ will be oriented parallel or antiparallel independently of the magnitude of H. Hence, θ does not change and therefore V does not change. This results in a straight line of V as a function of H. We would like to emphasize that the appearance of symmetric dips or peaks depends on the movement of the magnetization vector $\vec{M}$.

Nernst effects

In this section we start to introduce the thermal transport equations given by Eq. 3. A charge current $\vec{J}^c$ can be driven by a temperature gradient ∇T which is connected by the tensor $\tilde{\sigma}^{cq}$ to

$$\vec{J}^c = -\tilde{\sigma}^{cq} \nabla T. \tag{11}$$

In an open circuit a thermopower $\vec{E}$ is generated by the temperature gradient ∇T and we obtain the equation $\vec{E} = -\tilde{S}\nabla T$ with the Seebeck tensor[18]

$$\tilde{S} = \begin{pmatrix} S & S_N & 0 \\ -S_N & S & 0 \\ 0 & 0 & S_z \end{pmatrix}. \tag{12}$$

[18] J. E. Wegrowe et al. Physical Review B **89** (2014) 094409

This tensor looks very similar to the resistivity tensor (Eq. 5). When a temperature gradient is applied along a conductor, charge carriers with a higher thermal energy diffuse into the direction with lower thermal energy. In an open electrical circuit this charge current is compensated by the generated electric field. This is known as the *Seebeck effect*[19], which is a thermoelectric effect and given by

$$E_x = -S\nabla T_x \tag{13}$$

with the material dependent Seebeck coefficient S.[20] When two materials with different Seebeck coefficients are connected, it can be used as a temperature sensor. This is known as a *thermocouple*. The open ends of the thermocouple have to be at a known reference temperature. Then the measured voltage at the open ends give information about the temperature at the connected ends. Thermocouples are used in most experiments in this thesis to determine the temperature differences.

[19] T. J. Seebeck. Abh. Akad. Wiss. Berlin **1822** (1820-21) 189

[20] components of ∇T will be indicated as ∇T_x, ∇T_y and ∇T_z which are parallel to the axes (x, y, z) of the coordinate system used

Now, let us consider the Hall effect configuration presented in Fig. 1. When the applied charge current $\vec{J}$ is exchanged by a temperature gradient ∇T, a transverse motion still exists when an external magnetic field is present. This is called the *first*

Ettingshausen-Nernst effect named after Albert von Ettingshausen and Walther Nernst (simply referred to as *Nernst effects* in what follows).[21] Similarly to the Hall effects there are different types of Nernst effects. In a very simple picture, the analogy between the Nernst and Hall effects lies in the thermally driven charge currents due to the Seebeck effect compared to the applied charge currents. In an open circuit condition the transverse motion of the thermally driven charge carriers generates an electric field. The observed electric field $\vec{E}$ is a cross product of the temperature gradient ∇T and the external magnetic field $\vec{H}$ in the form

$$\vec{E} = \mu_0 N_{NE} \nabla T \times \vec{H} \tag{14}$$

with the Nernst coefficient N_{NE}. This is known as the conventional or *ordinary Nernst effect (ONE)*. The measured voltage is proportional to the external magnetic field H (cf. Fig. 2). In a ferromagnetic conductor we can find a similar effect to the AHE which is called the *anomalous Nernst effect* (ANE) and given by the equation

$$\vec{E} = N_{ANE} \nabla T \times \vec{M}. \tag{15}$$

The cross product between the temperature gradient ∇T and the magnetization $\vec{M}$ results in a hysteretical curve of V which is antisymmetric with respect to the external magnetic field H (cf. Fig. 3).

For the thermally driven counterparts of the AMR and PHE we only have to modify Eq. 8 and Eq. 9 by changing J_x to ∇T_x.[22] We end up with similar equations in the form

$$E_x = \nabla T_x \left(\rho_{\parallel} \cos^2(\theta) + \rho_{\perp} \sin^2(\theta)\right) \tag{16}$$

$$E_y = \nabla T_x \left(\rho_{\parallel} - \rho_{\perp}\right) \sin(\theta) \cos(\theta). \tag{17}$$

The counterpart of the AMR (Eq. 16) is known as *anisotropic magnetothermopower* (AMTP), and the counterpart of the PHE (Eq. 17) is the transverse AMTP, which is also known as the *planar Nernst effect* (PNE).

[21] A. von Ettingshausen and W. Nernst. Annalen der Physik **265** (1886) 343

[22] V. D. Ky. physica status solidi (b) **17** (1966) K207

Spintronics

Spin-dependent charge currents

In a conducting material a charge current $\vec{J}^c$ (Fig. 7 (a)) is spin polarized when there is a majority of electrons with a parallel spin $\vec{J}^c_\uparrow$ flowing in one direction (Fig. 7 (b)). Even when there is a minority of electrons with a spin in the opposite direction $\vec{J}^c_\downarrow$ we will have charge transport as well as spin transport. In terms of the formalism of Eq. 3 we get a spin current $\vec{J}^s = \vec{J}^c_\uparrow - \vec{J}^c_\downarrow$ accompanied to the charge current $\vec{J}^c = \vec{J}^c_\uparrow + \vec{J}^c_\downarrow$. These currents can be used in a broad range of spintronic applications.[23] The most famous example is the *giant magnetoresistance effect* (GMR) discovered independently by Albert Fert and Peter Grünberg in 1988.[24] A layer stack of two ferromagnetic electrodes (FM layers) separated by a non-magnetic metal (NM layer) of nanometer thickness acts as a spin valve. When the magnetization of the FM layers is aligned parallel the resistance for a charge current through the layer stack is smaller compared to an antiparallel alignment of the FM layers. The MR ratios[25] are in a range of about 10 % at room temperature. The different resistances are caused by a scattering of the charge carriers depending on their spin orientation relative to the magnetization direction of the FM layers. This effect is used in reading heads in hard drives for more efficient data storage.

After its discovery, the GMR effect opened the triumphal procession of further spintronic investigations. When the non-magnetic metal is replaced by a nanometer thin insulator (IN) like Al_2O_3 or MgO the MR effect is called *tunnelling magnetoresistance* (TMR). Here, the spin-dependent charge current is tunnelled through the insulating barrier with a spin-dependent tunnelling probability. This can be explained by a different amount of free states at the Fermi energy for the transmitted electrons with spin directions parallel and antiparallel to the magnetization of the entered FM layer. This was discovered by Michel Julliere[26] as early as in 1975 but was not noted as much as the discovery of the GMR because of the relatively small MR ratios below 1 %. Today, the TMR is in the focus of recent research for the next technique of advanced data storage due to MR ratios of over 600 % at room temperature[27] and nearly 2000 % at 4.2 K.[28] These FM/IN/FM layer stacks can be structured in so called *magnetic tunnel junctions* (MTJ) with dimensions down to 20 nm × 20 nm. These MTJs are switched from a parallel to an antiparallel state and reversed with

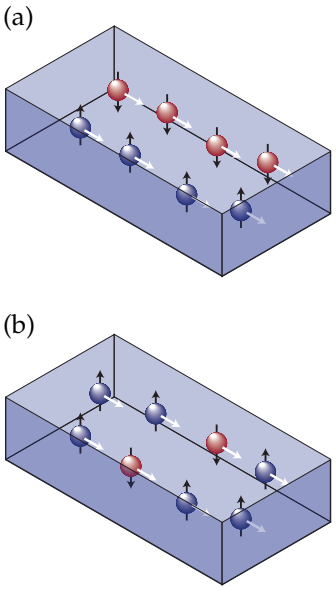

Figure 7: (a) A charge current $\vec{J}^c$ with the same amount of spin up and spin down electrons. (b) A spin polarized current with a majority of charge carriers with spin in one direction.

[23] S. D. Bader and S. S. P. Parkin. Annual Review of Condensed Matter Physics **1** (2010) 71

[24] M. N. Baibich et al. Physical Review Letters **61** (1988) 2472; G. Binasch et al. Physical Review B **39** (1989) 4828

[25] $MR = \frac{R_{ap} - R_p}{R_p}$

[26] M. Julliere. Physics Letters A **54** (1975) 225

[27] S. Ikeda et al. Applied Physics Letters **93** (2008) 082508

[28] H. Liu et al. Applied Physics Letters **101** (2012) 132418

an external magnetic field. This magnetic field switches one of the FM layers. The second FM layer has to get a larger coercive field or has to be pinned by an adjacent antiferromagnetic layer. Then it can be switched into an antiparallel state.

It becomes obvious that these MTJs are favoured for future data storage of one bit depending on the two states of resistance (low and high resistance equivalent to 0 and 1). Future progress in the research of MTJs will be the evolution of miniaturized devices and the disappearance of mechanical parts like, e.g., reading heads which move over the surface in hard drives. These mechanical parts limit reading times. One promising possibility of handling the latter issue is the so called *spin transfer torque* (STT) switching introduced by Slonczewski.[29] A sufficiently large charge current which will be spin polarized in the first FM layer and transmitted through the IN barrier should change the magnetization direction of the second FM layer into the opposite state. The magnetization dynamic in these processes can be described by the Landau-Lifshitz-Gilbert (LLG)[30,31] equation

$$\frac{\partial \vec{M}}{\partial t} = -\gamma \vec{M} \times (\mu_0 \vec{H}_{\text{eff}}) + \frac{\alpha_0}{M_S}\left[\vec{M} \times \frac{\partial \vec{M}}{\partial t}\right] \tag{18}$$

with the gyromagnetic ratio γ, the magnetization in saturation M_S, and the damping parameter α_0. The first term on the right hand side describes the precession of $\vec{M}$ around an effective magnetic field $\vec{H}_{\text{eff}}$ (Fig. 8) and the second term stands for the relaxation of the precession which is called *damping*. For the STT, Slonczewski[29] extended the right hand side by an additional term to describe the effect of the spin polarized charge current I from a *fixed layer* with fixed magnetization $\vec{M}_{\text{fixed}}$ into a *free layer* with magnetization $\vec{M}$. The additional term is given by, e.g., Ralph and Stiles[31] in the form

$$\frac{\partial \vec{M}_{\text{stt}}}{\partial t} = \eta \frac{\mu_B I}{eV} \vec{M} \times (\vec{M} \times \vec{M}_{\text{fixed}}) \tag{19}$$

with the charge I, the Bohr magneton μ_B, the elementary charge constant e, the volume V of the free layer and a layer structure parameter η. A high spin polarization P at the interface between the FM and IN layer is important for a large TMR effect as well as for small charge current densities during STT switching. The spin polarization P is defined as the ratio between the difference of spin up and spin down electrons divided by the sum of all electrons at the Fermi energy.[32] The best STT also occurs when the spin

[29] J. C. Slonczewski. Journal of magnetism and magnetic materials **159** (1995) L1

[30] L. D. Landau and E. Lifshitz. Phys. Z. Sowjet. **8** (1935) 153; T. L. Gilbert. Magnetics, IEEE Transactions on **40** (2004) 3443

[31] D. C. Ralph and M. D. Stiles. Journal of magnetism and magnetic materials **320** (2008) 1190

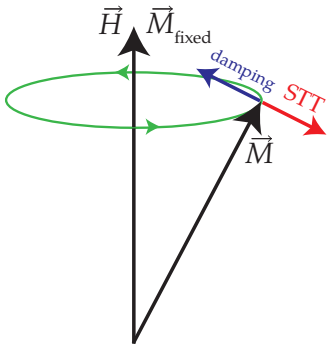

Figure 8: The magnetization $\vec{M}$ describes a precession around $\vec{H}$ and $\vec{M}_{\text{fixed}}$. The relaxation is represented by the damping. The spin transfer torque (STT) increases the precession of $\vec{M}$.

[32] $P = \frac{n^{\uparrow} - n^{\downarrow}}{n^{\uparrow} + n^{\downarrow}}$

orientation of the spin polarized charge current is perpendicular to the magnetization of the target FM layer (free layer). Then, the most angular momentum is absorbed in tilting the magnetization direction. The STT may also be reversed. This will be mentioned in the next section about pure spin currents.

Spin currents

A pure spin current can be created when an amount of electrons with one spin flows in one direction simultaneously to the same amount of electrons with the opposite spin flowing in the opposite direction (Fig. 9). In our formalism we have a spin current $\vec{J}^s = \vec{J}^c_\uparrow - \vec{J}^c_\downarrow \neq 0$, but $\vec{J}^c = \vec{J}^c_\uparrow + \vec{J}^c_\downarrow = 0$. There is no net charge current, only a pure spin current. Here, the spin is transported directly by moving electrons. A pure spin current can even exist without moving electrons in magnetic insulators, for instance. This spin current is produced by the generation of magnons - the quanta of spin waves. Here, spin transport is described by a current of angular momentum in one direction without any moving electrons.

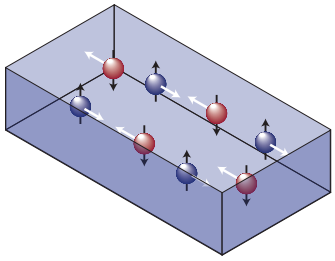

Figure 9: When the same amount of spin up and spin down electrons are moving in opposite directions a pure spin current $\vec{J}^s$ occurs.

The generation, manipulation and detection of spin currents are big challenges in spintronics. For the generation of pure spin currents there are some well established technique, for example the so called *spin pumping effect*[33] generated by, e.g., the *ferromagnetic resonance* (FMR).[34] The spin pumping effect is the reversal of the previously mentioned spin transfer torque. Here, a ferromagnetic/non-magnetic metal bilayer (FM/NM) is placed in a microwave cavity with a static external magnetic field $\vec{H}_0$ applied. The spin polarization of the ferromagnet is now aligned along $\vec{H}_0$. After that, a microwave AC magnetic field perpendicular to the static field excites a precession of the spins in the ferromagnet around $\vec{H}_0$. This precession is accompanied by a generation of magnons. The excitation is called ferromagnetic resonance due to a resonant absorption of electromagnetic energy in the ferromagnetic system. This absorption leads to a magnetization dynamic which can be described by the Landau-Lifshitz-Gilbert equation (Eq. 18). The precession of $\vec{M}$ is now around the static magnetic field $\vec{H}_0$ in place of $\vec{H}_{\text{eff}}$ of Eq. 18. The generated magnons are moving in the direction of the NM. The spin pumping arises at the FM/NM interface where a fraction of the spin current is transmitted into the NM material. The pumped spin current $\vec{j}_s^{\text{pump}}$ can be rewritten as[35]

[33] Y. Tserkovnyak et al. Physical Review Letters **88** (2002) 117601

[34] B. Heinrich et al. Physical Review Letters **90** (2003) 187601

[35] Y. Tserkovnyak et al. Physical Review Letters **88** (2002) 117601

$$\vec{j}_s^{\text{pump}} = \frac{\hbar}{4\pi}\left(g_r^{\uparrow\downarrow}\vec{M}\times\frac{d\vec{M}}{dt} - g_i^{\uparrow\downarrow}\frac{d\vec{M}}{dt}\right). \tag{20}$$

Here, $g_r^{\uparrow\downarrow}$ and $g_i^{\uparrow\downarrow}$ are the real and the imaginary part of the spin mixing conductance.[36] This factor describes the quality of the interface for the spin current transmission. Tserkovnyak et al.[37] point out that the adjacent NM is not a perfect spin sink and a back flow spin current $\vec{j}_s^{\text{back}}$ has to be considered. When both spin currents are not equal - this is the case for the steady state - we obtain a resulting spin current

$$\vec{j}_s = \vec{j}_s^{\text{pump}} - \vec{j}_s^{\text{back}} \tag{21}$$

which flows through the NM.

Another method for spin current generation is the *spin Hall effect* (SHE) which can be found in Eq. 3 in the connection of $\vec{J}^s = \tilde{\sigma}^{sc}\vec{E}$. The idea was first mentioned by Dyakonov and Perel in 1971.[38] The electrons of an electrical charge current are scattered depending on their spin due to the spin-orbit-coupling of the material. For Hirsch[39] this scattering was mainly caused by impurities, which refers to the same reasons already mentioned for the AHE and ANE. These are the skew-scattering and the side-jump effects. Instead, for Sinova et al.[40] this scattering can also be purely intrinsic, which is caused by the band structure of the material. However, the scattering is transverse to the charge current $\vec{j}_c$ and perpendicular to the spin polarization direction $\hat{s}$.[41] In a non-magnetic material the spins of all free electrons are equally distributed in all directions. Therefore, we will get the same amount of electrons scattered in opposite directions but with opposite sign of $\hat{s}$. This leads to a pure transverse spin current. The generated spin accumulation at the edges transverse to the charge current could be observed optically in semiconductors.[42]

The reverse process of the SHE is the *inverse spin Hall effect* (ISHE)[43] when a pure spin current is converted into a transverse charge current. In terms of the Onsager relations and Eq. 2 and 3 we have the connection $\vec{J}^c = \tilde{\sigma}^{cs}\nabla\mu_s$. The ISHE is one of the most important methods to detect spin currents in spintronics by now. Furthermore, it is also the method for spin current detection in this thesis. The relation in the conversion between the spin and charge currents can be described as the so-called spin Hall angle Θ_{SH} which is given by[44]

$$\theta_{\text{SH}} = \frac{\sigma_{xy}^s}{\sigma_{xx}^c}\frac{e}{\hbar} \tag{22}$$

[36] $g^{\uparrow\downarrow} = g_r^{\uparrow\downarrow} + g_i^{\uparrow\downarrow}$

[37] Y. Tserkovnyak et al. Physical Review Letters **88** (2002) 117601

[38] M. I. Dyakonov and V. I. Perel. JETP Letters **13** (1971) 467; M. I. Dyakonov and V. I. Perel. Physics Letters A **A 35** (1971) 459

[39] J. E. Hirsch. Physical Review Letters **83** (1999) 1834

[40] J. Sinova et al. Physical Review Letters **92** (2004) 126603

[41] $\hat{s} = -\frac{\vec{M}}{|\vec{M}|}$

[42] Y. K. Kato et al. Science **306** (2004) 1910; J. Wunderlich et al. Physical Review Letters **94** (2005) 047204

[43] E. Saitoh et al. Applied Physics Letters **88** (2006) 182509; H. Y. Inoue et al. Journal of Applied Physics **102** (2007) 083915

[44] A. Hoffmann. Magnetics, IEEE Transactions on **49** (2013) 5172

with the longitudinal charge conductivity σ^c_{xx} and the transverse spin Hall conductivity σ^s_{xy}. The ISHE was firstly measured in nanometer thin $Ni_{81}Fe_{19}$/Pt bilayers.[43] Here, the spin current was generated with the above mentioned method of FMR + spin pumping from the ferromagnetic $Ni_{81}Fe_{19}$ into the paramagnetic Pt film, which exhibits high spin-orbit-coupling. In the Pt the spin current $\vec{j_s}$ which has a spin orientation $\hat{s}$ parallel to the static external magnetic field $\vec{H}_0$ is converted into a charge current[45]

[45] J. Xiao et al. Physical Review B **81** (2010) 214418

$$\vec{j_c} = \theta_{SH} \frac{2e}{\hbar A} \vec{j_s} \times \hat{s} \tag{23}$$

with the contact area A of the FM/NM interface. However, in an open circuit condition the imbalance of charge carriers in the NM builds up an electric field which counteracts the driven charge current. This electric field can be written in the following form

$$\vec{E}_{ISHE} = D_{SHE} \vec{j_s} \times \hat{s} \tag{24}$$

with the material dependent ISHE efficiency D_{SHE}. This efficiency consists of the prefactors in Eq. 23 in addition to the electrical resistivity ρ of the NM film. Eq. 24 is consistent with the formalism of Eq. 3 and corresponds to the term $\vec{J^s} = \tilde{\sigma}^{sc}\vec{E}$.

A spin current through a non-magnetic metallic film which exhibits high spin-orbit coupling operates like a spin detector by only measuring an electrical voltage perpendicular to $\vec{j_s}$ and the spin orientation $\hat{s}$. The layer thickness of these spin detector materials is limited by the material dependent spin diffusion length λ_{sd}. This is a characteristic mean free path within the spin flips randomly due to collisions of the electron with other particles. The absolute value of the spin current j_s decays on its way through the NM layer when it is transmitted through the interface. The reduced spin current with a distance z from the interface can be written as[46]

[46] O. Mosendz et al. Physical Review Letters **104** (2010) 046601

$$j_s(z) = j_s^0 \frac{\sinh((z - t_N)/\lambda_{sd})}{\sinh(t_N/\lambda_{sd})} \tag{25}$$

with the thickness t_N of the NM layer. The spin current decreases rapidly in the NM material. Other important properties for the detection of spin currents are available in FMR measurements. The previously mentioned spin mixing conductance $g^{\uparrow\downarrow}$ can be determined with the linewidth[47] ΔH_{sp} of the ferromagnetic resonance peak by[48]

[47] full width at half maximum (FWHM)

[48] O. Mosendz et al. Physical Review B **82** (2010) 214403

$$g^{\uparrow\downarrow} = \frac{4\pi\gamma M_s t_{FM} \Delta H_{sp}}{g\mu_B\omega} \tag{26}$$

with the gyromagnetic ratio $\gamma = ge/2mc$, the thickness t_{FM} of the FM layer and the microwave angular frequency ω (cf. Hoffmann[49] and Mosendz et al.[50]). The linewidth ΔH_{sp} depends linearly on an effective damping parameter $\alpha_{eff} = \alpha_{sp} + \alpha_o$. This is a sum of the Gilbert damping parameter α_o we have introduced in the LLG equation (Eq. 18) and a spin pumping damping parameter α_{sp}. Then, the linewidth is given by $\Delta H_{sp} = \alpha_{eff}\omega/\gamma$. When the FM film is investigated by FMR without NM layer on top we obtain the Gilbert damping α_o by measuring ΔH.

[49] A. Hoffmann. Magnetics, IEEE Transactions on **49** (2013) 5172

[50] O. Mosendz et al. Physical Review Letters **104** (2010) 046601

Accompanied by the spin Hall effect there are many other effects and possible applications such as *spin-torque switching*.[51] Here, a charge current through a Ta film which is non-magnetic and exhibits high spin-orbit coupling generates an out-of-plane spin current due to the SHE. This spin current is used to switch the magnetization of the lower FM layer of a MTJ which is placed on top of the Ta film. The switching can be reversed by changing the sign of the charge current. This effect is equal to the previously mentioned STT but the spin torque is accomplished by a pure spin current instead of a spin polarized charge current.

[51] L. Liu et al. Science **336** (2012) 555

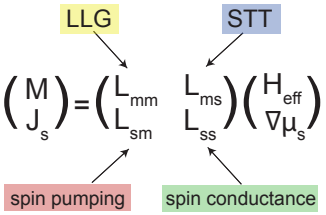

Figure 10: Response matrix between the magnetization M, the spin current J_s, the effective magnetic field H_{eff} and a spin driving force $\nabla\mu_s$.

For the sake of completeness we would like to give a short overview of the connection between the magnetization M and a pure spin current J_s. The spintronic phenomena described by the LLG, STT, spin pumping and spin conductance can be combined in a response matrix (Fig. 10).[52] H_{eff} was introduced in Eq. 18 and the *spin driving force* $\nabla\mu_s$ results from the difference of the spin-dependent chemical potentials $\mu^{\uparrow} - \mu^{\downarrow}$ which creates spin accumulation and a driving force into regions with lower spin accumulation. It becomes obvious by Onsager's symmetry relation (Eq. 2) that spin pumping and the STT are complementary to each other and connect the spin current with the motion of magnetization.

[52] A. Brataas et al. arXiv.org (2011). arXiv: 1108.0385

A very recently observed phenomenon which is based on an interplay between the SHE and its reversal process, the ISHE, is the so called *spin Hall magnetoresistance* (SMR).[53,54] This is a new kind of MR effect. When a charge current flows through a non-magnetic material with a high spin-orbit coupling there is a transverse spin current due to the SHE. The spin orientation is perpendicular to the charge current and the spin current direction. At the edges these spin currents are reflected due to the boundary conditions. After the reflection the ISHE converts this spin current back into a charge current which flows in the same direction as the applied charge current. An adjacent film of the magnetic insulator yttrium iron garnet can absorb the spin cur-

[53] H. Nakayama et al. Physical Review Letters **110** (2013) 206601

[54] M. Althammer et al. Physical Review B **87** (2013) 224401

rent by STT when the magnetization of the yttrium iron garnet is perpendicularly aligned to the spin orientation. The magnetization is controlled by an external magnetic field which is too low to influence the spin orientation of the spin current in the Pt. When the magnetization is parallel to the spin orientation of the spin current there is a reflection. The absorption and reflection of the spin current and the interplay of SHE and ISHE correspond to the two states of high and low resistance. This could be shown in collaboration with Althammer et al.[54] in similar yttrium iron garnet and nickel ferrite films which were used in this thesis.

Spincaloritronics

The generation of pure spin currents with heat is described by the field of spincaloritronics.[55] We already described thermoelectric effects where the electric field was exchanged by a temperature gradient and Ohm's law (Eq. 4) changes into the Seebeck effect (Eq. 13). The context becomes clear by Eq. 3 and the Onsager relations. The Seebeck effect connects the temperature gradient ∇T with a generated electric field $\vec{E}$ by a material dependent proportionality factor - the Seebeck coefficient S. It is well known, in a simple image, that thermal energy can activate the motion of particles as well as quasi particles. Phonons are an example of a thermally induced flow of quasi particles. Furthermore, the generation of thermally driven magnons is relatively new and of great interest in research at present. This is the connection $\vec{J}^s = -\tilde{\sigma}^{sq}\nabla T$ in Eq. 3. In the following passage, we will explain the rising of the spin Seebeck effect during the last years in chronological order. A theoretical point of view will be presented which is used in later discussions and arguments concerning the appearance of the spin Seebeck effect in the materials investigated.

[55] G. E. W. Bauer et al. Nature Materials **11** (2012) 391

Spin Seebeck effect

One of the main goals in spincaloritronics is the generation of thermally mediated spin currents. The key experiment in this branch is the *spin Seebeck effect* (SSE). The first observation of the SSE was reported in 2008 by Uchida et al.[56] in 20 nm thin permalloy (Py, $Ni_{81}Fe_{19}$) films with a 10 nm thin Pt strip as a spin detector. They considered a conventional thermocouple as reference. This reference is adopted to a ferromagnet where they considered the two spin channel model.[57] Each spin channel represents one conductor with its distinct Seebeck coefficient. Therefore, an im-

[56] K. Uchida et al. Nature **455** (2008) 778

[57] N. F. Mott. In: *Proceedings of the Royal Society of London. Series A*. vol. 153. 1936 699

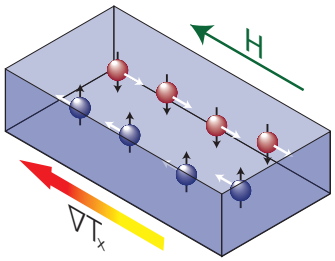

Figure 11: The two spin channels of a ferromagnet were considered as a thermocouple.

(a)

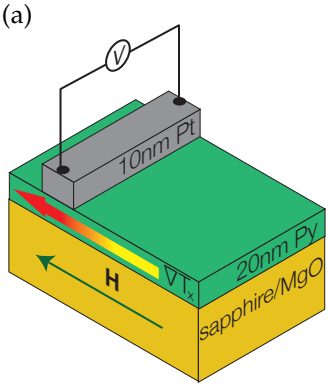

(b)

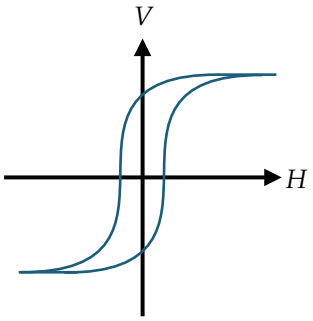

Figure 12: (a) First SSE configuration with Pt strip on the hot side of a Py film on a sapphire or MgO substrate. (b) The voltage V at the Pt strip as a function of the external magnetic field H.

balance of the spin was predicted in the ferromagnetic film when an in-plane temperature gradient ∇T_x was applied (Fig. 11).

This imbalance was expected between the hot and the cold side of the FM layer with an in-plane spin orientation when an external magnetic field lay parallel to ∇T_x. For the detection of the spin accumulation a thin Pt strip was used with a thickness of 10 nm, which is in the region of the spin diffusion length. It was not entirely reported what kind of driving force was exactly responsible for a spin current flowing perpendicularly from the Py layer into the Pt strip. Nevertheless, the ISHE in the Pt was expected to convert the spin current into a transverse charge current. An electromotive force described by Eq. 24 was expected to arise along the Pt strip which should be measurable as an electrical voltage. Therefore, the required orientations are the spin polarisation vector $\hat{s}$ aligned by the external magnetic field, which is parallel to ∇T_x, and an out-of-plane spin current $\vec{j}_s$. A detailed explanation for the driving force of this out-of-plane spin current was missing. The combination of an FM/NM layer system implies a diffusion of the spin from a region of spin accumulation to a region with no spin accumulation accompanied with the spin pumping effect from an FM into an NM layer.

However, the reported observations were a measurable voltage in a range of a few microvolt with a temperature difference ΔT_x of about 10 K over a length of 10 mm. The most striking behaviour was the variation of the voltage depending on the location of the Pt strip along the Py film (Fig 12 and Fig 13). The voltage decreased when the Pt strip was moved from the hot side to the cold side of the Py. In the middle of the Py film the ISHE voltage vanished completely. After that, a sign reversal in the voltage could be observed and the absolute value increased until the Pt strip reached the cold sample side. What was responsible for this sign reversal was the reversed spin current into the Pt between the hot and the cold sample ends. When the external magnetic field $\vec{H}$ was reversed the spin orientation $\hat{s}$ changed its sign simultaneously. This behaviour could be observed in magnetic field loop measurements. The obtained $V-H$ curves looked like typical $M-H$ hysteresis curves due to the magnetization switching of the FM layer. These $V-H$ curves were reversed when the Pt strip was placed from the hot to the cold sample side. Therefore, Uchida et al. concluded that this sign reversal has to come from a reversal of the spin current $\vec{j}_s$.

However, the first explanation by Uchida et al. was a sign change in $\hat{s}$ due to the imbalance of the spins with opposite direc-

tion between the hot and the cold sample side. This behaviour was not carefully explained. When the magnetization of the FM layer is in saturation all spins should be parallel aligned. After all, there is no difference in the observation when there are two spin currents with an antiparallel spin orientation in the same direction or two spin currents with a parallel spin orientation in opposite directions.

Furthermore, the cross product of Eq. 24 (ISHE) could be further confirmed by measurements involving rotation of the external magnetic field in the sample plane. The observation was a cos function when the magnetic field direction started from parallel to the temperature gradient. The sign of this cos function changed when the Pt strip moved from the hot to the cold sample side. When the voltage was measured directly on the Py film the ISHE voltage vanished completely even at the sample edges when the spin detector was missing.

This spin accumulation thermocouple analogy was controversially discussed. It is based on the two spin channel model which has to withstand over a lengthscale of a few millimeters, the length of the Py film. This is much longer than the above mentioned spin diffusion length of a few, tens, or even hundreds of nanometers depending on the material, but still smaller. An alternative and theoretically motivated explanation was given by Xiao et al. in 2010.[58] They criticised the view that the two spin channels should be short circuit due to spin-flip scattering along the millimeter scale. They proposed a difference between the sub-systems of the magnon temperature T_m in the FM layer and the electron temperature T_e in the NM layer. The latter should be equal to the phonon temperature T_p in the NM layer due to a strong electron-phonon interaction. This difference was assumed as the driving force for a thermally activated spin pumping effect. A more detailed description of the magnon-phonon interaction due to their relaxation behaviour was given by Sanders and Walton.[59] The explanation by Xiao et al.[58] is mostly based on their work.

We would like to reduce the complete theory to the main arguments. In the work of Xiao et al.[58] the magnetization $\vec{M}$ in the FM layer is represented by a single domain in the so-called macrospin model. At a non-zero temperature T the magnetization $\vec{M}$ is thermally activated and therefore $\dot{\vec{M}} \neq 0$.[60] This leads to a spin pumping driven spin current $\vec{j}_s^{\text{pump}}$ given by Eq. 20. This is accompanied by a back flow spin current $\vec{j}_{\text{back}}$ and can be written

(a)

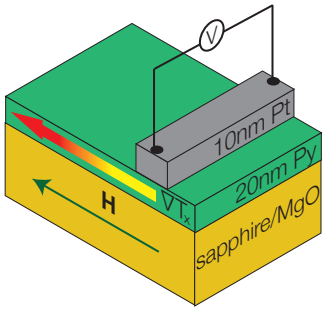

(b)

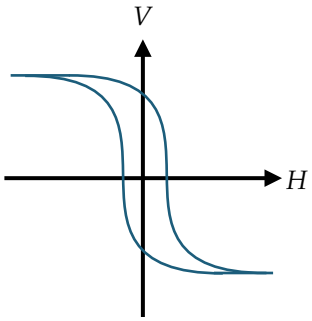

Figure 13: (a) First SSE configuration with Pt strip on the cold side of a Py film on a sapphire or MgO substrate. (b) The voltage V of the Pt strip as a function of the external magnetic field H.

[58] J. Xiao et al. Physical Review B **81** (2010) 214418

[59] D. Sanders and D. Walton. Physical Review B **15** (1977) 1489

[60] $\dot{\vec{M}} = \frac{d\vec{M}}{dt}$

[61] J. Xiao et al. Physical Review B **81** (2010) 214418

by Xiao et al.[61] as

$$\vec{j}_s^{\text{back}}(t) = -\frac{M_s V}{\gamma}\gamma\vec{M}(t) \times \vec{H}_{\text{r}}(t) \tag{27}$$

with a random magnetic field $\vec{H}_{\text{r}}$ which acts on the thermally activated magnetization. The spin current $\vec{j}_s^{\text{pump}}$ is proportional to the magnon temperature T_m in the ferromagnet and the back flow spin current $\vec{j}_s^{\text{back}}$ is proportional to the electron temperature T_e in the non-magnetic material. Regarding Eq. 21 which tells us that the resultant spin current is the sum of both we obtain

$$\vec{j}_s \propto T_m - T_e = \Delta T_{\text{me}} \tag{28}$$

[62] M. Schreier et al. Physical Review B **88** (2013) 094410

When Eq. 23 for the ISHE is used a formula for the measured SSE voltage can be created which was later drafted by Schreier et al.[62] from Xiao et al.[61] in the form

$$V_{\text{SSE}} = \frac{g_r^{\uparrow\downarrow}\gamma\hbar k_B}{2\pi M_s V_a}\Delta T_{\text{me}} \cdot \frac{2e}{\hbar}\theta_{SH}\rho l \cdot \eta \cdot \frac{\lambda}{t}\tanh\left(\frac{t}{2\lambda}\right). \tag{29}$$

In the first fraction there are all properties concerning the FM layer. There are the real part of the spin mixing conductance $g_r^{\uparrow\downarrow}$ (cf. Eq. 20 and Eq. 26), the gyromagnetic ratio γ, and the magnetic coherence volume V_a (cf. Xiao et al.[61] and Schreier et al.[62]). ΔT_{me} is the temperature difference between the magnons in the FM and the electrons in the NM. The NM layer properties are the spin Hall angle θ_{SH} (cf. Eq. 22), the electrical resistivity ρ and the distance l between the voltage contacts. The constant η stands for a back flow correction factor for a spin current which diffuses back from the NM into the FM layer. The last terms describe the penetration depth with the spin diffusion length λ and the thickness t of the NM layer.[62]

Transverse spin Seebeck effect

[63] K. Uchida et al. Nature **455** (2008) 778

The SSE on Py as it was measured by Uchida et al.[63] in 2008 was obtained in the so-called *transverse* configuration (TSSE), because the detected spin current which is usually out-of-plane to the FM/NM system is transverse to the applied temperature gradient. In what follows the spin Seebeck effect in this configuration will be called TSSE.

[64] K. Uchida et al. Nature Materials **9** (2010) 894

After the first observation in Py films, two further material systems came into the focus of TSSE investigations at the same time. In 2010 Uchida et al.[64] investigated the TSSE in the magnetic

insulator yttrium iron garnet (YIG). The observed behaviour of the voltage measured on the Pt strip was the same compared to Py which led to a similar interpretation of the TSSE. In this sample system there are no free charge carriers in the ferromagnet, only thermally activated magnons. The theory by Xiao et al.[65] that the driving force of the spin current is the difference between the magnon temperature in the FM and the electron temperature in the NM could still explain the observations.

[65] J. Xiao et al. Physical Review B **81** (2010) 214418

Moreover, in the same year Jaworski et al.[66] investigated the ferromagnetic semiconductor GaMnAs. The behaviour of the transverse voltage observed at a Pt strip was also mostly the same compared to the investigation on Py by Uchida et al.[63] The most striking additional contribution of this publication was a cut of the FM layer in the middle of the sample. There was no connection between the hot and the cold sample side of the FM layer except through the insulating and non-magnetic GaAs substrate. A sign reversal of the observed ISHE voltage between the hot and the cold side of the sample was still obtained. Therefore, the dominant effect was attributed to the TSSE. They claimed that a connection between both sides could only be realized by phonons in the substrate.

[66] C. M. Jaworski et al. Nature Materials **9** (2010) 898

Furthermore, Jaworski et al.[66] presented the first concerns about unintended side effects which where investigated as follows. Instead of Pt strips they used Pt point contacts at the sample ends transverse to the temperature gradient. The transverse voltage was measured at these Pt contacts. Moreover, they used GaMnAs samples with an out-of-plane magnetization. They observed an effect which they attributed to the ANE given by Eq. 15. There was no sign reversal between the hot and the cold sample end. The effect completely disappeared when Pt strips instead of point contacts were used. They assumed that the Pt shorted out the effect, because the Pt had a much smaller resistance than the GaMnAs. After that, they deposited Pt point contacts on GaMnAs films with an in-plane magnetization and observed an ANE added by a PNE (Eq. 17). Again, a sign reversal between the hot and the cold end was not observed. They concluded that the ANE was a result of spurious out-of-plane temperature gradients.

In 2011 Bosu et al.[67] presented a TSSE investigation in the highly spin polarized Heusler compound Co_2MnSi with an adjacent Pt strip near one sample edge. They did measurements on Co_2MnSi/Pt and on Py/Pt as a reference to compare the results with the work of Uchida et al.[63] The observations were mostly the same, but they also considered an unintended ANE in addition

[67] S. Bosu et al. Physical Review B **83** (2011) 224401

to the ISHE voltage due to spurious out-of-plane temperature gradients. However, they obtained a sign change in the voltage between the hot and the cold sample ends measured at the Pt strip. The voltage was proportional to the temperature difference but the slope of this proportionality was dissimilar between the hot and the cold side. They tested the same measurements on Py samples without Pt on top and obtained a voltage proportional to the temperature difference with the same sign on both sample ends but also with different slopes at the hot and the cold end, respectively. They observed the same behaviour for Co_2MnSi as well as Py films. Furthermore, a series of thicker Co_2MnSi samples showed an increase of the unintended ANE. They concluded that this was due to a superposition of a TSSE which shows a sign reversal and an ANE which shows no sign change in the voltage when the Pt strip changes from the hot to the cold side. They could not observe a significant influence of the high spin polarization of Co_2MnSi compared to a conventional FM alloy like Py.

[68] S. H. Wang et al. Physical Review B **88** (2013) 214304

In 2013 Wang et al.[68] reported an attempt to separate the ANE and TSSE contributions by measuring and comparing Py/Py/Pt and Py/Pt/Py structures. In the latter structure they expected that a possible TSSE would cancel itself out by contributions from the top and bottom Py films which should have opposite signs. They could observe a clear PNE with about 64 % of the measured voltage. In reference measurements they estimated an ANE contribution due to an unintended out-of-plane temperature gradient of about 26 %, and the remaining 10 % were attributed to a possible SSE. However, the authors were not able to attribute these 10 % unequivocally to the TSSE. It is very likely that the difference in the voltage measurement for the comparison samples is a result of a mutable out-of-plane temperature gradient obtained by mounting the samples on the copper heaters, by different contacting and a result of different spin-mixing conductances of the interfaces due to variations within the preparation process. All this will be described in more detail in the following experimental chapters. Furthermore, when this voltage contribution can be attributed to the SSE it was not completely ruled out that it is generated by the out-of-plane temperature gradient which also causes the ANE. This is a different SSE configuration which will be described in the next section.

[69] G. Siegel et al. Scientific Reports **4** (2014) 4429

Last year, Siegel et al.[69] reported TSSE observations in Bi-YIG/Pt bilayers. However, they have not shown the characteristic sign change between the hot and cold sample side. This would

have been important for an unequivocal attribution of the effect to the TSSE. It is highly probable that their observations are due to unintended out-of-plane temperature gradients.

The previously mentioned publications by Uchida et al.[70] for TSSE investigations on Py/Pt and YIG/Pt, Jaworski et al.[71] for investigations on GaMnAs/Pt and Bosu et al.[72] for investigations on Co_2MnSi/Pt were obtained in only two different setups.[73] These publications are the only reports about the SSE in the configuration of a transverse measured voltage (i.e. TSSE) at an adjacent spin detector material with an in-plane temperature gradient along different FM materials. Further reports of measurements in this configuration were obtained in the same groups.

The TSSE reported by Uchida et al.[70] attracted great attention in the communities of spintronics as well as thermoelectric science. The high number of citations (over 430 since 2008) conjectures the number of groups in the world who tried to reproduce the results, first of all in Py thin films with an adjacent Pt strip. In Tab. 1 a compilation of all reports is listed for all attempts to reproduce the measurements from the first reports of the TSSE in different material systems. Of course, this list only regards attempts which were published afterwards. However, the number of different groups and setups shows how many physicists took an opposite point of view on the observed results.

[70] K. Uchida et al. Nature **455** (2008) 778

[71] C. M. Jaworski et al. Nature Materials **9** (2010) 898

[72] S. Bosu et al. Physical Review B **83** (2011) 224401

[73] Bosu et al. and Uchida et al. obtained their results in the same setup for SSE measurements.

Longitudinal spin Seebeck effect

The advantage of a magnetic insulator with no free charge carriers was used by Uchida et al.[74] in 2010 to investigate the SSE in a second configuration. The magnetic insulator YIG was completely covered by a thin Pt layer. This bilayer was sandwiched between a heat bath and a heat sink. They could report that an applied out-of-plane temperature gradient drives a parallel spin current with a spin orientation controlled by an external magnetic field which is applied in the sample plane. This spin current enters the Pt layer and is converted into a measurable voltage due to the ISHE. The fact that the detected spin current is parallel to the temperature gradient is why it is called the *longitudinal* SSE. The spin Seebeck effect in this configuration will be called the LSSE in the following. The theory by Xiao et al.[75] can be adopted for the LSSE. Here, the explanation of the driving force given by the difference between the magnon temperature in the FM and the electron temperature in the NM is more intuitive for a longitudinally generated spin current.

[74] K. Uchida et al. Applied Physics Letters **97** (2010) 172505

[75] J. Xiao et al. Physical Review B **81** (2010) 214418

Although, the TSSE is generally controversially discussed, in ferromagnetic metals like Py as well as in magnetic insulators like YIG, the LSSE configuration is now well established and was reproduced by many groups. It was also observed in many different garnets and ferrites which served as a magnetic insulator material (e.g. Uchida et al.[76]).

There are different methods of heating which can be used to generate an out-of-plane temperature gradient. In 2012, Weiler et al.[77] presented the LSSE in YIG/Pt with a laser heating technique instead of copper block heating. The laser-spot with a diameter of 10 μm scanned the landscape of the Hall-bar patterned YIG/Pt bilayer. Another heating method was introduced by Schreier et al.[78] in 2013. They used a charge current through the Pt layer for heating the sample. A heat sink at the bottom ensured the generation of an out-of-plane temperature gradient. However, a large contribution of an unintended side effect which was symmetric with respect to the magnetic field had to be disentangled. The solution was a reversal of the charge current through the Pt. A sign reversal of the symmetric contribution could be observed, but the LSSE kept its sign while the direction of the temperature gradient did not change. The symmetric contribution was assumed to be the SMR effect. This contribution could be removed by taking the sum of both charge current directions. The remaining voltage was the LSSE contribution.

A community of four groups did LSSE as well as FMR spin pumping experiments on similar YIG/Pt samples to compare the sign of their results by using the same convention of vector directions for their measurement configuration (temperature gradient, external magnetic field and the polarisation of the multimeter). The work of Schreier et al.[79] has shown that the sign was equal between all groups for the ISHE voltage observed in LSSE and FMR spin pumping experiments, respectively. Afterwards, they defined the spin Hall angle of Pt with a positive sign to decide between materials with positive (e.g. Pt) and negative (e.g. Ta) spin Hall angles in the future literature.

For the investigation of the time and length scales of the generated spin current Agrawal et al.[80] presented time resolved LSSE measurements. They used a 6.7 μm thick YIG film with a 10 nm thin Pt layer on top and found a diffusion length of about 500 nm for thermal magnons which propagate into the Pt. They used a modulated laser beam to heat up the sample from above and a heat sink below the sample ensured the generation of an out-of-plane temperature gradient. They monitored the evolution

[76] K. Uchida et al. Physical Review B **87** (2013) 104412; K. Uchida et al. Applied Physics Letters **97** (2010) 262504

[77] M. Weiler et al. Physical Review Letters **108** (2012) 106602

[78] M. Schreier et al. Applied Physics Letters **103** (2013) 242404

[79] M. Schreier et al. Journal of Physics D: Applied Physics (2014) 025001

[80] M. Agrawal et al. Physical Review B **89** (2014) 224414

time of the LSSE signal and observed that the effect arises in the first microsecond. Due to the fact that this rising time is different from the rising time of the laser (200 ns) and the rising time of the temperature gradient over the interface (20 ns) they concluded that the LSSE is a sum of an interface and a bulk contribution. The interface contribution comes from the difference between the magnon temperature T_m in the FM layer and the electron temperature T_e in the NM layer. The bulk contribution, however, comes from thermally excited magnons generated in the whole FM film. The sum of both contributions is described by Agrawal et al.[80] as

$$V_\mathrm{LSSE}(t) \propto \alpha \int_{\delta d}^{0} \nabla T_y(y,t)dy + \beta \int_0^l \nabla T_y(y,t) \exp\left(\frac{-y}{L}\right)dy \qquad (30)$$

with the out-of-plane temperature gradient ∇T_y, the thickness l of the FM layer, the effective magnon diffusion length L and the effective thickness δd of the interface. Here, α is a parameter for magnon-electron coupling between the FM and NM layer and β is a parameter for the magnon-magnon interaction in the FM layer. After that, they extracted an intrinsic time evolution constant of about 343 ns for the LSSE based on simulations of the temperature gradient evolution in the sample.

Roschewsky et al.[81] were also able to report time resolved LSSE measurements, but on thinner YIG($t < 65\,\mathrm{nm}$)/Pt($t < 20\,\mathrm{nm}$) bilayers. They could not verify the magnon diffusion length reported by Agrawal et al.[80] due to their thinner YIG films, but they have shown by lock-in measurements with modulation frequencies up to 30 MHz that there is no decay of the SSE for times larger than 5 ns. The deviation in the magnon diffusion length of 500 nm reported by Agrawal et al.[80] and 110 nm reported by Kehlberger et al.[82] can be explained by their different measurement methods, the sample thicknesses and sample properties like different magnetic damping of the YIG and different interface conditions.

Recently, there were investigations reported by Geprägs et al.[83] on the magnetic insulator $Gd_3Fe_5O_{12}$ (GIG) which is closely related to YIG. However, GIG shows a very interesting temperature dependent behaviour of the magnetization. Instead of the non-magnetic yttrium in YIG it was replaced by gadolinium which is ferromagnetic at temperatures below 290 K. The gadolinium contributes a magnetic sublattice to the two magnetic iron sublattices. The magnetization of the gadolinium sublattice is temperature dependent. Therefore, GIG shows a compensation

[81] N. Roschewsky et al. Applied Physics Letters **104** (2014) 202410

[82] A. Kehlberger et al. arXiv.org (2013). arXiv: 1306.0784v1

[83] S. Geprägs et al. arXiv.org (2014). arXiv: 1405.4971v1

point where the net magnetization of the sum of all sublattices is zero. Below this compensation point the net magnetization of the GIG rises again due to increasing magnetization in the gadolinium sublattice at lower temperatures. Below the compensation point the magnetization is aligned antiparallel to the magnetization above the compensation point. However, in an external magnetic field it can be aligned parallel to $\vec{H}$ at above and below this compensation point. First theoretical ideas about the LSSE in antiferromagnets and compensated ferrimagnets were published by Ohnuma et al.[84] in 2013. They gave rise to the question whether each magnetic sublattice drives a spin current generated by the LSSE or whether the net magnetization drives only one spin current. In GIG the spin current is presented by thermally excited magnons in the magnetic and insulating material. According to the report by Geprägs et al. they performed experiments independently in two groups and two setups with two similar samples which were also prepared independently. They surprisingly observed two changes in sign of the measured ISHE voltage instead of only one, which they had expected, while the magnetization shows only one compensation point in the range of the temperature investigated. There is no clear explanation up to now, but suggestions lead to a Gd-Gd-exchange around 80 K where the second sign reversal can be observed. However, the results give rise to the conclusion that the observed spin currents due to the LSSE in the ferrimagnet investigated do not mirror the net magnetization. Therefore, investigation on other garnets which also show compensation points in their ferrimagnetic behaviour will become very interesting in view of further investigation of magnetic sublattices. In general, the LSSE as a technique of investigating magnetic sublattices represents a breakthrough in the research of magnetic materials which opens a new field of research.

[84] Y. Ohnuma et al. Physical Review B **87** (2013) 014423

Magnetic proximity effect in magnetic insulator/ Pt bilayers

Further, we would like to discuss the issue of spin polarization at the interface of magnetic insulator/Pt bilayer systems. This issue is one of the most critical problems, which is also controversially discussed in the recent literature about SSE investigations, when Pt is used as a spin detector. It is one of the most popular spin detector materials which is known as a heavy metal with a rela-

tively high spin orbit coupling. Furthermore, the deposition of Pt is a very simple step in the whole sample preparation compared to compounds with larger predicted spin Hall angles. However, the reported spin Hall angles of Pt range from 0.012 ± 0.002 reported by Feng et al.[85], obtained in spin pumping experiments, and 0.11 ± 0.08 reported by Althammer et al.[86], achieved by SMR experiments. Nevertheless, spin diffusion lengths vary from (8.3 ± 0.9) nm to (1.5 ± 0.5) nm, respectively. A very thin Pt layer in the range of $1 - 10$ nm is sufficient for spin detection.

[85] Z. Feng et al. Physical Review B **85** (2012) 214423

[86] M. Althammer et al. Physical Review B **87** (2013) 224401

Pt nearly fulfills the Stoner criterion for ferromagnetic ordering.[87] The product of the exchange coupling J and the density of states at the Fermi energy $N(E_F)$ should satisfy

$$JN(E_F) > 1. \tag{31}$$

[87] E. C. Stoner. In: *Proceedings of the Royal Society of London. Series A*. 1938 372

For Pt the density of states at the Fermi energy exhibits a relatively large value of ≈1.74 states/eV/spin.[88] When Pt comes into contact with a ferromagnetic material, the first monolayers can become spin polarized. Spin polarized Pt could be observed in Ni/Pt and Fe/Pt multilayers with magnetic moments of about $0.2\,\mu_B$/atom and $0.5\,\mu_B$/atom, respectively.[89] The measurement technique typically used for the investigation of magnetic moments is x-ray magnetic circular dichroism (XMCD) which was presented by Schütz et al.[90] in 1987 (cf. De Groot[91]). In XMCD the difference in the absorption of left- and right-circular polarized light with the element specific absorption energy gives information about the magnetic moment in the investigated element. However, the observed magnetic moment is a mean value for the whole investigated film which makes it difficult to measure spin polarization at the interface of a bilayer system. This difficulty is reflected in the recent discussion triggered by the reports of Geprägs et al.[92] who did not observe any evidence of a magnetic proximity effect in YIG/Pt and Lu et al.[93], who detected a spin polarization of the Pt at the interface. Both positions are supported by XMCD measurements.

[88] G. Y. Guo et al. Physical Review B **89** (2014) 214406

[89] F. Wilhelm et al. Physical Review Letters **85** (2000) 413; W. J. Antel et al. Physical Review B **60** (1999) 12933

[90] G. Schütz et al. Physical Review Letters **58** (1987) 737

[91] F. M. F. De Groot. Journal of electron spectroscopy and related phenomena **67** (1994) 94

[92] S. Geprägs et al. Applied Physics Letters **101** (2012) 262407

[93] Y. M. Lu et al. Physical Review Letters **110** (2013) 147207

A more beneficial method for this issue is x-ray resonant magnetic reflectivity (XRMR) presented by Geissler et al.[94] in 2001 on Co/Pt bilayers (cf. Macke and Goering[95]). In conventional x-ray reflectometry (XRR) measurements the interference of the incident beam and the reflected beam at the surface and the interfaces is used to determine the film thicknesses of the layers and the surface roughness. In XRMR the incident beam is left or right circular polarized which gives rise to dichroism if the investigated element is spin polarized. The observed magnetic moment

[94] J. Geissler et al. Physical Review B **65** (2001) 020405

[95] S. Macke and E. Goering. Journal of Physics: Condensed Matter **26** (2014) 363201

is thickness independent and only regards the spin polarization at the interface. For this reason we investigated the interface of FM/Pt bilayer systems (e.g. $NiFe_2O_4$/Pt) with XRMR to determine a possible spin polarization of the Pt film at the interface to consider proximity Nernst effects in our transport measurements. The results are presented in more detail by Kuschel et al.[96]. The conclusion from these investigations is that a possible magnetic moment of Pt is below the measurement sensitivity limit (e.g. $0.02\,\mu_B$ per Pt atom in $NiFe_2O_4$/Pt bilayers). However, calculations by Schreier et al.[97] and Weiler et al.[98] for YIG/Pt indicate that Pt should have an anomalous Nernst coefficient three orders of magnitude larger than Ni even when a completely spin polarized Pt film is assumed which would be extremely large. Furthermore, Kikkawa et al.[99] have shown that a possible ANE contribution due to magnetic proximity effects is negligibly small compared to the observed LSSE signal.

[96] T. Kuschel et al. Physical Review Letters **115** (2015) 097401

[97] M. Schreier et al. Physical Review B **88** (2013) 094410

[98] M. Weiler et al. Physical Review Letters **108** (2012) 106602

[99] T. Kikkawa et al. Physical Review Letters **110** (2013) 067207

Side effects in SSE measurements

The overview of the SSE given so far represents the beginning of this thesis. We investigated the TSSE as well as the LSSE in all kind of FM systems - metals, materials with semiconducting properties, insulators. For FM metals we will present the results already published.[100] This will be supplemented by our collaborators work in collaboration with Schmid et al.[101] The main idea behind further measurements in terms of the TSSE despite the already existing publications was the detailed investigation of all unintended side effects like the PNE and ANE which appeared desultorily in all reports of Tab. 1. We investigated these Nernst effects in terms of a misinterpretation of the TSSE in FM metals. This was done parallel to works published by other groups in

[100] D. Meier et al. Physical Review B **88** (2013) 184425

[101] M. Schmid et al. Physical Review Letters **111** (2013) 187201

	First report of TSSE	no TSSE found
metal	Uchida, K. et al. Nature **455** (2008) 778	Huang, S. Y. et al. Phys. Rev. Lett. **107** (2011) 216604 Avery, A. et al. Phys. Rev. Lett. **109** (2012) 196602 Schmid, M. et al. Phys. Rev. Lett. **111** (2013) 187201 Meier, D. et al. Phys. Rev. B **88** (2013) 184425 Bui, C. T. and Rivadulla, F. Phys. Rev. B **90** (2014) 100403(R)
semicondutor	Jaworski, C. M. et al. Nature Mater. **9** (2010) 898	Soldatov, I. V. et al. Phys. Rev. B. **90** (2014) 104423
insulator	Uchida, K. et al. Nature Mater. **9** (2010) 894	Meier, D. et al. Nat. Commun. **6** (2015) 8211

Table 1: Publications on TSSE experiments in different materials. Comparison between the first reports and reports with no TSSE in similar experiments.

the recent years. We will discuss these reports and compare their results with our observations. For semiconductors Soldatov et al.[102] just recently presented a paper for GaMnAs and did not observe a TSSE either. Instead, they also observed unintended Nernst effects. For TSSE measurements in magnetic insulators like YIG Uchida and co-workers were the only people who reported an observation. In our own work, we set a further focus on magnetic insulators because Nernst effects are suppressed due to the absence of free charge carriers.[103] Furthermore, we have to consider the possibility of magnetic proximity effects in Pt when it is in contact with a FM layer. Pt is near the Stoner criterion of a ferromagnet. This can lead to spin polarization of the Pt at the interface. This results in magnetic proximity induced Nernst effects which will be called *proximity Nernst effects* (anomalous Nernst as well as planar Nernst).

[102] I. V. Soldatov et al. Physical Review B **90** (2014) 104423

[103] D. Meier et al. Nature Communications **6** (2015) 8211

In Fig. 14 both SSE configurations are shown: on the one hand the transverse configuration with a temperature gradient ∇T typically aligned in the film plane (Fig. 14 (a)) and on the other hand the longitudinal configuration with ∇T typically aligned out-of-

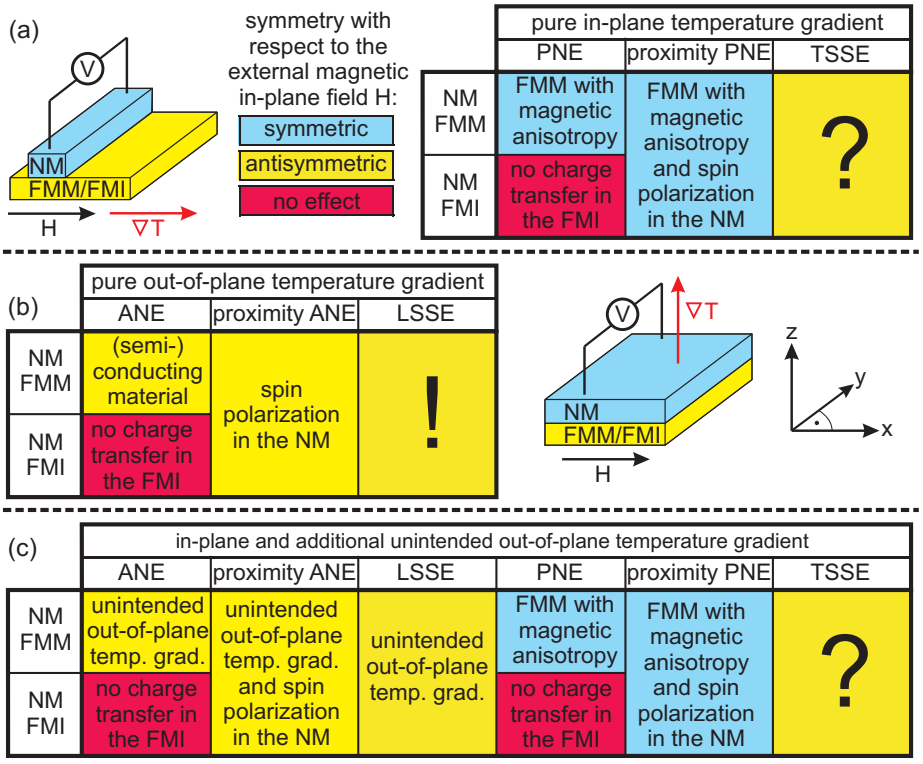

Figure 14: Summary of effects in SSE experiments for FMM/NM and FMI/NM bilayers and given symmetry with respect to the external magnetic in-plane field H for antisymmetric magnetization reversal processes. (a) Pure in-plane ∇T for TSSE measurements. (b) Pure out-of-plane ∇T for LSSE measurements. (c) In-plane and unintended out-of-plane ∇T.

plane (Fig. 14 (b)). In both configurations the external magnetic field H lies in the film plane. The ISHE voltage is measured perpendicularly to H in both cases. For the transverse configuration the NM layer is limited to a strip which is located near the edge of the FM layer, whereas the NM layer in the longitudinal configuration can cover the FM layer completely.

The *effect zoo* we have considered in our research on FM/NM bilayer systems is listed in Fig. 14 and coded by a coloured scheme to distinguish its symmetry with respect to H or even its appearance. We also distinguish between NM layers on ferromagnetic metals (FMM) and magnetic insulators (FMI). In the transverse configuration (Fig. 14 (a)) for FMM/NM bilayers the effect of interest is the TSSE which can easily be separated from unintended PNE and proximity PNE contributions by its different symmetries. In FMI/NM bilayers the PNE can be neglected, but a proximity PNE may occur which is also easy to disentangle from a TSSE. For the longitudinal configuration the ISHE voltage due to the LSSE in FMM/NM bilayers can be overlapped by contributions of the ANE as well as proximity ANE. The separation is much more complicated due to the same symmetry with respect to H. In FMI/NM bilayers, instead, an ANE can be neglected while a proximity ANE should be considered. We have to add up both lists of possible effects when there is a mixture of in-plane and out-of-plane temperature gradients (Fig. 14 (c)). For FMM/NM bilayers the complete *zoo* of effects is possible and has to be included in the evaluation of experimental results. Therefore, both symmetric as well as antisymmetric contributions are possible, but each contribution also contains different effects, which makes it tedious to separate each part according to its origin. For FMI/NM it becomes much easier to distinguish between the effects. ANE and PNE can be neglected due to the lack of charge carriers in the FMI layer. The proximity PNE is the only effect which is symmetric with respect to H. Next it has to be determined if the NM layer is spin polarized or not to exclude a proximity ANE contribution from an LSSE in the measured ISHE voltage.

Our present work contains experiments to investigate the contributions of all these effects when in-plane and out-of-plane temperature gradients on FMM/NM and FMI/NM bilayers are applied.

Spin Seebeck effect in permalloy

In this chapter we will present the investigation of the spin Seebeck effect in thin Py films. The material will be illustrated very briefly and we will give an overview of the previous investigation. The main part of this chapter is dedicated to the experimental results and their discussion, which will be completed by a short outlook into the future of ferromagnetic metals for spin caloric applications. Most of these results were published in 2013.[104]

[104] D. Meier et al. Physical Review B **88** (2013) 184425

Permalloy

Permalloy (Py) is a ferromagnetic compound of about 81 % nickel and 19 % iron. It shows very high magnetic permeability. The relative permeability is about 100 000.[105] Therefore, it is used as a magnetic core material or magnetic field shielding. A very low coercive field of a few *Oersted* makes it a very soft magnetic material. Py can obtain a small uniaxial magnetic anisotropy due to the deposition process.[106] It is also a very interesting material in spintronics, especially for spin pumping experiments. In Py/Pt bilayer systems the ISHE were used to observe spin currents generated by spin pumping in the Py for the first time, which was done in 2006.[107] The use of Py/Pt bilayers to investigate spin dynamics by spin pumping is still very up-to-date.[108] Since these experiments the appearance of spin currents in these sample systems has been well understood. Therefore, Py/Pt was one of the most favoured sample systems for the first spincaloritronic experiments, especially for the spin Seebeck effect.

The Py films in this thesis were deposited via e-beam evaporation and magnetron sputtering on MgO (001) and sapphire (0001) substrates. Uchida et al.[109] decided to use sapphire substrates. They claimed that the thermal conductivity of their substrates was similar to the thermal conductivity of the deposited Py

[105] D. C. Jiles. Introduction to Magnetism and Magnetic Materials, Second Edition, CRC Press, 1998

[106] S. Chikazumi. Journal of the Physical Society of Japan **11** (1956) 551; Joy F. Dillinger and R. M. Bozorth. Physics **6** (1935) 279

[107] E. Saitoh et al. Applied Physics Letters **88** (2006) 182509; M. V. Costache et al. Physical Review Letters **97** (2006) 216603

[108] D. Wei et al. Nature Communications **5** (2014) 3768; M. Obstbaum et al. Physical Review B **89** (2014) 060407

[109] K. Uchida et al. Nature **455** (2008) 778

films. This should reduce any out-of-plane temperature gradients due to different thermal conductivity values. We used sapphire substrates with a thermal conductivity of $\sigma = 42\,\mathrm{W\,m^{-1}\,K^{-1}}$ at 25 °C and MgO substrates with $\sigma = 30\,\mathrm{W\,m^{-1}\,K^{-1}}$ from *CrysTec GmbH*.[110] Compared to Py with a thermal conductivity of about $46.4\,\mathrm{W\,m^{-1}\,K^{-1}}$ reported by Ho et al.[111] sapphire is the preferred substrate with a lower mismatch. However, we investigated Py films on both substrates. Furthermore, we carried out different surface treatments of the substrates like Ar^+ etching before the Py deposition to investigate the influence of different interface conditions.

[110] CrysTec GmbH. `http://www.crystec.de/daten/al2o3.pdf`. [Online; accessed 03-February-2015]. 2015; CrysTec GmbH. `http://www.crystec.de/daten/mgo.pdf`. [Online; accessed 03-February-2015]. 2015

[111] C. Y. Ho et al. Journal of Physical and Chemical Reference Data **7** (1978) 959

Previous reports

In Tab. 1 the first reports of TSSE in metals, semiconductors and insulators are listed. They are opposed to reports on investigations in the same and similar material systems with no TSSE observation. The first of these opposite reports was the work of Huang et al.[112] about temperature gradients in thin films on substrates. The focus was set on the assumption that the substrate was much thicker than the thin film, which can lead to unintended out-of-plane temperature gradients when the thermal conductivities are different. They investigated Py films of 20 nm to 300 nm thickness patterned in Hall bars deposited on 500 µm thick Si substrates. For the in-plane temperature gradient they used a resistive heater near the Py Hall bar on one sample side and a Cu block as a heat sink on the opposite side of the sample. Their observation was an antisymmetric voltage with respect to the external magnetic field, but without any sign change between the hot and the cold side of the sample. When the heater was placed closer to the Hall bar a sign change in the voltage was obtained on the hot side but the cold side kept its sign. However, they observed the same sign and sin function symmetry in magnetic field rotation measurements by reversal of the temperature gradient. This leads to the conclusion that the observed effect was driven by an out-of-plane instead of an in-plane temperature gradient. It should be emphasized that this observation was done without any spin detector material on top of the Py film. An observation of a possible TSSE could be excluded. Then the main effect can be attributed to an ANE in the ferromagnetic Py layer. A PNE could be neglected because a contribution symmetric with respect to H was not obtained. In

[112] S. Y. Huang et al. Physical Review Letters **107** (2011) 216604

further measurements an additional Pt layer on top of the Py/Si system could not lead to any different observations except for a small reduction of the magnitude. There was no TSSE contribution in Py films with Pt strips at all. They recommended using free standing films without substrates. Only a pure PNE in 20 µm thin Fe foil confirmed a solely in-plane temperature gradient. However, they used a heater located on top or at the bottom of the bilayer systems, which makes it difficult to get a pure in-plane temperature gradient without any out-of-plane contributions.

One year later Avery et al.[113] reported TSSE measurements in 20 nm thin Py and Ni films on 500 nm thin suspended Si-N. They assumed a *zero substrate* limit to reduce the heat flow through the substrate underneath. The samples contained Pt strips at the ends of the Py and Ni films to detect possible spin currents. However, the observed voltage could be attributed to a pure PNE and no TSSE contribution was obtained. The voltage was symmetric with respect to the external magnetic field, which was supported by a $\sin \cdot \cos$ symmetry given by Eq. 17 when the magnetic field was rotated in the sample plane. They estimated an upper limit of a possible TSSE driven ISHE voltage, if there is any contribution hidden in the measurement signal. This was the experimental error of about 5 nV.

[113] A. Avery et al. Physical Review Letters **109** (2012) 196602

The work of Schmid et al.[114] in 2013 was done in collaboration with our group. The samples used were identical to the samples presented in our work. Generally, they observed two different features in their TSSE investigations. The first one was a symmetric contribution of the voltage with respect to the magnetic field which showed a $\sin \cdot \cos$ symmetry when the magnetic field was rotated in the sample plane. This contribution can be attributed to the PNE. The second contribution showed an antisymmetric voltage with respect to the magnetic field and a cos function in a magnetic field rotation. This could be attributed to the ANE as well as the TSSE. However, they have shown that the antisymmetric part increases monotonically when the temperature T_{Pt} at the Pt strip increases in a range below and above room temperature. This behaviour was independent of the temperature gradient direction ($\Delta T = \pm 25\,\mathrm{K}$) and was even observed when no temperature gradient was applied ($\Delta T = 0\,\mathrm{K}$). Therefore, the antisymmetric part could not be attributed to the TSSE but to the ANE. The reason for the generated ANE has to be an out-of-plane temperature gradient produced by the Peltier elements which were used for heating. The samples were not clamped, either.

[114] M. Schmid et al. Physical Review Letters **111** (2013) 187201

Their conclusion was supported by reference measurements on samples with a Cu strip instead of a Pt strip. For these samples the same behaviour was observed. However, there should be no ISHE voltage signal detectable in Cu. Schmid et al. also revealed an upper limit for a possible TSSE which was about 20 nV in Py/Pt samples, which is within their experimental error.

Experimental results

[115] K. Uchida et al. Nature **455** (2008) 778

The first SSE report in 2008 by Uchida et al.[115] describes investigations on thin Py films in the transverse geometry (Fig. 15). The first step in our investigations is to reproduce this experiment. The temperature gradient ∇T_x is applied along the sample plane parallel to an external magnetic field $\vec{H}$. The sample is located between two copper blocks. While Uchida et al. fixed the sample ends on top of the copper blocks, we clamped the sample ends between the copper blocks and copper plates to promote in-plane thermal flux and avoid unintended out-of-plane temperature gradients. The substrate was not fully covered by the Py to prevent electrical contact between the metallic film and the copper clamps. Here, the Py film of $5 \times 3\,\mathrm{mm}^2$ in lateral dimensions and 20 nm of thickness was deposited via e-beam evaporation on top of a $10 \times 10\,\mathrm{mm}^2$ substrate. The spin current detector was a 100 µm wide Pt strip of 10 nm thickness which was deposited via magnetron sputtering on one side of the Py film. The strip was aligned perpendicularly to the temperature gradient ∇T_x over the complete substrate of 10 mm.

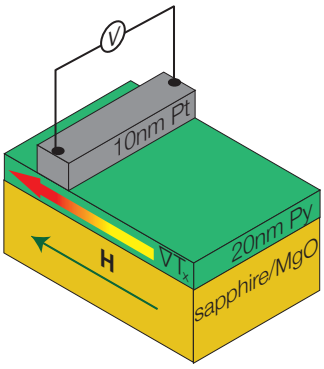

Figure 15: TSSE configuration: The temperature gradient ∇T and the external magnetic field H are parallel aligned and applied in the sample plane. The voltage V is measured transversely at the ends of the Pt strip.

In-plane temperature gradients

Thermoelectric measurements are very sensitive concerning unintended heat flow which can appear in all parts of the measurement system. Among these sensitive parts are the electrical contacts we have to use to measure the voltage. In the case of the spin Seebeck effect the ends of the Pt strip have to be contacted. The best way to reduce unintended heat flow through the wiring is to use very thin tips or wires with a small contact area on the Pt strip. Therefore, we started using Au bonding wires with a diameter of 25 µm. The contacting was done by ultrasonic wedge bonding with a *Hybond Model 572A Wedge Bonder*. The Au wire was pressed with an ultrasonic pulse of 62 kHz to remove contamination between wire and sample. A low force between 0.15 – 2 N was used to promote diffusion between the materials,

for a time between 20 – 400 ms. This leads to a contact area of about 25 – 50 µm in diameter without any considerable damage to the Pt film.

For further prevention of thermal conduction and convection between the sample and the sample holder with the surroundings we performed the first measurements in vacuum. Thermal fluctuation could be minimized and can be attributed to thermal radiation and low thermal conduction due to the connection between the sample holder and the chamber.

In Fig. 16 - Fig. 18 the voltage signal V at the ends of the Pt strip is shown as a function of the external magnetic field H. For each graph we changed the direction of the in-plane magnetic field with a fixed azimuthal angle α with respect to the x-axis (elongated sample direction). In the TSSE configuration ∇T_x should also lie along the x-direction. For each α the magnetic field H was changed starting at −100 Oe to 100 Oe and back to −100 Oe again for a complete magnetic field loop. This measurement reveals the symmetry of the appearing effects. For a TSSE we expect an antisymmetric behaviour of V with respect to H when we switch the magnetization directions. This can be compared to Eq. 24 (ISHE) because the cross product is responsible for the angle dependency. The temperature difference in Figs. 16 to 18 was fixed at $\Delta T = 35\,\mathrm{K}$ and the angle α was varied between 0 – 90°. The Pt strip was located on the hot side of the Py film. The reference temperature T_0 was defined by the cold sample side and fixed at room temperature. Air cooling through the copper block ensured the maintenance of T_0 despite heat dissipation.

In Fig. 16 (a) the external magnetic field H was intentionally applied parallel to ∇T_x in the sample plane ($\alpha = 0°$). The ob-

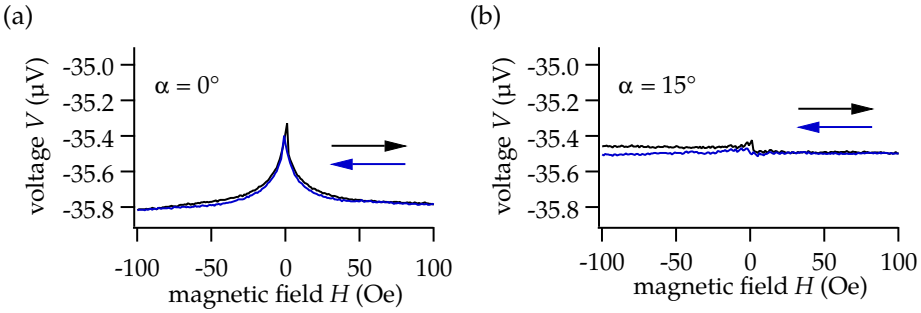

Figure 16: Transverse voltage V as a function of the external magnetic field H which is aligned in-plane with a fixed angle α with respect to the in-plane temperature gradient ∇T_x. (a) for $\alpha = 0°$ and (b) $\alpha = 15°$. The temperature difference was fixed at $\Delta T = 35\,\mathrm{K}$.

tained voltage signal V is symmetric with respect to H. For large absolute values of H the same saturated voltage V_{sat} is reached (−35.8 µV). There are two peaks around 0 Oe which do not overlap. Furthermore, they do not have exactly the same height. For zero field there is a crossing point of the two branches at −35.4 µV.

The reason for the different heights of the peaks is the step size of the magnetic field sweep during the measurement. Here, the step size was 1 Oe with a delay time of 1 s between each measurement step. The voltage was measured with a *Keithley Nanovoltmeter 2182A* with an adjusted integration time of 20 ms of the A/D converter inside the multimeter. The multimeter was also adjusted in the *moving average* mode with a stack of 50 values to obtain the best signal filtering. Here, the multimeter determines the average about the last 50 measured values. Therefore, an integration time of 20 ms leads to a delay time of 1 s between each magnetic field step to get a genuine signal V for a certain magnetic field value H. Now we changed the angle between the long sample axis (x-direction) and the magnetic field vector $\vec{H}$ to $\alpha = 15°$ (Fig. 16 (b)). The observed curve shows a nearly straight line around −35.5 µV. Small peaks around 0 Oe can be assumed and there is no difference between the left and the right hand side for V_{sat} except for a small difference due to a thermal drift of the voltage between the start and the end of the measurement. When we change the angle to $\alpha = 30°$ and $\alpha = 45°$ (Fig. 17 (a) and (b)) we observe two minima instead of two maxima around 0 Oe. The saturated voltage V_{sat} increases and the minima are more distinct for both angles, respectively. The crossing point of about −35.4 µV of the two branches is the same compared to the measurements with the previous angles α. When we increase α to 75° and 90° (Fig. 18) there are still two minima with a

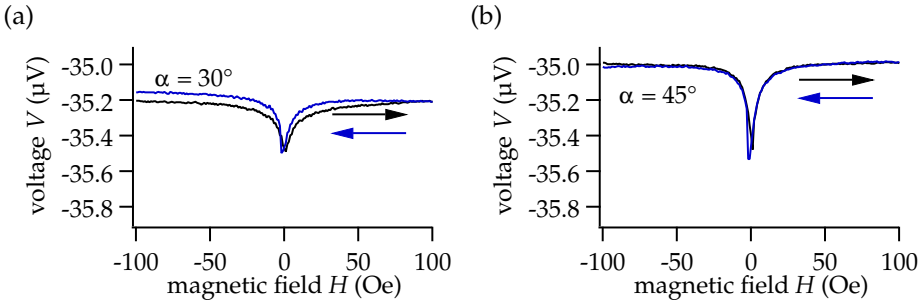

Figure 17: Transverse voltage V as a function of the external magnetic field H which is aligned in-plane with a fixed angle α with respect to the in-plane temperature gradient ∇T_x. (a) for $\alpha = 30°$ and (b) $\alpha = 45°$. The temperature difference was fixed at $\Delta T = 35$ K.

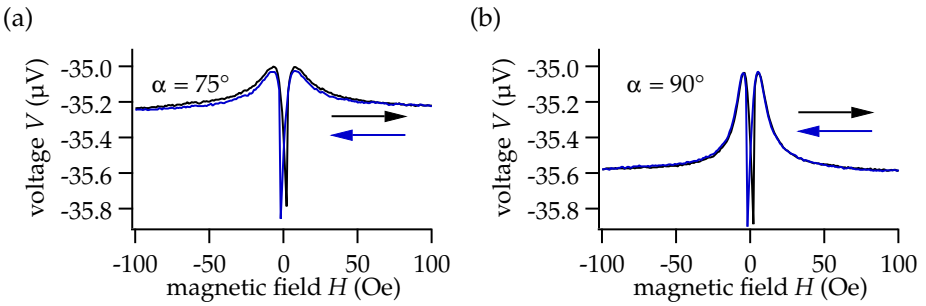

Figure 18: Transverse voltage V as a function of the external magnetic field H which is aligned in-plane with a fixed angle α with respect to the in-plane temperature gradient ∇T_x. (a) for $\alpha = 75°$ and (b) $\alpha = 90°$. The temperature difference was fixed at $\Delta T = 35\,\mathrm{K}$.

crossing point at $-35.4\,\mu\mathrm{V}$. However, when the magnetic field H is increased in both directions there are local maxima of about $-35.0\,\mu\mathrm{V}$. This is remarkably the same voltage as the saturated value for $\alpha = 45°$. For larger magnetic fields H a saturated value is obtained. In the range between $-100\,\mathrm{Oe}$ to $-90\,\mathrm{Oe}$ and $90\,\mathrm{Oe}$ to $100\,\mathrm{Oe}$ the average voltage was calculated and plotted as a function of the angle α shown in Fig. 19 (a). The saturated voltage shows a significant part of a twofold sin curve of α. Therefore, a complete 360° rotation of H was done in the sample plane with an absolute value of $100\,\mathrm{Oe}$. The curve obtained can be fitted by a function in the form of $A \cdot \sin(2(\alpha + \alpha_0))$ with an amplitude of $A = 700\,\mathrm{nV}$ and a phase shift of $\alpha = -7°$ (Fig. 19 (a)). For a better comparison of the switching behaviour three particular curves for α (0°, 15° and 45°) are plotted in Fig. 19 (b). The switching

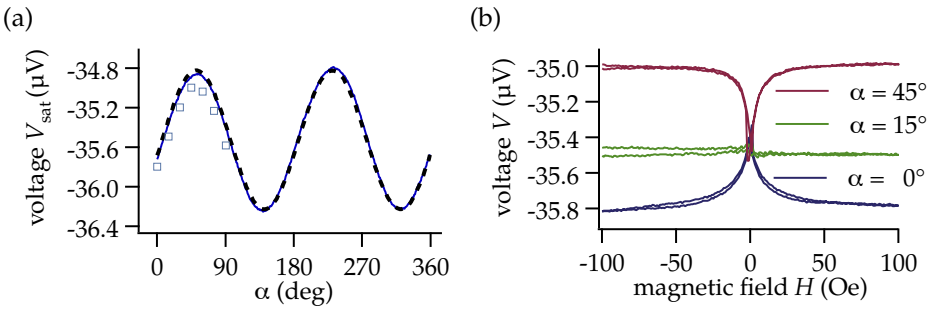

Figure 19: (a) The transverse voltage V_{sat} in saturation as a function of the angle α between the magnetic field $\vec{H}$ and the x-direction where the in-plane temperature gradient ∇T_x is applied for an absolute value $|\vec{H}| = 100\,\mathrm{Oe}$ and a temperature difference $\Delta T = 35\,\mathrm{K}$ (solid line) compared to a fit sine function (dashed line), added to the saturated voltage from Figs. 16 to 18 (squares). (b) The voltage V as a function of H for different angles α and $\Delta T = 35\,\mathrm{K}$.

behaviour is different for angles below and above 15°.

All measurements in Fig. 16 - Fig. 18 are symmetric with respect to the external magnetic field H. Therefore, we can exclude the TSSE which shows an antisymmetric behaviour with respect to H. There was no reproducible difference between the saturated voltages for positive and negative magnetic fields inside the experimental sensitivity limit which could lead to a TSSE contribution. There is not even an unintended ANE due to parasitic out-of-plane temperature gradients. Therefore, we can assume that we have created a completely in-plane temperature gradient ∇T_x without any out-of-plane components ∇T_z. The results shown in Fig. 16 - Fig. 18 can be perfectly explained by the PNE. Here, the absolute voltage depends on the angle φ between the magnetization vector $\vec{M}$ and the temperature gradient in the film plane ∇T_x. The field rotation measurement in Fig. 19 (a) already verifies the $\sin(\varphi)\cos(\varphi)$ characteristic of the PNE (Eq. 17). Here, it can be assumed that the magnetization vector $\vec{M}$ of the Py film is completely saturated and aligned parallel to the magnetic field vector $\vec{H}$ with an absolute value of 100 Oe. For this reason the angle α is comparable to the angle φ. A twofold sin curve reflects the symmetry of the observed effect. When α is fixed we can also achieve a voltage signal symmetric with respect to H. When H is large enough we can find the same voltage we obtain in the field rotation measurement for a certain α ($\approx \varphi$). When the absolute value of H is decreased $\vec{M}$ rotates in the film plane and both φ and V vary. For $\alpha = 15°$ (Fig. 16 (b)) we can observe no considerable variation in the voltage signal compared to other angles α. We can assume that we found the magnetic easy axis of a uniaxial magnetic anisotropy (UMA) along this direction. For any value of H the magnetization vector $\vec{M}$ of the Py film is aligned along this direction and the angle φ does not change. Due to the symmetry we obtain the same voltage signal for $\alpha = 195°$. Now we understand how φ and V change for $\alpha \neq 15°$. The magnetization $\vec{M}$ is aligned parallel to the magnetic field vector $\vec{H}$ for sufficiently large field values. When the absolute value of H decreases the magnetization vector $\vec{M}$ rotates into the magnetic easy axis. It depends on the direction of H (and therefore on the angle α) whether the angle between $\vec{M}$ and ∇T_x (i.e. φ) decreases or increases when the magnetic field H is decreasing. This leads to the appearance of either voltage maxima or minima during a magnetic field sweep. For angles α larger than 45° we observe both maxima and minima. Here, the magnetization vector $\vec{M}$

crosses $\varphi = 45°$ where the voltage signal V reaches its maximum.

However, in the $\sin^2(\alpha)$ fit function we achieved a phase shift of $\alpha_0 = -7°$. This can be explained by a tilt of the temperature gradient ∇T_x off the x-direction. In Fig. 20 (b) the exact directions of ∇T, the UMA and the external magnetic field $\vec{H}$ are sketched with respect to the sample orientation. It is possible to calculate the angle φ between ∇T and $\vec{M}$ during the magnetization reversal process for each measurement in Fig. 16 - Fig. 18. We take Eq. 17 for the PNE in the form $V \propto \sin 2\varphi \nabla T$. The voltage can be normalized (V_{norm}) such that the maximum voltage corresponds to the value 1 for $\varphi = 45°$ when $\sin(2 \cdot 45°)$ has its maximum. Furthermore, the saturated value (at $H = \pm 100$ Oe) for $\varphi = \alpha - 7°$ is related to $\sin(2 \cdot (\alpha - 7°))$. In case of $\alpha = 75°$ the saturation value is related to $\sin(2 \cdot (75° - 7°)) \approx 0.7$. Now, we can calculate the angle $\varphi = \frac{1}{2}\arcsin(V_{\text{norm}})$ and plot it against H (Fig. 20 (a)). Regarding the range of the $\frac{1}{2}\arcsin$ function only angles between 0° and 45° can be accessed. For the dashed box in Fig. 20 (a) we can find a multi domain state. In this area the magnetization vector $\vec{M}$ remains in the direction of the UMA. The magnetic moments of individual domains switch step by step. In this area the voltage caused by the PNE acts the same way as though the magnetization vector was still rotating until it reaches $\varphi = 0°$ and

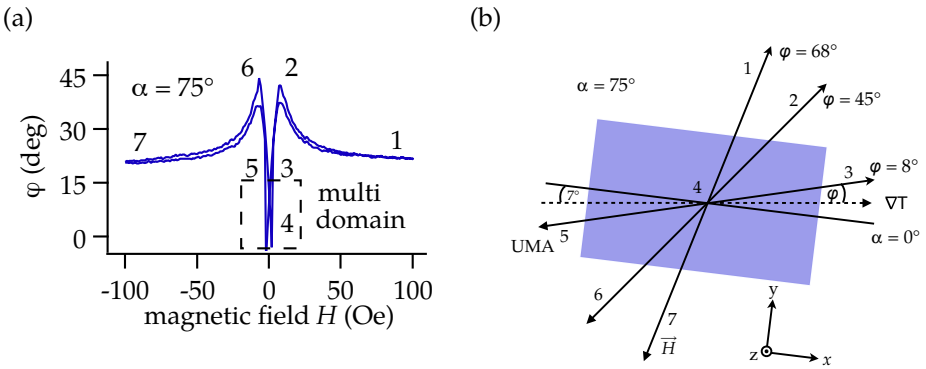

Figure 20: (a) The angle φ of the magnetization $\vec{M}$ with respect to ∇T as a function of the external magnetic field H applied at an angle $\alpha = 75°$ with respect to the x-axis. The calculated range of φ is limited from 0° to 45° due to the $\frac{1}{2}\arcsin$ function we used. In the multi-domain state M decreases without changing φ (dashed box). (b) The reversal process of $\vec{M}$ during the variation of H applied along $\alpha = 75°$. When H decreases $\vec{M}$ rotates coherently from no. 1 via no. 2 into the magnetic easy direction (no. 3). In magnetic remanence (no. 4) the total magnetization is zero due to the multi-domain state. When H increases the mono-domain state is reached (no. 5). After that, $\vec{M}$ rotates coherently via no. 6 to no. 7.

the PNE voltage vanishes. When the magnetic moments of all domains have switched, we leave the multi domain state area and the magnetization vector rotates genuinely with the denoted angle φ. Nevertheless, it is possible to reconstruct the complete magnetization reversal process (cf. Fig. 20 (b)).

We can conclude that we are able to apply a reliable in-plane temperature gradient in this kind of setup which solely produces a PNE in the Py film. The crucial indicator for this conclusion is the measured voltage which is completely symmetric with respect to the external magnetic field H. A missing ANE guarantees that an unintended out-of-plane temperature gradient can be neglected. Therefore, we can also neglect difficulties in the separation of overlapping voltage contributions from different effects. However, when an antisymmetric contribution is missing it can be concluded that there is no TSSE within the experimental sensitivity limit.

[116] K. Uchida et al. Nature **455** (2008) 778

The main differences in measurement technique between Uchida et al.[116] and the one we used for the results presented are contacting the Pt strip with a micro probing system and the ambient conditions. Uchida et al.[116] used a micro probing system with thin tungsten tips (W tips) instead of bonding wires. Next we would like to check if there are any differences in the measurements when we also use W tips in a micro probing system to contact the Pt. In addition, this is performed under ambient conditions.

W tips with a general diameter of 500 µm and a contact area of about 10 µm in diameter were used to contact the ends of the Pt strip. The measurements presented in what follows were performed under ambient conditions. The sample was again clamped between two copper blocks with copper plates on top to apply carefully a completely in-plane temperature gradient and

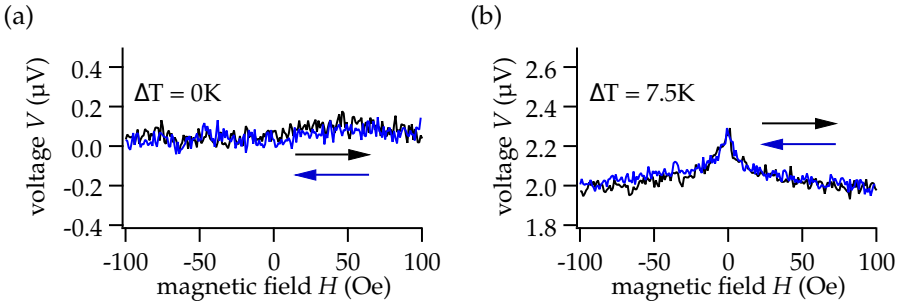

Figure 21: Transverse voltage V as a function of the external magnetic field H for different in-plane temperature gradients. (a) for $\Delta T = 0\,\mathrm{K}$, (b) for $\Delta T = 7.5\,\mathrm{K}$.

neglect out-of-plane components. One block was heated with a resistive Joule heater, the other one could be kept at room temperature by an air cooling system through the block to use it as a heat sink. The temperatures were measured on both blocks with K-type thermocouples, simultaneously. In Fig. 21 and Fig. 22 you can see the results for different in-plane temperature gradients. A temperature difference of $\Delta T = 0\,\mathrm{K}$ in Fig. 21 (a) shows no significant effect considering the experimental accuracy which is noisier than the results we obtained in vacuum with a bonding wire contacting. By applying various temperature differences, you can achieve a series of completely symmetric voltage curves. The voltage can be compared to the measurement in Fig. 16 (a) obtained with the same fixed angle $\alpha = 0°$. The different properties are the offset voltage V_{off} at 0 Oe and the magnitude V_{diff} of the effect (the difference between the saturated voltage V_{sat} and the maximum voltage around 0 Oe). V_{diff} is proportional to the temperature difference ΔT between the copper blocks which is shown in Fig. 23. These measurements are also consistent with the PNE we already observed in the vacuum setup with a bonding wire contacting. The proportionality of the magnitude with the temperature difference verifies the PNE as well as the symmetry of the voltage as a function of the magnetic field. There is also no evidence of a TSSE as well as an ANE which would result in an antisymmetric contribution. Therefore, we can conclude that our setup with a micro probing system and measurements under ambient conditions is accurate enough to verify the obtained results previously in vacuum with a bonding wiring. Again, a reliable in-plane temperature gradient ∇T_x was applied and there is no evidence for an unintended out-of-plane temperature gradient ∇T_z which would result in an ANE and therefore in an antisymmetric contribution of the voltage.

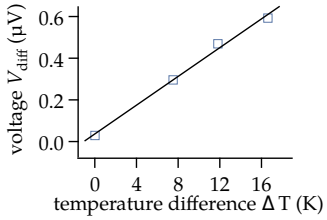

Figure 23: The difference between the saturated voltage at high magnetic fields and the maximum voltage V_{diff} as a function of the temperature difference ΔT between the sample ends.

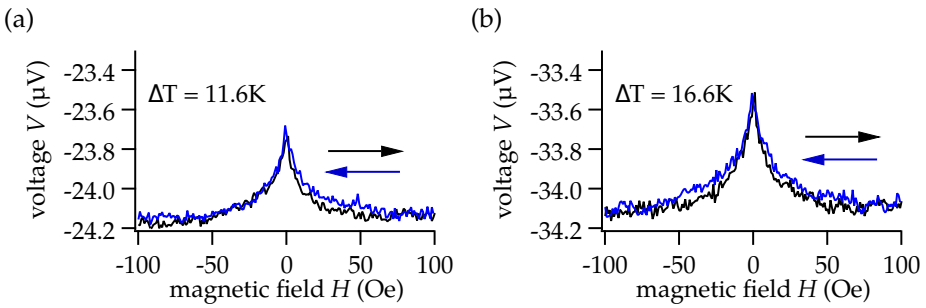

Figure 22: Transverse voltage V as a function of the external magnetic field H for different in-plane temperature gradients. (a) for $\Delta T = 11.6\,\mathrm{K}$, (b) for $\Delta T = 16.6\,\mathrm{K}$.

In several publications for TSSE measurements on Py/Pt films when an antisymmetric contribution of the measured voltage was observed it could be explained by an ANE due to a missing sign change shown by a reversal of the in-plane temperature gradient (cf. Tab. 1).[117] The reported ANE was induced by unintended out-of-plane temperature gradients due to improper sample mounting. In most cases the sample was not clamped between copper block and copper plate but only positioned on top of copper blocks. The substrates are much thicker than the thin films on top and - due to different thermal conductivities of the different layers - there are temperature drops at the interfaces. This can cause an out-of-plane temperature gradient and an ANE arises.

[117] S. Y. Huang et al. Physical Review Letters **107** (2011) 216604; A. Avery et al. Physical Review Letters **109** (2012) 196602; M. Schmid et al. Physical Review Letters **111** (2013) 187201; D. Meier et al. Physical Review B **88** (2013) 184425

Now, we want to investigate what happens when an out-of-plane temperature gradient ∇T_z is intentionally applied (Fig. 24). This way we can study the behaviour of the antisymmetric contribution in the voltage measured. This will also answer the question whether an unintended ∇T_z generates an ANE which can be misinterpreted as a TSSE.

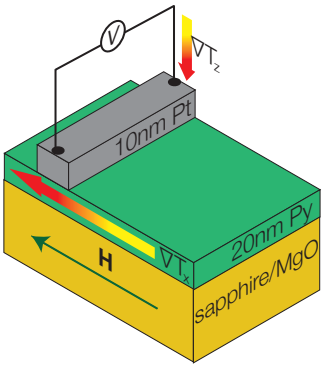

Figure 24: TSSE configuration: Temperature gradient ∇T_x and the external magnetic field H are parallel aligned and applied in the sample plane. The voltage V is measured transversely at the ends of the Pt strip. An out-of-plane temperature ∇T_z can be intentionally induced by the electrical contacts on the Pt strip.

We want to keep a precisely controllable in-plane temperature gradient. Therefore, the sample is still clamped between the copper blocks. For an intentionally applied out-of-plane temperature gradient we use the contact tips on the Pt strip. By using thicker tips and increasing the contact area between tip and Pt strip we obtain a second heat sink for the heat flow in the sample. Both an in-plane heat flow between the copper blocks and an out-of-plane heat flow from the sample into the contact tips are expected. In comparison to thinner contact tips this heat flow should be large enough to generate a measurable ANE in the Py film. In the following experiments, we used Au tips with a general diameter of 1 mm and a contact area of about 0.28 mm² which varied depending on the angle of the tip with respect to the sample plane, the pressure of the contacting and the shape of the sharpened tip. Therefore, the absolute value of the heat flow through the tip was not precisely controllable and could vary for each new contacting of the sample.

In Fig. 25 the voltage V at the ends of the Pt strip is plotted as a function of the external magnetic field H for two different in-plane temperature gradients. In Fig. 25 (a) the temperature difference is $\Delta T = 10\,\mathrm{K}$ and in Fig. 25 (b) we applied $\Delta T = 20\,\mathrm{K}$ between the sample ends. The absolute voltage range is different

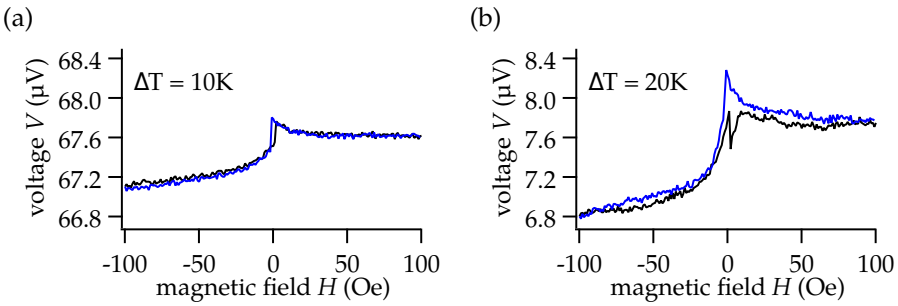

Figure 25: Transverse voltage V as a function of the external magnetic field H for different in-plane temperature gradients ∇T_x in addition to an intentionally induced out-of-plane temperature gradient ∇T_z through the contact tips. (a) For $\Delta T = 10\,\mathrm{K}$, (b) for $\Delta T = 20\,\mathrm{K}$.

for both measurements, but the relative scaling range is equal for a better comparison of the magnitudes. The magnitudes for measurements with an antisymmetric contribution are defined as the voltage in saturation (V_{sat}) minus the offset voltage (V_{off}). Therefore, both saturated voltages in a range between $-100\,\mathrm{Oe}$ to $-90\,\mathrm{Oe}$ (V^{-}_{sat}) and $90\,\mathrm{Oe}$ to $100\,\mathrm{Oe}$ (V^{+}_{sat}) were averaged and $V_{\mathrm{sat}} = (V^{+}_{\mathrm{sat}} - V^{-}_{\mathrm{sat}})/2$ was calculated. The offset voltage was averaged by $V_{\mathrm{off}} = (V^{+}_{\mathrm{sat}} + V^{-}_{\mathrm{sat}})/2$. In Fig. 26 the antisymmetric part (a) and the symmetric part (b) of Fig. 25 were separated mathematically and plotted separately. Each plot contains the curves for $\Delta T = 10\,\mathrm{K}$ and $20\,\mathrm{K}$ together with the reference measurement for $\Delta T = 0\,\mathrm{K}$. The offset voltage V_{off} was removed to compare the curves in the same range. One can see that V_{sat} of the antisymmetric part is proportional to ΔT as well as V_{diff} of the symmetric part. We already defined V_{diff} in the previous section as the difference between the voltage in saturation V_{sat} and the maximum voltage which can be found around $0\,\mathrm{Oe}$. The symmetric part can be

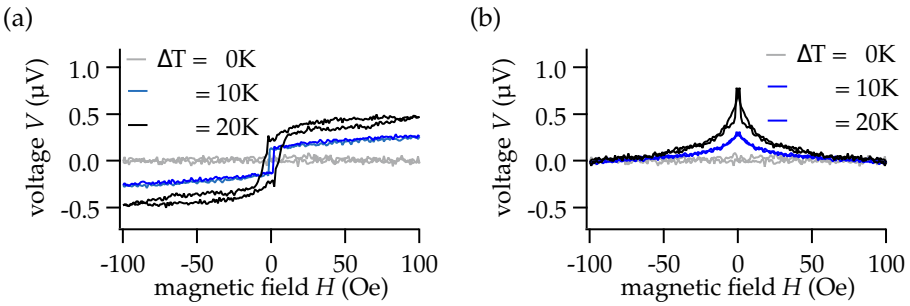

Figure 26: Mathematical separation of the transverse voltage V into an antisymmetric part (a) and a symmetric part (b) as a function of the external magnetic field H for different in-plane temperature gradients ∇T_x.

properly attributed to the PNE driven by the applied in-plane temperature gradient ∇T_x. The antisymmetric part is now an additional contribution caused by using thicker contact tips on the Pt strip. In the previous section we have shown measurements with Au bonding wires on the Pt strip. These measurements were dominated by a symmetric signal and no antisymmetric contribution could be observed. Therefore, we can assume that the antisymmetric part in Fig. 26 (a) is not effected by the tip material used (Au or W), but a result of a second heat sink due to a larger contact area and an unintended out-of-plane temperature gradient ∇T_z as a consequence. For this reason we can attribute the antisymmetric part to the ANE described by Eq. 15.

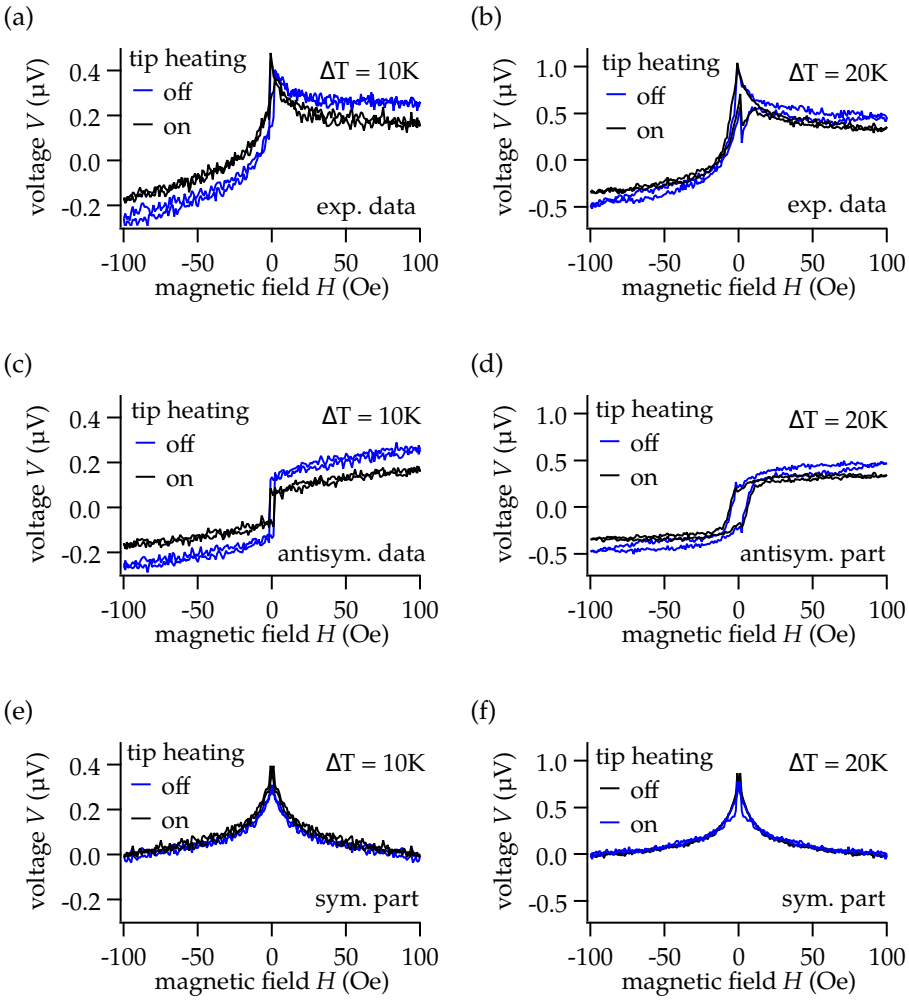

Figure 27: (a),(b) Experimental data of the transverse voltage V as a function of the external magnetic field H for $\Delta T = 10\,\mathrm{K}$ and $\Delta T = 20\,\mathrm{K}$, respectively. V was measured with and without Au tip heating with a power of 0.07 W and 0.15 W, respectively. (c),(d) The antisymmetric part of the experimental data. (e),(f) The symmetric part of the experimental data.

In the next step, we influenced the out-of-plane temperature gradient by heating one of the Au tips with a glued 1.5 kΩ resistor (Fig. 28). This resistor is only thermally connected to the tip and electrically insulated. By voltages up to 35 V heating powers up to 0.8 W can be created.

In Fig. 27 the graphs previously shown (cf. Fig. 26) with in-plane temperature differences $\Delta T = 10\,\mathrm{K}$ and $\Delta T = 20\,\mathrm{K}$ were taken and compared with measurements with the same ΔT combined with a heated Au tip. In the case of $\Delta T = 10\,\mathrm{K}$ it was heated with a power of 0.07 W and for $\Delta T = 20\,\mathrm{K}$ with a power of 0.15 W in order to see an influence. The antisymmetric and the symmetric contributions were also separated mathematically. It becomes obvious that V_{sat} in the antisymmetric part decreases for a heated Au tip. The symmetric part, however, does not show any significant change. Since we did the same external magnetic field reversal measurement we can assume that the Py film went through the same magnetization reversal process. Therefore, we can conclude that the in-plane temperature gradient ∇T_x shows no significant change but the out-of-plane temperature gradient ∇T_z was varied regarding Eq. 15. The curves with tip heating indicate a reduction of V_{sat}. The intentionally produced heat flow from the Au tip counteracts the heat flow produced in the heated Cu block which goes through the sample. The temperature gradient ∇T_z is reduced and the ANE is depressed. The PNE instead is not significantly influenced, which means that the temperature gradient ∇T_x is not significantly dominated by the tip heating.

Now, we will confirm the direction of the heat flow by eliminating the in-plane temperature gradient and set $\Delta T_x = 0\,\mathrm{K}$, but keep on the tip heating with a power of 0.07 W. Fig. 29 again shows the measured voltage V as a function of the external magnetic field H. In Fig. 29 (a) one can see the voltage signal measured. In Fig. 29 (b) the voltage is plotted in the absence of V_{off}. The value achieved for V_{sat} shows the opposite sign to V_{sat} in Fig. 27. This can be attributed to the fact that the out-of-plane heat flow component generated by the heated sample from the in-plane temperature gradient is cancelled. The out-of-plane heat flow is only produced by the heated tip. Therefore, the effective out-of-plane temperature gradient shows a reversal compared to the initial situation. The change of sign in the ANE driven voltage due to a reversal of the out-of-plane temperature gradient can be misinterpreted as the expected change of sign in the ISHE voltage of the TSSE which is expected as a result of a reversal of the in-plane temperature gradient. In all realized experiments no

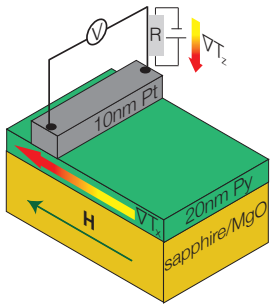

Figure 28: TSSE configuration with tip heating: Temperature gradient ∇T_x and the external magnetic field H are parallel aligned and applied in the sample plane. The voltage V is measured transversely at the ends of the Pt strip. An out-of-plane temperature ∇T_z can be intentionally induced by an attached resistor R at the electrical contacts on the Pt strip.

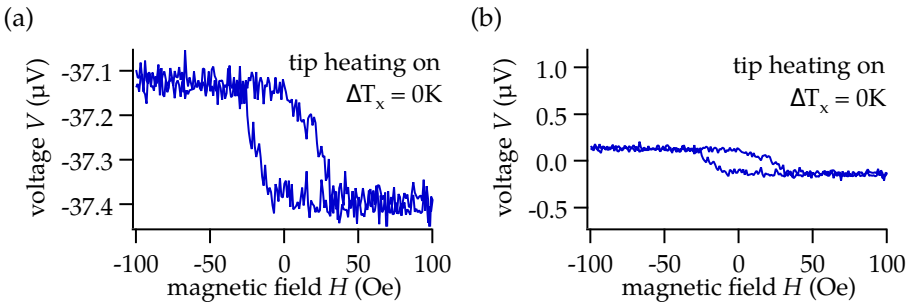

Figure 29: (a),(b) Experimental data of the transverse voltage V as a function of the external magnetic field H with no in-plane temperature gradient ∇T_x but with a heated Au tip to produce an out-of-plane temperature gradient ∇T_z. (a) Experimental data with offset, (b) the same measurement without offset voltage (centered around 0 μV) plotted at a larger scale for better comparison to the previous data.

change of sign could be observed by moving the Pt strip from the hot to the cold sample end. Furthermore, when an unintended out-of-plane temperature gradient ∇T_z appears with a different sign from one sample end to the other, an unintended ANE with different sign could appear which would be misinterpreted as a TSSE. This fact shows that utmost care is required by realizing this kind of experiment.

Discussion

In all measurements we induced a solely in-plane temperature gradient by clamping the samples between two copper plates on each side. Furthermore, we achieved a pure PNE when thin W tips or thin Au bonding wires were used. There was no significant and consistent difference between the saturated voltages for positive and negative magnetic field which would produce a measurable ANE signal. This would even be expected for small out-of-plane temperature gradients. This unintended out-of-plane contribution could only be obtained by using thicker needles with a larger contact area to get a second heat sink for the heat produced on the hot side of the sample. Then a measurable antisymmetric contribution was achieved with respect to the magnetic field. The antisymmetric voltage contribution can be attributed to the ANE considering that this contribution could not be observed by using thinner Au bonding wires. However, this effect was obtained at the ends of a Pt strip on top of the Py film when a possible TSSE can be detected. Huang et al.[118] have only investigated Py films without Pt or with a complete Pt film on

[118] S. Y. Huang et al. Physical Review Letters **107** (2011) 216604

top. The latter would short-circuit the complete sample. Jaworski et al.[119] reported to suppress this effect when they measured the voltage on the Pt strip instead of Pt point contacts on GaMnAs. We could not observe a complete suppression of the ANE signal by using a Pt strip.

Avery et al.[120], in their work, estimated an upper limit for the TSSE which was the experimental error of about 5 nV. In our investigations we can also estimate a possible upper limit for the TSSE. We take the measurement shown in Fig. 16 (a) obtained with a temperature difference of $\Delta T = 35\,\mathrm{K}$ where the noise was among the samllest we obtained. We can estimate a difference in the saturated voltage for positive and negative magnetic fields. A difference of about 30 nV can be obtained. Nevertheless, the sign of this difference was not consistent when several measurements with the same parameters were compared. No significance was found in this difference. Moreover, Uchida et al.[121] reported an ISHE voltage per Kelvin of temperature difference measured on a 4 mm long Pt strip of about $2.6 \times 10^{-7}\,\mathrm{V\,K^{-1}}$. For a TSSE contribution of about 30 nV we would obtain a value of about $0.008\,57 \times 10^{-7}\,\mathrm{V\,K^{-1}}$ on a 5 mm long Pt strip with the same width and thickness of 100 µm and 10 nm, respectively. The temperature gradient was applied over the same length of 10 mm and the Py thickness was also the same of about 20 nm.

The work of Schmid et al.[122] reveals an upper limit of about 20 nV for the TSSE in Py/Pt samples which is inside their experimental error. This corresponds to a value of $0.008 \times 10^{-7}\,\mathrm{V\,K^{-1}}$ when a temperature difference of $\Delta T = 25\,\mathrm{K}$ is applied between the sample ends. The samples used where identical to the samples presented in this work.

Wang et al.[123] managed to present the same contributions of PNE and ANE compared to our results in Py/Pt films. It can be assumed that their unintended out-of-plane temperature gradient was caused by mounting the sample on copper blocks without clamping, large areas of electrical contacts which were not further described except for the use of silver paste for the Cu wires, and radiation into the atmosphere. The attempt to separate the antisymmetric voltage into an ANE and a possible SSE contribution cannot exclude any experimental error by comparing different samples or the existence of the LSSE instead of the TSSE. Our measurements show the enormous effect of the measurement conditions which can influence the voltage signal by adding unintended side effects.

[119] C. M. Jaworski et al. Nature Materials **9** (2010) 898

[120] A. Avery et al. Physical Review Letters **109** (2012) 196602

[121] K. Uchida et al. Journal of Applied Physics **107** (2010) 09A951

[122] M. Schmid et al. Physical Review Letters **111** (2013) 187201

[123] S. H. Wang et al. Physical Review B **88** (2013) 214304

When different Py/Pt samples are compared which are used in TSSE investigations one of the most important properties is the spin-mixing conductance $g^{\uparrow\downarrow}$. A small or even suppressed spin-mixing conductance at the interface can keep the spin current from entering the spin detector material. Then, no ISHE voltage can be measured and the TSSE is not detectable. For the investigated Py/Pt samples in this work both the Py and the Pt were deposited in-situ with no vacuum break. Schmid et al.[124] did spin pumping experiments on identical samples and were able to determine a value of $g^{\uparrow\downarrow} = 2 \times 10^{15}\,\mathrm{m}^{-2}$. This value is four orders of magnitude smaller than theoretically predicted and experimentally confirmed values of about $g^{\uparrow\downarrow} = 2 \times 10^{19}\,\mathrm{m}^{-2}$ reported by other groups.[125] This is, of course, one of the main points of criticism in the argument for a suppressed TSSE. Unfortunately, there are no reported values of the spin-mixing conductance in the first and only reports of the TSSE in Py/Pt samples.

[124] M. Schmid et al. Physical Review Letters **111** (2013) 187201

[125] O. Mosendz et al. Physical Review B **82** (2010) 214403; Q. Zhang et al. Applied Physics Letters **99** (2011) 172105

However, our investigations summarize the appearance of unintended Nernst effects for different contacting methods. We were able to obtain and assign measurements with solely in-plane temperature gradients but with no TSSE in the voltage. After that, we managed to induce an out-of-plane temperature gradient to produce voltage contributions which are antisymmetric with respect to the external magnetic field. These antisymmetric contributions can seem like a TSSE, but we were able to distinguish between a genuine TSSE and an unintended ANE. The antisymmetric contribution was, therefore, attributed to the ANE and a significant TSSE contribution could definitely not be observed.

The ferromagnet Py itself and in combination with an adjacent spin detector like Pt are still very interesting for further investigations in spintronics. These investigations include the generation of spin currents due to spin pumping experiments and the detection of these spin currents due to the ISHE in the Pt. Spin dynamics and of course all related parameters such as spin diffusion length, spin mixing conductances of the interface and spin Hall angles of different spin detector materials can be measured very easily with Py. It turned out that spincaloritronics experiments, especially the generation of pure spin currents driven by heat, are very difficult to perform. However, Py and ferromagnetic conductors in general are not out of the game in spincaloritronics. Further investigations and new techniques for distinguishing between spin currents and spin-dependent charge currents are required.

Spin Seebeck effect in yttrium iron garnet

This chapter deals with the investigation of the spin Seebeck effect on the magnetic insulator yttrium iron garnet ($Y_3Fe_5O_{12}$, YIG). In the beginning we introduce the sample system and give an overview of the main physical properties. Furthermore, the main advantages of this material for spin caloric applications will be illustrated. In the main part of this chapter the experimental results are presented. After that, these results are discussed in terms of the observed effects and their importance for spin caloritronics. We complete this chapter with a short conclusion and an outlook on further applications of magnetic insulators. Most of the results were published in 2015.[126]

[126] D. Meier et al. Nature Communications **6** (2015) 8211

Yttrium Iron Garnet

The magnetic insulator yttrium iron garnet ($Y_3Fe_5O_{12}$, YIG) is a compound of 160 atoms per unit cell with a lattice constant of 1.238 nm. Each unit cell contains 8 formula units of $Y_3Fe_5O_{12}$. It is a network consisting of alternating $Fe^{3+}O_4$-tetrahedrons and $Fe^{3+}O_6$-octahedrons which share common corners. Inside this tetrahedron-octahedron network one can find Y^{3+} ions which form $Y^{2+}O_8$-dodecahedrons. The Y^{3+} ions have no unpaired electrons, which causes in $S = 0$ and $L = 0$ for the total spin and total orbital angular momentum, respectively. They do not contribute to the net magnetization. The Fe^{3+} ions have five unpaired electrons in d orbitals which lead to $S = 5/2$ and $L = 0$. The Fe^{3+} sub lattices are antiparallel aligned due to a super exchange interaction through the oxygen ions. For each formula unit there are two Fe^{3+} on the octahedral sites which contribute with $10\mu_B$ and three Fe^{3+} on the tetrahedral sites which contribute with $15\mu_B$ in the opposite direction. This results in a ferrimagnetic state with $5\mu_B$ at 0 K.[127]

[127] A. Paoletti. Physics of Magnetic Garnets (1978)

Property	Value	Unit	Ref.
Lattice constant a_0	1.238	nm	(a)
Curie temperature T_C	272	°C	(a)
Saturation magnetization	1700	gauss	(a)
Ferrimagnetic resonance line width ΔH	0.2 to 7.0	Oe	(a)
Damping constant	8.58×10^{-5}		(b)
Resistivity	3×10^{11}	Ω cm	(a)

Table 2: Main properties of YIG taken from (a) T. H. Ramsey and (b) H. Chang et al.[128] The damping constant by H. Chang et al. is currently the lowest damping for nanometer thick FM films.

A summary of the most important properties of YIG is presented in Tab. 2 taken from T. H. Ramsey and H. Chang.[128] Due to the large number of atoms in the unit cell YIG has a very large lattice constant of about 1.238 nm. A Curie temperature of about 272 °C assures a stable magnetic state at room temperature. Furthermore, YIG is a very good insulator with a band gap of about 2.7 eV which results in high resistivity.[129]

For deposition processes the substrates typically used are gadolinium gallium garnet ($Gd_3Ga_5O_{12}$, GGG) and yttrium aluminium garnet ($Y_3Al_5O_{12}$, YAG). GGG exhibits the same lattice constant which makes it one of the most popular substrates for YIG fabrication. Unfortunately, one of the disadvantages is that YIG and GGG are almost indistinguishable in x-ray diffraction $\Theta - 2\Theta$ scans, which are often used for characterisation during the fabrication process. Furthermore, GGG shows a large paramagnetic contribution in magnetization measurements. However, one alternative method for evaluating its crystallinity is FMR. YIG has got the lowest magnetic damping factor known up to now with values of about 1×10^{-3} in thin (6 nm to 27 nm) sputtered films[130] and 6.7×10^{-5} in 1.3 µm thick films[129] deposited by liquid phase epitaxy. Thus, YIG films which have grown more crystalline show a smoother FMR peak with a narrow linewidth which is proportional to the damping constant. Instead, YAG substrates are not paramagnetic, but at high temperatures, which are necessary for crystalline film growth, aluminium can diffuse into the YIG. This diffusion can cause two sublayers, YIG and $Y_3Fe_{5-x}Al_xO_{12}$, which can both show an exchange coupling.[131]

Due to extremely low damping and the lack of charge carriers YIG offers a high potential for investigations on magnons, the quanta of spin waves. This field of research is called *magnonics*.[132]

[128] T. H. Ramsey. Journal of the American Ceramic Society **42** (1959) 645; H. Chang et al. IEEE Magnetics Letters **5** (2014) 6700104

[129] Y. Kajiwara et al. Nature **464** (2010) 262

[130] T. Liu et al. Journal of Applied Physics **115** (2014) 17A501

[131] E. Popova et al. The European Physical Journal B **31** (2003) 69

[132] A. A. Serga et al. J. Phys. D: Appl. Phys. **43** (2010) 264002

The utilization of YIG as a waveguide for spin waves with a relatively long propagation distance leads to spin-wave logic devices like magnon transistors[133] which give rise to magnonic based computers.[134]

[133] A. V. Chumak et al. Nature Communications **5** (2014) 4700

[134] B. Leven et al. Physik in unserer Zeit **46** (2015) 34

The first results of YIG films we are presenting were investigated in terms of the SSE in the transverse configuration. Therefore, a temperature gradient ∇T_x was applied in the in-plane direction with a parallel aligned external magnetic field $\vec{H}$ as shown before for Py/Pt. The YIG films we used were mostly fabricated by pulsed laser deposition (PLD) from a stoichiometric polycrystalline target. During the growth process the substrate was heated at a temperature of about 710 °C and for the oxidation an oxygen pressure of about 10 mTorr was fixed. The laser beam had a frequency of 10 Hz and an energy density of 0.8 J cm^{-2}.

Experimental results

TSSE measurements on YIG/Pt

For the TSSE measurements a 180 nm thick YIG film deposited on 5×5 mm^2 GGG (111)-oriented substrates by PLD were used. A 10 nm thin Pt strip was deposited on top by magnetron sputtering through a split mask on one side of the YIG film with a width of 100 µm. The YIG film shows a saturation magnetization of $M_S = 120$ kA m^{-1} and a coercive field of about 100 Oe. Measurements in the TSSE configuration on YIG/Pt were obtained in vacuum and under ambient conditions. For the measurements in vacuum the Pt strip was contacted by Au bonding wires with 25 µm in thickness. Furthermore, for the measurements under ambient conditions the Pt strip was contacted by W and Au tips with different diameters and contact areas. Therefore, a micro probing system was used which was introduced for the investigations on Py/Pt films. It could be shown that both setups have the ability to apply a pure in-plane temperature gradient without any unintended out-of-plane contributions when the sample is clamped and thin tips or needles with a sufficiently small contact area are used for measurements under ambient conditions. First of all, the sample was measured in vacuum to get the best resolution in the voltage measurement as obtained for Py/Pt films when Au bonding wires were used. Therefore, the sample was clamped between two copper blocks to apply the in-plane temperature gradient. No further electrical insulation was needed due to the insultating GGG substrate below as well

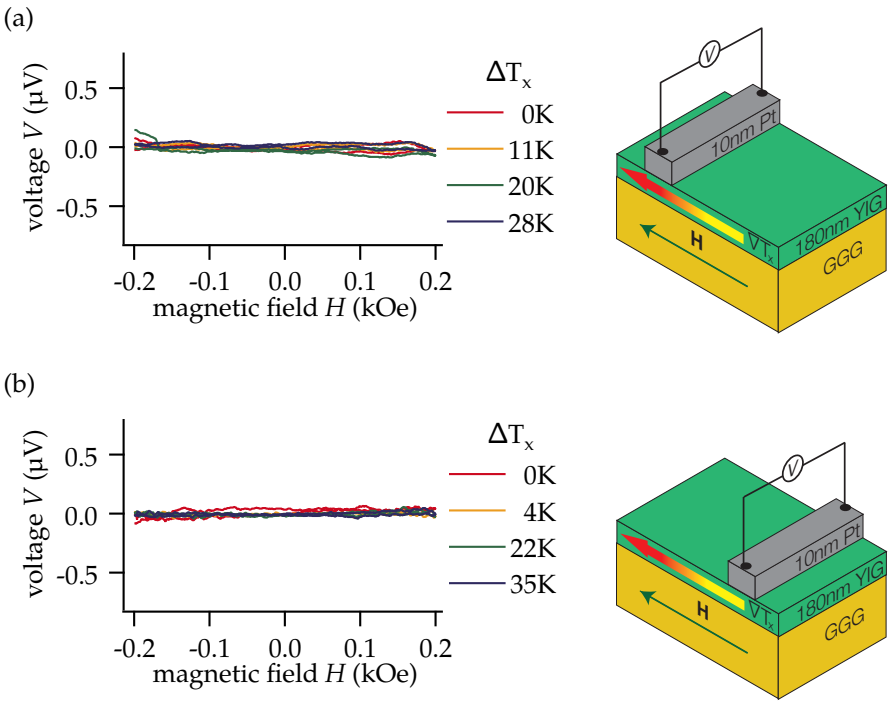

Figure 30: Transverse voltage V as a function of the external magnetic field H measured in vacuum with thin Au bonding wires on the Pt strip (right sketch) for different in-plane temperature gradients ∇T_x. (a) Pt strip on the hot side, (b) Pt strip on the cold side of the sample.

as the insulating YIG film on top of the sample. The Pt strip was placed near the hot sample side which was contacted by the Au bonding wires to measure the transverse voltage as a function of the external magnetic field which was applied parallel to ΔT_x. This measurement was done for various temperature differences including $\Delta T_x = 0\,\mathrm{K}$ (Fig. 30). We could not observe any significant variation in the voltage within the sensitivity limit of about $\pm 20\,\mathrm{nV}$ when the magnetic field was varied. This was obtained for Pt strip on the hot (Fig. 30 (a)) as well as for Pt strip on the cold sample side (Fig. 30 (b)). These results exclude the appearance of all effects listed in Fig. 14 we are considering. In particular, there is no evidence of the TSSE within the sensitivity limit.

In the next step the sample was mounted in the setup for measurements under ambient conditions. Here, the micro probing system was used to contact the Pt strip. At first, the Pt strip was contacted with thin W tips with a contact area of about $A = 0.003\,\mathrm{mm}^2$. Much attention was paid to contact the Pt very carefully to prevent any out-of-plane temperature gradient contributions. This was successful for Pt strip on the hot sample side, which can be seen in Fig. 31 (a). There is no significant effect within a measurement sensitivity limit of about $\pm 40\,\mathrm{nV}$. For each

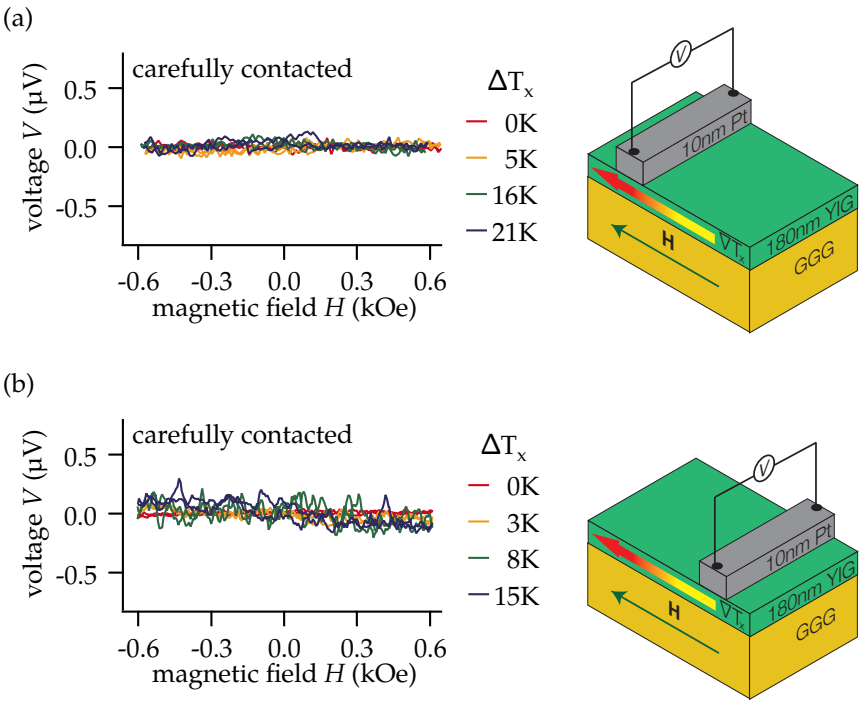

Figure 31: Transverse voltage V as a function of the external magnetic field H measured under ambient conditions with thin W tips on the Pt strip (right sketch) for different in-plane temperature gradients ∇T_x. The W tips were carefully contacted to reduce a large contact area. (a) Pt strip on the hot side, (b) Pt strip on the cold side of the sample.

ΔT_x the standard deviation of the voltage ranges between 25 nV for $\Delta T_x = 0$ K and 40 nV for $\Delta T_x = 21$ K. These values are in the order of the typical signal-to-noise-ratio recorded by using a Keithley 2182A Nanovoltmeter and a micro probing system for sample contacting. It can also be compared to the sensitivity limit we achieved for Py/Pt films.

However, for Pt strip on the cold side (Fig. 31 (b)) we can observe an antisymmetric effect in the voltage V with respect to H for the largest temperature difference ($\Delta T_x = 15$ K). The difference between the saturated values for large positive and negative magnetic fields (V_{sat}) is evidence for one of the antisymmetric effects listed in Fig. 14 for FMI/NM bilayer systems. In YIG no Nernst effects can appear due to the absence of charge carriers. Furthermore, XRMR measurements on YIG/Pt films showed no evidence of magnetic proximity effects and thus no spin polarization of the Pt at the interface.[135] Therefore, we can neglect any Nernst effects evoked by a spin-polarized Pt layer. The only possible effect we can consider from Fig. 14 should be a TSSE generated by the in-plane temperature gradient when we assume that there are no unintended out-of-plane contributions. Never-

[135] F. Della Coletta et al. ESRF annual report, HC-1500, 2014

theless, there is no observable effect for Pt strip on the hot side, especially no effect with a reversed sign. Therefore, we exclude the appearance of the TSSE and attribute the antisymmetric effect to the LSSE produced by an unintended out-of-plane temperature gradient due to careless and stronger contacting.

For proving this assumption we investigated the behaviour of different W and Au tips with different contact areas to manipulate the out-of-plane heat flow. In Fig. 32 measurements are displayed for Pt strip on the hot and the cold sample side which was contacted with W and Au tips with different contact areas A. It can be seen that the antisymmetric effect in the voltage V with respect to the external magnetic field H which was obtained for a large in-plane temperature gradient in Fig. 31 was strongly increased. This was achieved even for the same W tips but with stronger contacting. Furthermore, the effect generally increases when the contact area A increases. This is observed for W as well as Au tips and for Pt strip at the hot and the cold sample side. However, the antisymmetric effect is larger for Pt strip on the hot side compared to Pt strip at the cold side when the same tips are used. Nevertheless, the sign of V_{sat} is the same for both sample sides. $V_{\mathrm{sat}} = (V^{+}_{\mathrm{sat}} - V^{-}_{\mathrm{sat}})/2$ was already defined for previously shown measurements on Py. For YIG the region for the determi-

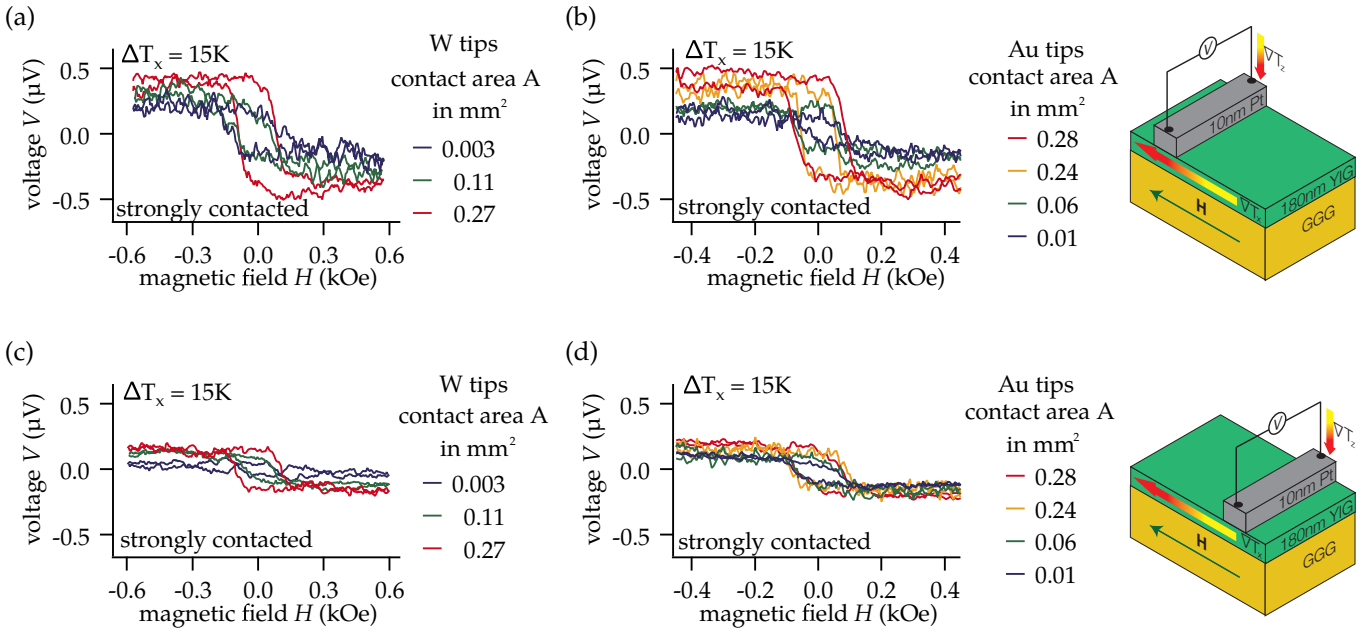

Figure 32: Transverse voltage V as a function of the external magnetic field H measured under ambient conditions on the Pt strip (right sketch) with W and Au tips of different diameters and different contact areas A for $\Delta T_x = 15\,\mathrm{K}$. The W and Au tips were strongly contacted to produce a large contact area. Pt strip on the hot side contacted with W tips (a) and Au tips (b), Pt strip on the cold side contacted with W tips (c) and Au tips (d).

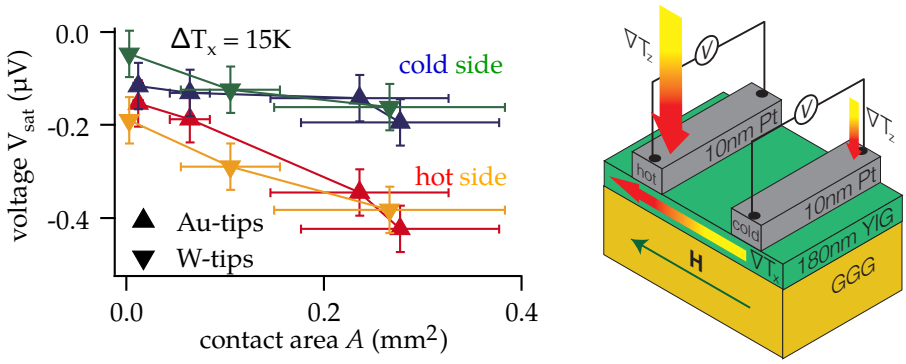

Figure 33: The ISHE voltage magnitude V_{sat} as a function of the heated Au tip temperature T_{needle} for different in-plane temperature gradients ∇T_x and Pt strip on the hot and the cold side of the sample.

nation of V_{sat} was extended between $500\,\text{Oe} < H < 600\,\text{Oe}$ and $-600\,\text{Oe} < H < -500\,\text{Oe}$ for V_{sat}^{+} and V_{sat}^{-}, respectively. Therefore, we can again exclude the TSSE and find further evidence of the previously mentioned assumption of a generated LSSE driven by an out-of-plane temperature gradient induced by heat flow through contact tips with a large contact area.

In Fig. 33 the voltage in saturation taken from all curves in Fig. 32 are plotted as a function of the contact area A for the W and Au tips. Due to the fact that the real attached contact area could not be reproduced sufficiently we estimated the average between the possible maximum contact area and a sufficiently low area. This leads to relatively large error bars. However, for Pt strip on the hot and the cold side the sign of V_{sat} is the same. Furthermore, the absolute value of V_{sat} decreases for smaller contact areas of the tips used for both materials (W and Au). It is obvious that the temperature difference between the sample and the contact tips is responsible for the magnitude of V_{sat} which is larger on the hot compared to the cold sample side as well as the size of the contact area which causes a considerable heat sink for an out-of-plane heat flow.

For further investigation of the out-of-plane temperature gradient we tried to intentionally control the out-of-plane heat flow. Therefore, we used the thickest Au tips with $A = 0.28\,\text{mm}^2$ and the glued resistor for heating one tip. Measurements with Pt strip on the hot and cold side of the YIG film were performed as well as measurements with various in-plane temperature gradients and various out-of-plane temperature gradients with intentional heating of the Au tips. The results of these measurements are presented in Fig. 34 (a) to 34 (d) and Fig. 36 (a) to 36 (d).

The voltage again shows antisymmetric behaviour with respect to the external magnetic field which could not be attributed to the TSSE. The most adequate test to prove this fact is again to change the in-plane temperature gradient direction which is equal to changing the Pt strip from hot to cold. In Fig. 34 (a) to 34 (d) the red curves indicate when thick Au tips are used without any heating. Each curve shows a hysteretical behaviour with a magnitude V_{sat} with the same sign. In Fig. 34 (a) the effect nearly vanishes but a clear sign of the magnitude can be determined ($\Delta T_x = 10\,\mathrm{K}$). The magnitude increases with larger temperature differences to $\Delta T_x = 30\,\mathrm{K}$ (Fig. 34 (b)). On the hot side even a temperature difference of $\Delta T_x = 5\,\mathrm{K}$ is large enough to generate a distinct magnitude (Fig. 34 (c)). This magnitude increases remarkably for $\Delta T_x = 10\,\mathrm{K}$ (Fig. 34 (d)).

Now, we can intentionally influence this out-of-plane heat flow by heating one Au tip. This heating was done for all previously used in-plane temperature gradients with the Pt strip on both sample sides. The temperature of the Au tip is denoted in terms of the room temperature RT = 296 K added by a value x for a particular amount of heating. The temperature of the tip was obtained in a reference measurement achieved with a thermocouple on the Au tip. In Fig. 35 this temperature T_{needle} is shown as a func-

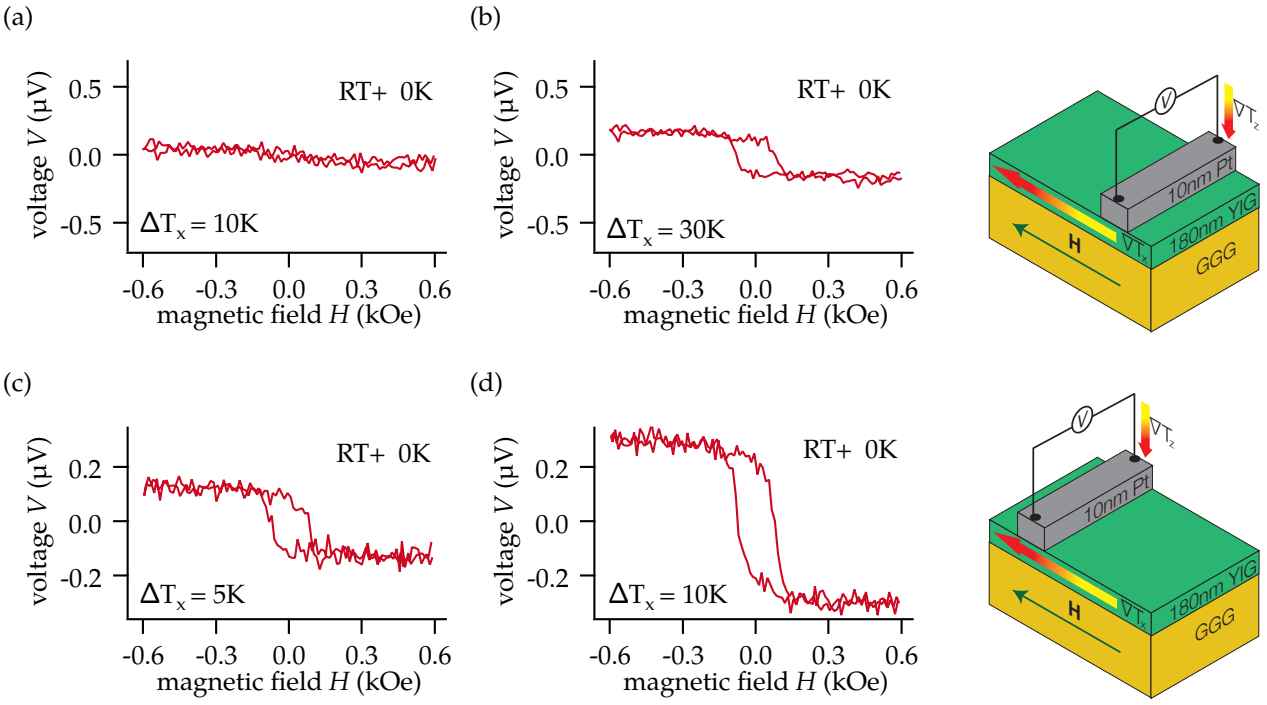

Figure 34: Transverse voltage V as a function of the external magnetic field H measured with Au tips on the cold side with $\Delta T_x = 10\,\mathrm{K}$ (a) and 30 K (b). Measurements with Au tips on the hot side with $\Delta T_x = 5\,\mathrm{K}$ (c) and 10 K (d).

tion of the applied resistor power P_{needle}. An almost proportional behaviour can be observed regarding heat loss over the whole needle into the environment, which explains a deviation of the data for larger heating powers from the linear fit function. If we now increase the heating power P_{needle} of the Au tip for a certain in-plane temperature gradient ΔT_x, we can observe a decreasing magnitude which results in a change of sign and an increasing magnitude in the opposite direction. A generic measurement for this behaviour is shown in Fig. 36 (c). We start with a measurement without heating the Au tip (RT + 0 K). When we heat the tip slightly the magnitude decreases (RT + 3 K) and changes its sign when the heating power increases (RT + 17 K). This can be further increased by a larger Au tip temperature (RT + 31 K). When we estimate V_{sat} for all measurements in Fig. 36 it can be plotted against the Au tip temperature T_{needle} (Fig. 37). For each in-plane temperature gradient the sign of V_{sat} is the same when the Au tip is not heated (cf. Fig. 37 at RT). Furthermore, the sign is the same for Pt strip located on the hot side as well as on the cold side of the YIG. The value of V_{sat} increases with T_{needle} in all cases but with different slopes. The slope is larger for Pt strip located on the cold side. Here, the out-of-plane heat flow due to the heated sample is much smaller on the cold side compared to

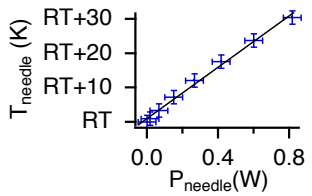

Figure 35: Au tip temperature T_{needle} for different heating powers P_{text} at a glued resistor.

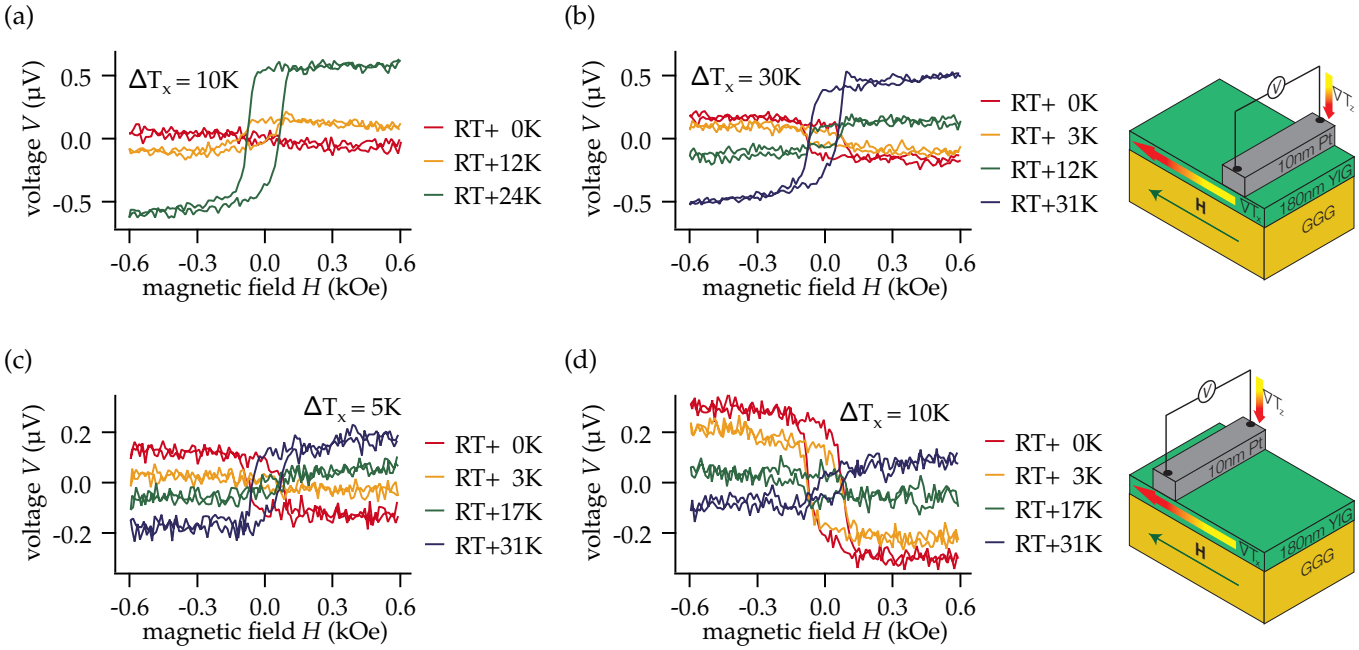

Figure 36: Transverse voltage V as a function of the external magnetic field H measured with Au tips on the cold side with ΔT_x = 10 K (a) and 30 K (b). Measurements with Au tips on the hot side with ΔT_x = 5 K (c) and 10 K (d). For each ΔT_x one Au tip on the Pt strip was heated to a temperature T_{needle} = RT + xK.

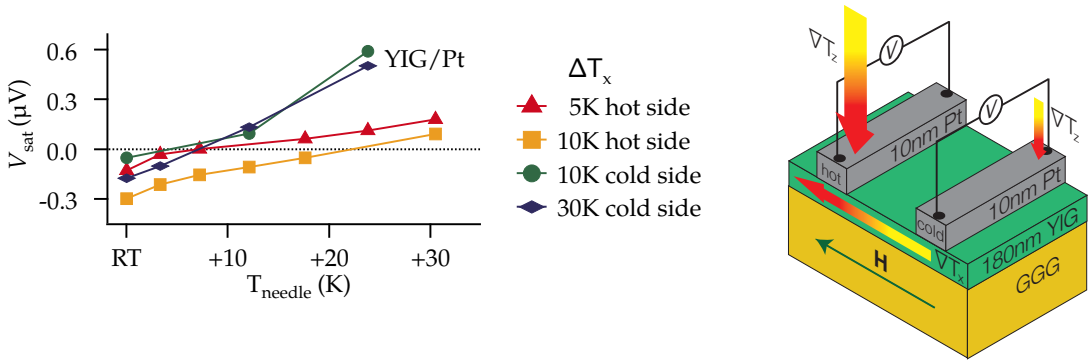

Figure 37: The ISHE voltage magnitude V_{sat} as a function of the heated Au tip temperature T_{needle} for different in-plane temperature gradients ∇T_x and Pt strips on the hot and the cold side of the sample.

the hot side. It is easier for the heated Au tip to counteract this heat flow. This results in a faster increase of V_{sat}. For all ΔT_x and Pt strips on the cold side and on the hot side there is a needle temperature T_{needle} where V_{sat} vanishes completely. Here, the heat flow generated by the heated needle and the heat flow due to the heated sample must be the same with the opposite sign. The different slopes lead to the location for this crossing point on the zero line of V_{sat}. For larger ΔT_x this point is found at larger needle temperatures.

LSSE measurements on YIG/Pt

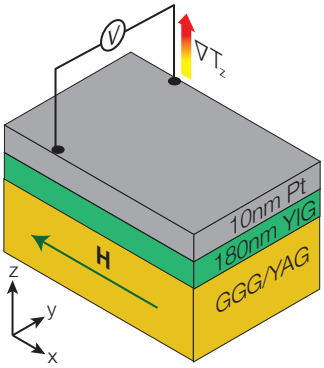

Figure 38: Bilayer stack of the investigated samples: Pt as a spin detector material on top of the YIG deposited on a GGG or YAG substrate.

For LSSE measurements it is not necessary to have structured samples like Pt strips or Hall bars. Therefore, the investigated samples mostly consisted of a bilayer of a thin YIG film and an ultra-thin film of a normal metal as the spin detector. Here, this normal metal was usually Pt due to the high spin orbit coupling which is preserved for many established deposition techniques. For fundamental investigations of the LSSE behaviour the sample was simply clamped between two copper blocks from the top and the bottom side of the film plane to generate an out-of plane temperature gradient ∇T_z. The YIG films in this part were grown on insulating GGG as well as YAG substrates, but on top a piece of sapphire substrate was used for electrical insulation between the Pt and the upper copper block. The upper side was not completely covered to allow enough space for electrical contacting of the Pt on the edges of the bilayer film. An external magnetic field was applied perpendicularly to both, ∇T_z and the direction of the electric field which was measured between the electrical contacts (y-direction). Therefore, H was applied along the x-

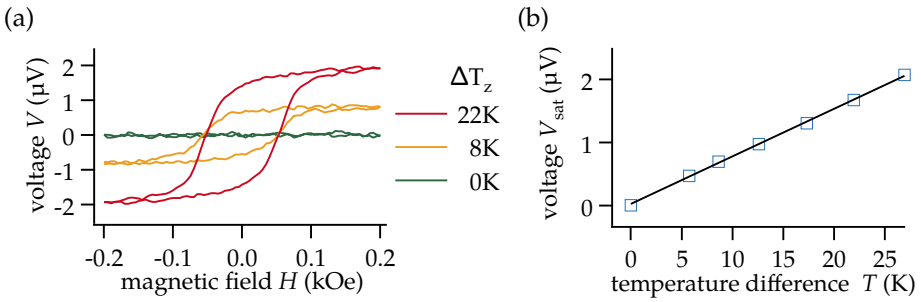

Figure 39: LSSE measurement on YIG/Pt: The ISHE voltage was measured at the ends of the Pt strip for various out-of-plane temperature gradients ∇T_z (a). (b) The proportionality of the voltage in saturation V_{sat} as a function of the temperature difference ΔT_z between the copper blocks.

direction (Fig. 38). All LSSE measurements on YIG/Pt were done in vacuum.

Next we measured the LSSE directly on the YIG/Pt sample which we used for measurements in the TSSE configuration in the previous section. The two layers had a thickness of 180 nm and 10 nm for the YIG and Pt, respectively. The sample was clamped between two copper blocks with a 0.5 mm thick sapphire substrate on top of the sample. The copper block on top acted as a heat source while the copper block at the bottom was the heat sink. The temperature difference was measured between the copper blocks with two K-type thermocouples. The external magnetic field could be applied and rotated in the film plane up to 10 kOe.

In Fig. 39 (a) LSSE measurements for three exemplarily chosen out-of-plane temperature gradients are shown. The voltage V measured at the ends of the Pt strip is plotted as a function of the external magnetic field H which fulfills the cross product of Eq. 24 for a detected LSSE due to the ISHE. For large external magnetic fields the spin polarization vector $\vec{\sigma}$ of the YIG is perpendicular to the electrical contacts, and the thermally driven spin current $\vec{j}$ is parallel to the temperature gradient ∇T_z (Fig. 38). The reversal of $\vec{\sigma}$ accompanied by the reversal of H leads to the sign change of V. The voltage in saturation V_{sat} is shown in Fig. 39 (b) for various out-of-plane temperature differences ΔT_z. It clearly shows the proportionality as assumed for the LSSE. These results support our observations of the LSSE due to unintended out-of-plane temperature gradients in the TSSE configuration on the same sample which was presented in the previous section. In the next step another YIG film with a thickness of 130 nm deposited by PLD with two 8 nm thick Pt strips on top was measured (Fig. 40). The

voltage V is shown as a function of the external magnetic field H for various angles α between H and the x-direction. The saturated voltage in Fig. 40 vanishes for $\alpha = 90°$ when $\vec{H}$ is aligned parallel to the electrical contacts viz. along the Pt strip. This is consistent with the ISHE where the voltage should vanish when $\vec{M}$ accompanied by the spin direction of the thermally driven spin current is aligned parallel to the electrical contacts.

Apart from the expected LSSE which is indicated in the voltage in saturation there are maxima and minima around $H = 0$ Oe. One possible explanation for the appearance of these maxima and minima is a movement of the magnetization vector into a magnetic easy axis due to a magnetic anisotropy in the film plane of the YIG. The electrical contacts are sensitive to measure a large ISHE voltage when the magnetization vector is close to 0° with respect to the x-direction. The observed voltage is larger around $H = 0$ Oe when the magnetization rotates into the easy axis. This happens when the magnetic easy axis is closer to the x-direction than the magnetic field direction. Here, the magnetization vector $\vec{M}$ made a complete rotation of 360° (antisymmetric reversal process). $\vec{M}$ crosses the magnetic easy axis twice but in opposite directions. Three of the curves are magnified in a smaller voltage range in Fig. 40 (b) to make their switching behaviour more visible. The switching behaviour between different angles α cannot be compared in exact detail because the maxima and minima can differ depending on the step size of the magnetic field.

In the next step we investigated a 4 µm YIG film grown on a 6×2 mm² GGG substrate with 0.5 mm in thickness with a 10 nm thin Pt film on top. In Fig. 41 (a) - (f) the voltage between the two electrical contacts on the Pt film along the y-direction is

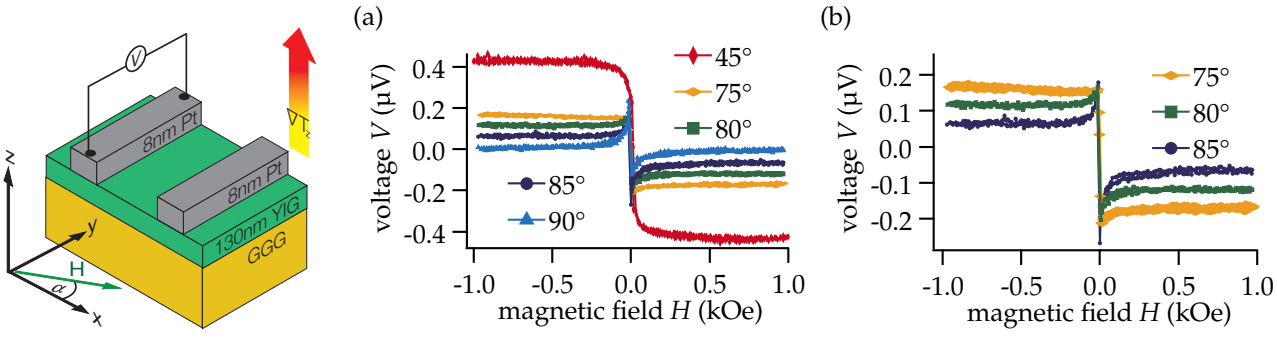

Figure 40: LSSE measurement on YIG/Pt: The ISHE voltage was measured at the ends of one of the Pt strips for various angles α of the external magnetic field H with respect to the x-direction. The out-of-plane temperature difference ΔT_z between the copper blocks was fixed at 14 K.

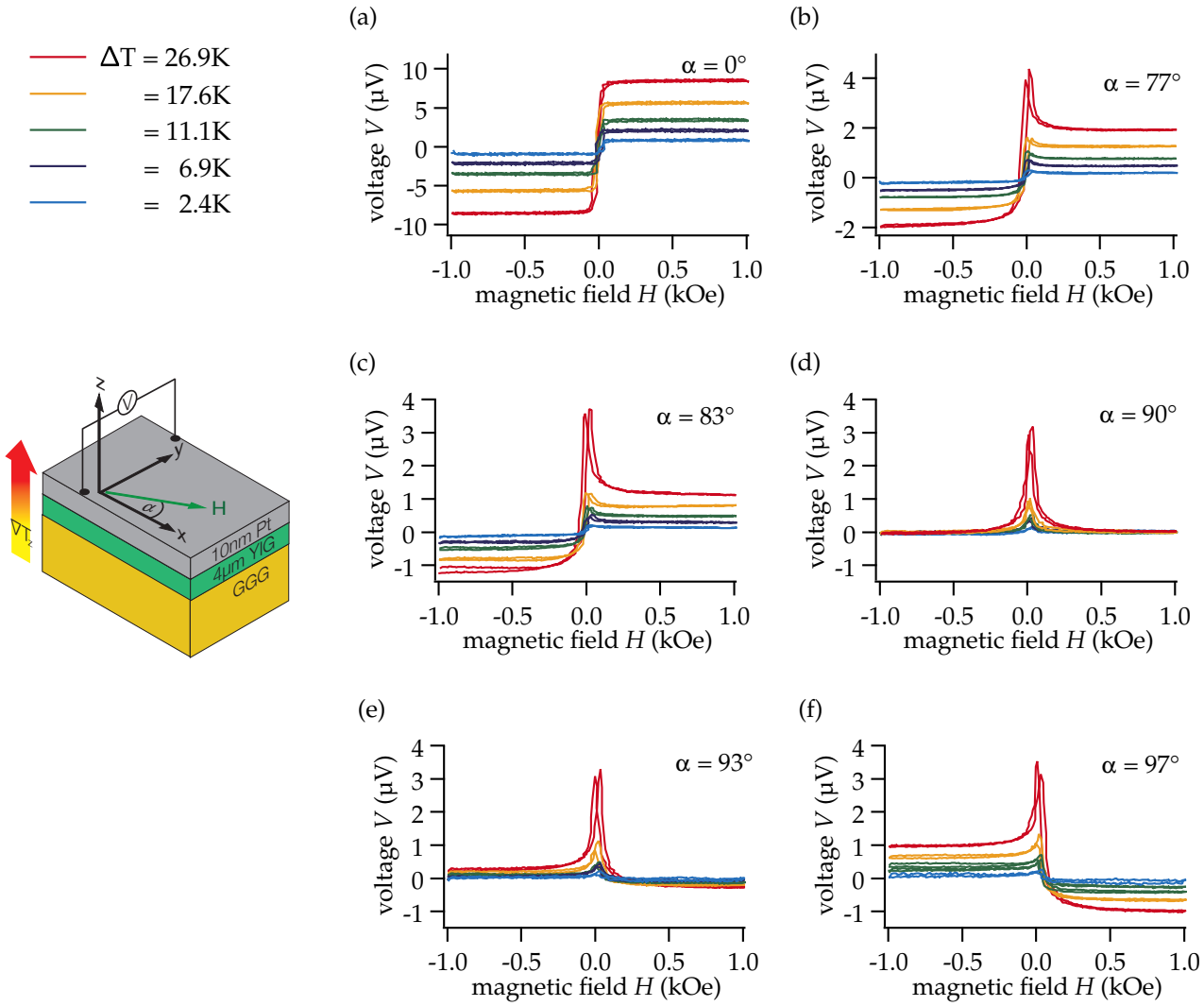

Figure 41: LSSE measurement on YIG/Pt: The ISHE voltage was measured at the ends of the Pt film for various angles α of the external magnetic field H with respect to the x-direction. The out-of-plane temperature gradient was varied with the result that ΔT_z between the copper blocks was increased.

shown as a function of the external magnetic field H applied in the film plane with an angle α with respect to the x-direction for various temperature differences ΔT_z. In Fig. 41 (a) one can see the hysteretical behaviour of the voltage V, antisymmetric with respect to H. V_{sat} is clearly proportional to the temperature difference between the copper blocks (Fig. 42). When we change the angle α of the external magnetic field H with respect to the x-direction the saturated voltage V_{sat} decreases until $\alpha = 90°$ where the ISHE voltage (V_{sat}) vanishes completely (Fig. 41 (d)). The entire angle dependency of the ISHE voltage can be seen in Fig. 43. The data were obtained with an absolute value of 1 kOe for H and a temperature difference of $\Delta T_z = 26.9$ K. We get a cos function as expected from the ISHE (Eq. 24).

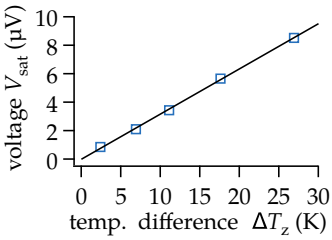

Figure 42: Proportionality of the ISHE voltage with the temperature difference ΔT_z.

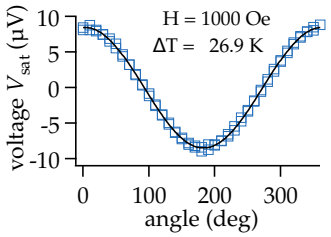

Figure 43: Angle dependency of the ISHE voltage V_{sat} with the angle α between the x-axis and the magnetic field direction $\vec{H}$.

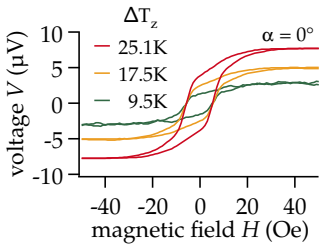

Figure 44: LSSE measurements in a smaller magnetic field range with the angle α = 0° between the x-axis and the magnetic field direction $\vec{H}$.

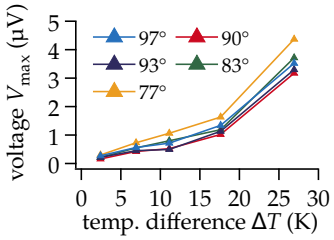

Figure 45: The magnitude V_{max} of the peaks (maximum value) for different angles α as a function of the temperature difference ΔT_z.

[136] J. Xiao et al. Physical Review B **81** (2010) 214418

[137] M. Schreier et al. Physical Review B **88** (2013) 094410

[138] J. Flipse et al. Nature Nanotechnology **7** (2012) 166

Additional LSSE measurements are shown in Fig.44 in a smaller magnetic field range for three different in-plane temperature gradients for $\alpha = 0°$. The switching of V with the magnetic field H can be clearly observed. We can estimate a coercive field H_C of the YIG film of about 5 Oe.

Furthermore, for angles $\alpha \neq 0°$ we can find two maxima around $H = 0$ Oe. The magnitudes of these peaks were estimated from the symmetric part of the curves. They are the difference between the peak value and the value in saturation. These maxima grow when ΔT_z increases (Fig. 45). The increase is not proportional with ΔT_z but similar for all α. This effect cannot be related to the PNE because YIG is an insulator and Pt shows no spin polarization. However, there is one condition under which symmetric behaviour occurs. The magnetization vector has to rotate symmetrically during the reversal process. This means that it only rotates back and forth on one side of the film plane (0° - 180°) instead of doing a complete rotation (0° - 360°), which is the case for the YIG/Pt sample with the much thinner YIG film presented in Fig. 40.

Discussion

First, we would like to discuss the measurements in terms of the TSSE. In YIG/Pt bilayers the driving force for a thermally activated spin current is the difference between the magnon temperature T_m in the YIG and the electron temperature T_e in the Pt. Xiao et al.[136] discussed the temperature difference ΔT_{me} of the origin of the thermally induced spin current in the same year when the TSSE was firstly observed in YIG/Pt bilayers. We want to determine this temperature difference to estimate a possible TSSE contribution. ΔT_{me} can be inferred from the recorded voltage as[137]

$$\Delta T_{me} = \frac{V_{sat}\,\pi\,M_S\,V_a\,t_{Pt}}{g_r\,\gamma\,k_B\,e\,\Theta_{SH}\,\rho_{Pt}\,l_{Pt}\,\lambda\,\tanh(t/2\lambda)}. \qquad (32)$$

Here, V_a is the magnetic coherence volume, g_r is the real part of the spin mixing conductance, γ is the gyromagnetic ratio, k_B is the Boltzmann constant, e is the elementary charge, Θ_{SH} is the spin Hall angle, and λ is the spin diffusion length of the NM material. The two temperature model has proved successful in relating ΔT_{me} to the phonon temperature, accessible in experiments (Schreier Schreier et al.[137] and Flipse et al.[138]). We simulate the phonon and magnon temperatures assuming 1D transport in our films and disregard the influence of thermal contact resistance

Fig. at RT	exp. ΔT_x (K)	exp. $\lvert V_{sat}\rvert$ (nV)	calc. $\lvert\Delta T_{me}\rvert$ (μK)	calc. $\lvert\Delta T_z\rvert$ LSSE (mK)
34 (a)	10	50	0.5	2.0
34 (b)	30	170	1.8	6.7
34 (c)	5	130	1.4	5.1
34 (d)	10	300	3.2	12

Table 3: The calculated values of ΔT_{me} for the measured values of V_{sat} taken from Fig. 34 (a) to 34 (d) and the corresponding ΔT_z (LSSE).

other than the coupling between magnons and electrons. This yields a value ΔT_z, the (phonon) temperature drop across the YIG film, for which the experimentally measured V_{sat} is obtained. We assume $\rho_{Pt} = 40\,\mu\Omega\,\text{cm}$. All material dependent YIG parameters were taken from Schreier et al.[137] In Tab. 3 we present the calculated ΔT_{me} for V_{sat} taken from Fig. 37 at RT (Fig. 34 (a) to 34 (d)) and the corresponding ΔT_z (LSSE). The ΔT_z obtained are of the order of a few millikelvins. It is reasonable to assume that such values can be induced by, e.g., thick contact tips, especially considering that our initial simplifications should lead to an overestimation of ΔT_z (cf. Schreier et al.[137]). The transverse spin Seebeck configuration was investigated in detail by Schreier et al.[137] It was found that for $\Delta T_x = 20\,\text{K}$ the obtained ΔT_{me} is well below 1 μK, even at the very edge of the sample where ΔT_{me} is maximized. This further supports the notion that spurious out-of-plane gradients are responsible for the voltages observed in our samples. This out-of-plane gradient can generate an ANE, proximity ANE or LSSE. However, an ANE is not possible due to the lack of free charge carriers in the YIG and the non-ferromagnetic Pt region which is not in contact with the FM layer. The proximity ANE due to possible spin polarized Pt which is in contact with the YIG can also be excluded by XRMR measurements at identical samples[139] as well as XMCD measurements by Geprägs et al.[140] which confirm the XRMR data. However, Kikkawa et al.[141] were able to show that a potential contribution of a proximity ANE additional to an LSSE is negligibly small. They measured their YIG/Pt bilayer system in two configurations and changed the directions of the temperature gradient and the external magnetic field. For an out-of-plane temperature gradient and an in-plane magnetic field there is an LSSE as well as a possible proximity ANE signal in the transverse voltage on the Pt film. When the temperature gradient is applied in-plane with an out-of-plane magnetic field

[139] F. Della Coletta et al. ESRF annual report, HC-1500, 2014

[140] S. Geprägs et al. Applied Physics Letters **101** (2012) 262407

[141] T. Kikkawa et al. Physical Review Letters **110** (2013) 067207

the proximity ANE is the only contribution, because an LSSE driven spin current cannot be detected. They determined an upper limit of a possible proximity ANE contribution of less than 5 % of the measured voltage. This supports our conclusion that the main antisymmetric contribution in our measurements is the LSSE, which is driven by an out-of-plane temperature gradient. The required temperature differences which are necessary for an LSSE (cf. Tab. 3) confirm that the observed magnitudes in the ISHE voltage are in a realistic range of order. This is consistent with the measurements in direct LSSE configuration from Fig. 39. In these measurements a few kelvins are necessary to obtain ISHE voltages in the same range. However, we took into account that the measured temperature difference is obtained between the copper blocks. These blocks are separated not only from the YIG film but also by a 0.5 mm thick sapphire substrate on top and a 0.5 mm thick GGG substrate at the bottom of the YIG.

We do not observe any symmetric contribution for ∇T_x without tip heating (Fig. 34). Therefore, PNE and proximity PNE contributions can also be excluded. Nevertheless, we find a small symmetric contribution for strong tip heating as demonstrated in Fig. 36 (b) for ΔT_{needle} = RT+31 K. In the region of H_C small peaks are visible under symmetrization of the voltage (Fig. 46 (a)). This can be extracted by a numerical separation of the experimental data into the antisymmetric and the symmetric part (Fig. 46 (b) and (c)). The symmetric part hints at the existence of an additional magnetothermopower effect potentially induced by a temperature gradient ∇T_y along the Pt strip. This is evidence of being thermally driven SMR (cf. Nakayama et al.[142] and Althammer et al.[143]). This would not be a combination of SHE and ISHE but a spin Nernst effect (SNE) accompanied by an ISHE.

[142] H. Nakayama et al. Physical Review Letters **110** (2013) 206601

[143] M. Althammer et al. Physical Review B **87** (2013) 224401

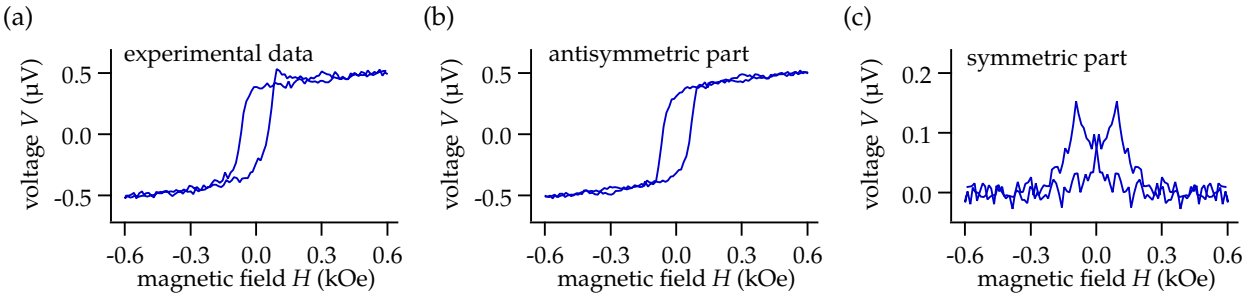

Figure 46: (a) Experimental data of the voltage V as a function of H taken from Fig. 36 (b) with ΔT_x = 30 K and a needle temperature T_{needle} = RT + 31 K separated numerically in the antisymmetric part (b) and the symmetric part (c).

Here, we have no induced charge current that drives an SHE but a temperature gradient which generates a thermally driven charge current. This produces the analogy between the SHE and SNE. The reflected spin current at the interface and conversion into a measurable charge current, or electrical voltage, should still be the ISHE. Further investigations should answer the question if a reflected spin current due to the SNE gives rise to an inverse SNE (ISNE) which would be the conversion of a transverse heat flow out of a thermally induced spin current due to the SNE. However, further investigations beyond this work are needed to identify the real origin of the observed phenomena in Fig. 46 (c).

Recently, Wegrowe et al.[144] used anisotropic heat transport as an interpretation for the measured voltages using in-plane temperature gradients. In their work, they derived the anisotropic field-dependent temperature gradient in metallic as well as insulating FM materials from the Onsager reciprocity relations.[145] Therefore, the thermocouple effect between the FM, the NM and the contacting tips can generate field-dependent voltages if there is a difference in the Seebeck coefficients. In our investigated systems, the Seebeck coefficients are indeed different for YIG, Pt and the contact tips. However, since we do not observe a field-dependent variation of the ISHE voltage by using thin W tips, any anisotropic field-dependent heat transport can be excluded as the reason for the observed voltages.

The antisymmetric effect in our measurements with intentionally applied in-plane temperature gradient can be identified as the LSSE which was verified by controlling the needle temperature and varying the out-of-plane temperature gradient. Taken together, in all our experiments in TSSE configuration on magnetic insulators, we thus only observe LSSE-type signatures. These LSSE voltages can be reminiscent of a TSSE-type response if an unintentional (or intentional) ∇T_z is present. This shows that the utmost care is required if one is to interpret magnetothermopower effects in terms of the TSSE.

Our observations on YIG/Pt in the TSSE configuration (Fig. 36) were measured using the convention presented by Schreier et al.[146] and we obtained the same sign of the spin Hall angle in Pt with our explanation of the temperature gradient directions. In all our LSSE investigations we can find the same sign for the spin Hall angle in Pt. We want to emphasize that this is not a sufficient but a necessary condition to address the voltage signal to a converted ISHE voltage due to a detected spin current driven by the LSSE.

[144] J. E. Wegrowe et al. Physical Review B **89** (2014) 094409

[145] L. Onsager. Physical Review **37** (1931) 405

[146] M. Schreier et al. Journal of Physics D: Applied Physics (2014) 025001

In our LSSE investigations we used YIG films of different thicknesses in the range of about 60 nm up to bulk like thicknesses of about 4 μm. In the paper of Kehlberger et al.[147] from 2013 they tried to find out whether the LSSE is a bulk or an interface effect. For this reason they carried out thickness dependent measurements which have shown a saturation of the LSSE signal normalized by the YIG thickness. They concluded that there is a characteristic propagation length of thermally excited magnons in the YIG. These magnons can reach the Pt where they are detected in terms of the ISHE. They evaluated a propagation length of about 110 nm. However, they had to use YIG/Pt samples which were prepared equally in such a way that the interface for samples of the same series is equal in that it prevents different spin-mixing conductances. In our case all the YIG films were not prepared in the same manner, nor was the adjacent Pt film. Therefore, the comparison of ISHE voltages between samples of different thicknesses is not favourable. We have to assume different interfaces for each sample. This leads to different spin-mixing conductances, which makes it impossible to compare the results across all samples. Furthermore, the thermal contact between the heater and the samples can differ for all samples. That is one critical point why the work of Kehlberger et al. is controversially discussed. Later we will mention some solutions to this kind of problem.

In Eq. 24 it becomes obvious that the ISHE voltage reaches its maximum when the external magnetic field is aligned perpendicular to the electrical contacts on the NM layer. Otherwise, the ISHE voltage decreases in a cos form, as Fig. 43 has shown for angles α between the external magnetic field and the x-direction which lies perpendicular to the electrical contacts. Kehlberger et al.[148] used the LSSE to investigate the magnetic properties in YIG films. They used the fact that the ISHE voltage due to Eq. 24 mirrors the projection of the magnetization to the direction perpendicular to the electrical contacts viz. the x-direction in our case. When a magnetic field is swept in both directions with a certain angle α one can see the reversal process of the magnetization vector in low magnetic fields. This reversal process depends on anisotropies of the FM material accompanied by hard and easy axis for the magnetization. We could use the same argumentation for the Py/Pt films and the reversal process of the magnetization in Py which gave us the change in voltage due to the PNE. Therefore, the PNE and the LSSE are good methods for the investigation of these reversal processes in ferromagnetic

[147] A. Kehlberger et al. arXiv.org (2013). arXiv: 1306.0784v1

[148] A. Kehlberger et al. Journal of Applied Physics **115** (2014) 17C731

metals and insulators, respectively.

We have shown angle dependent LSSE measurements in Fig. 40 and Fig. 41. For the voltage in saturation we could see the typical cos behaviour of the LSSE which has its maximum for a magnetization perpendicular to the electrical contacts and its minimum for magnetization parallel to the contacts. In the range with lower magnetic fields we can see a different behaviour for both samples. This difference is apparent in an antisymmetric and a symmetric magnetization reversal process for the YIG films with thicknesses of 130 nm and 4 µm, respectively. This can be realized by a complete rotation of the magnetization $\vec{M}$ for the antisymmetric reversal process and by a rotation between 0° - 180° back and forth for the symmetric reversal process. The appearance of an antisymmetric reversal process is an argument against a possible PNE due to a spin polarized Pt interface or a possible SMR driven by the generated ISHE voltage which is still present when the external magnetic field H is parallel to the electrical contacts. The PNE as well as the SMR are symmetric effects with respect to H and the symmetric reversal process in Fig. 41 for the 4 µm thick YIG film could be misinterpreted by one of these phenomena. However, the PNE could be neglected previously. The SMR, nevertheless, can also be neglected by regarding the direction of the maxima for angles α above and below 90°. The ISHE voltage would change its sign and the generated SMR would change from maxima to minima.

An antisymmetric magnetization reversal process could be observed by Kehlberger et al.[148] in 300 nm and 20 nm thin YIG films prepared by PLD, whereas Weiler et al.[149] have observed a symmetric magnetization reversal process in a 10 nm thin YIG film which was also prepared by PLD. A thickness dependency cannot be recognized when our measurements are compared to the literature data. However, angle dependent LSSE measurements are helpful in determining magnetic properties such as anisotropies on magnetic insulators. Even on very thin films where other magnetometry methods have the disadvantage of influence by simultaneously measuring the substrate. For instance, a perpendicularly magnetized YIG film would cause the ISHE voltage to disappear with a small external magnetic field. In this direction the electrical contacts are not sensitive to any spin currents because Eq. 24 would result in zero when the spin current and the spin direction are parallel.

[149] M. Weiler et al. Physical Review Letters **108** (2012) 106602

In conclusion of this chapter, we have shown different measurement configurations for the spin Seebeck effect on the magnetic insulator yttrium iron garnet (YIG). In the transverse configuration, which was already used for the ferromagnetic conductor Py, no spin Seebeck effect (TSSE) could be detected. However, we obtained contributions of the longitudinal spin Seebeck effect (LSSE) due to unintended out-of-plane heat flows caused by the electrical contacts. Other side effects which were possible in this measurement configuration could be neglected. The LSSE, instead, could be investigated directly in more detail. We have shown the typical behaviour of this effect and have discussed it in more detail in the context of the current literature.

The future of magnetic insulators in spintronics, magnonics and especially spincaloritronics is wide-ranging from further basic research of pure spin currents, material science in finding and tailoring new magnetic insulators for applications to the adaptation of this material class into devices and logics for information technology. The spin Seebeck effect, especially in the reproducible configuration of the LSSE, is well established in magnetic insulators like YIG. Therefore, it can be used for the investigation of magnetic properties in this material class. The focus will be set on the investigation of magnetic sublattices of antiferromagnets and compensated ferromagnets as described, e.g., by Ohnuma et al.[150]

[150] Y. Ohnuma et al. Physical Review B **87** (2013) 014423

Spin Seebeck effect in nickel ferrite

This chapter deals with the investigation of the spin Seebeck effect on the ferrimagnetic compound nickel ferrite ($NiFe_2O_4$, NFO). In this thesis we investigated NFO films which showed semiconducting behaviour due to a reduced band gap and, therefore, thermally activated charge carrier transportation. We will introduce the material system and give an overview of the main physical properties. Furthermore, the main idea to use this material for the investigation of spin caloric effects will be illustrated. The main part of this chapter is devoted to presenting the experimental results. After that, we will discuss the results in terms of the observed effects and their importance in spin caloritronics. Most of these results were published in 2013 and 2015.[151]

[151] D. Meier et al. Physical Review B **87** (2013) 054421; D. Meier et al. Nature Communications **6** (2015) 8211

Nickel ferrite

The ferrimagnet nickel ferrite ($NiFe_2O_4$, NFO) is a compound belonging to the spinel group but with the inverse spinel structure. Materials with the inverse spinel structure AB_2O_4 consist of two tetrahedrons with half of the B^{3+} cations occupied at the *A* sites and one octahedron with the A^{2+} and the other half of the B^{3+} ions equally distributed at the *B* sites.[152] As in the case of YIG there are 8 formula units in one unit cell. Each unit cell consists of 56 atoms. This results in a lattice parameter of about 0.834 nm. The magnetic moment comes from the Ni^{2+} ions on the *B* sites while the magnetic moments from the Fe^{3+} cations on the *A* and *B* sites are antiferromagnetically coupled through a super exchange interaction over the oxygen atoms.[153] This results in a ferrimagnetic state with $2\mu_B$ per formula unit. The NFO films which were used in this thesis were prepared by direct liquid injection chemical vapour deposition (DLI-CVD). In the DLI technique a liquid solution of two precursors [$Ni(acac)_2$ and $Fe(acac)_3$] in the molar ration of 1:2 and the solvent *N*,*N*-dimethyl formatted (DMF) are vaporized at a temperature of 175 °C to obtain a film growth rate

[152] N. Li et al. Chemical Vapor Deposition **17** (2011) 261

[153] D. Fritsch and C. Ederer. Physical Review B **82** (2010) 104117

Property	Value	Unit	Ref.
Lattice constant a_0	0.834	nm	(a)
Curie temperature T_C	$\approx$ 860	°C	(b)
Saturation magnetization	3100 to 3800	gauss	(a)
Damping constant	4.5×10^{-3}		(c)
Resistivity	(1.13–2.66)×10^4	Ω cm	(d)

Table 4: Properties of $NiFe_2O_4$ taken from (a) Li et al., (b) Dionne, (c) Yager et al. and (d) Rai et al.[154]

[154] N. Li et al. Chemical Vapor Deposition **17** (2011) 261; Gerald F. Dionne. Journal of Applied Physics **63** (1988) 3777; W. A. Yager et al. Physical Review **80** (1950) 744; R. C. Rai et al. Applied Physics A **106** (2012) 207

[155] C. Klewe et al. Journal of Applied Physics **115** (2014) 123903

[156] Q.-C. Sun et al. Physical Review B **86** (2012) 205106

[157] R. C. Rai et al. Applied Physics A **106** (2012) 207; J. Haetge et al. Inorganic chemistry **49** (2010) 11619; S. N. Dolia et al. Indian Journal of Pure and Applied Physics **44** (2006) 774; S. Balaji et al. Materials Science and Engineering: B **119** (2005) 119; R. D. Waldron. Physical Review **99** (1955) 1727

in a range of 10 to 18 nm min^{-1}. NFO films with thicknesses of 1 to 1.2 μm were deposited at substrate temperatures between 500 to 800 °C. Here, $MgAl_2O_4$ (MAO) (100)-oriented substrates were used which have a lattice parameter of 0.808 nm. The mismatch between the NFO and the MAO substrate leads to tetragonal distortion and horizontal stretching of the lattice parameter.[155]

Recent optical spectroscopy measurements show an indirect band gap of about 1.6 eV in the minority channel and a direct band gap of about 2.4 to 2.8 eV for NFO films of thicknesses between 150 to 270 nm.[156] Other experimental data for the optical band gap range from 0.33 eV to 3.7 eV for thin films as well as for the bulk.[157] Further relevant parameters are shown in Tab. 4.

The prepared and investigated NFO films in this thesis show semiconducting behaviour with low activation energy of about 0.09 eV for thermally excitable charge carriers. The electrical conductivity is controllable by varying the temperature due to the semiconducting properties. Therefore, the ANE induced by a conductive NFO film can be suppressed at low temperatures. This makes it very interesting for the investigation of spin caloric transport phenomena.

TSSE measurements on NFO/Pt

First of all, TSSE measurements on NFO/Pt were done in vacuum at room temperature. A 5 × 10 mm^2 NFO film of 1 μm thickness with a 10 nm thin Pt strip on one sample side was investigated. This sample was contacted and measured in the same way as we investigated the YIG/Pt film in terms of the TSSE in vacuum. Therefore, the ends of the Pt strip were contacted with 25 μm thin Au bonding wires and glued to copper wires with silver paste for the voltage measurement. The sample was clamped between two copper blocks for the in-plane temperature gradient. The

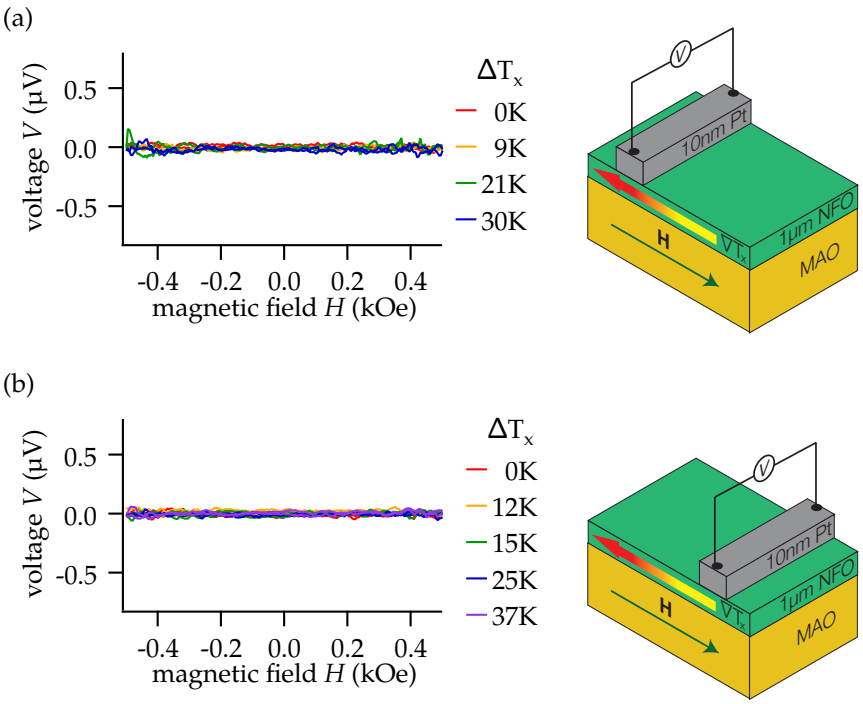

Figure 47: Measurements on NFO/Pt in the TSSE configuration for different in-plane temperature gradients performed under vacuum. The Pt strip was contacted with 25 μm thin Au bonding wires and was located (a) on the hot side and (b) on the cold side.

in-plane temperature difference ΔT_x was determined between the copper blocks.

In Fig. 47 the measurements for Pt strip on the hot and the cold side are displayed. The transverse voltage V is plotted as a function of the external magnetic field H. No significant effect can be observed within a sensitivity limit of about ±20 nV, which is comparable to the measurements on YIG/Pt we also performed in vacuum. We find no TSSE nor any other antisymmetric side effects which were driven by an unintended out-of-plane temperature gradient.

In the next step, the influence of an out-of-plane heat flow on NFO/Pt induced by contact tips has to be investigated in detail to get an impression of induced magnitudes of V_{sat}. Therefore, the next measurements were performed under ambient conditions and the Pt strip was contacted by the same tips we used for the YIG/Pt bilayers. The Pt strip is contacted by the thinnest W tips with a contact area of $A = 0.003\,\mathrm{mm}^2$. The measurements are shown in Fig. 48. A clear antisymmetric effect is obtained with the Pt strip located on the hot side, whereas a possible effect with the Pt strip on the cold side is hard to imagine within the measurement sensitivity. However, a strong contacting of the Pt

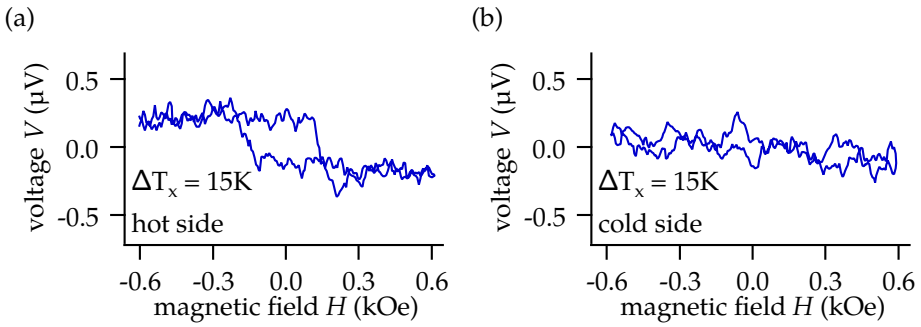

Figure 48: Measurements on NFO/Pt in the TSSE configuration performed under ambient conditions. The in-plane temperature difference ΔT_x was fixed at 15 K with Pt strip located on the hot side (a) and the cold side (b). The voltage V was measured by using thin W tips with a contact area $A = 0.003\,\mathrm{mm}^2$.

strip is assumed to be the reason for the observed effect. This promotes a larger contact area and, therefore, the appearance of an out-of-plane temperature gradient which leads to one of the effects presented in Fig. 14. The absence of sign change reversal leads to the absence of the TSSE which could also not be observed even when the Pt strip was contacted by sufficiently thin Au bonding wires. A temperature gradient ∇T_z out-of-plane would

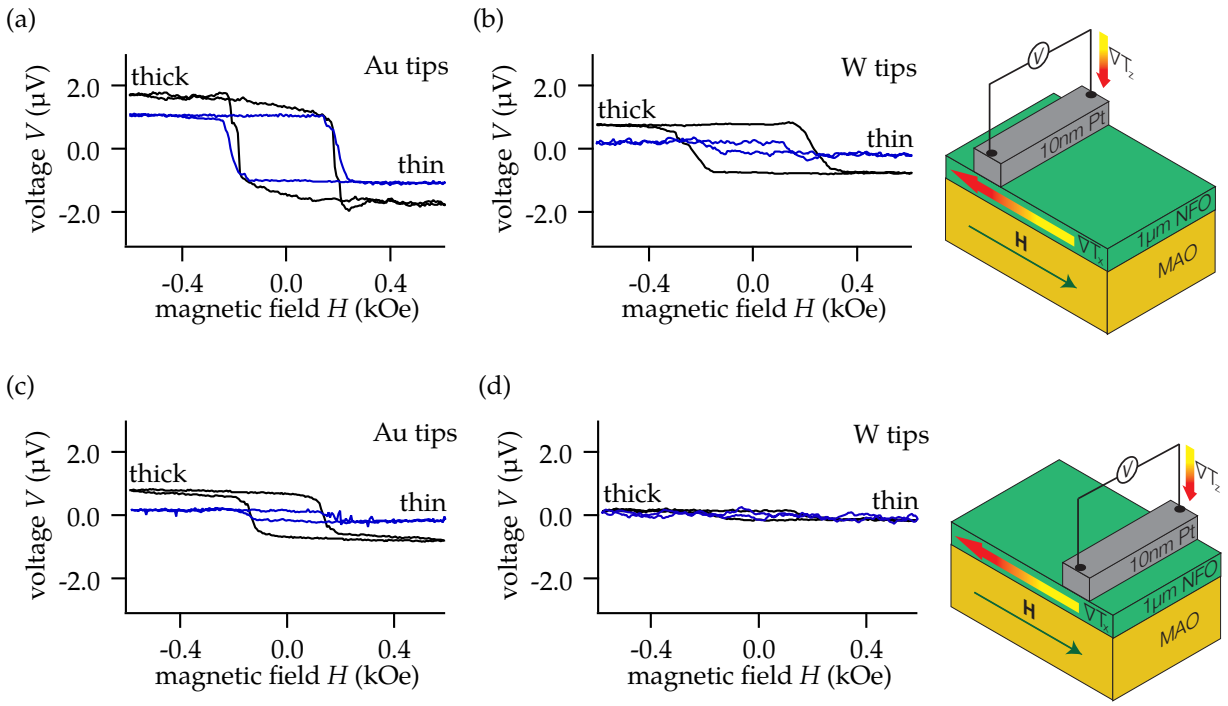

Figure 49: Measurements on NFO/Pt in the TSSE configuration performed under ambient conditions. The in-plane temperature difference ΔT_x was fixed at 15 K and the Pt strip was contacted by different W and Au tips for Pt strip locations (a), (b) on the hot side and (c), (d) on the cold side. The contact areas are $A = 0.28\,\mathrm{mm}^2$ and $A = 0.06\,\mathrm{mm}^2$ for the thick and thin Au tips and $A = 0.27\,\mathrm{mm}^2$ and $A = 0.003\,\mathrm{mm}^2$ for the thick and thin W tips, respectively.

cause an LSSE, ANE or proximity ANE (Fig. 14).

The influence of different tips with different contact areas A were also investigated on NFO/Pt in the same way we did on YIG/Pt. In Fig. 49 measurements for Pt strip located on the hot and the cold side are plotted. The Pt was contacted with thick and thin Au and W tips, respectively. An antisymmetric effect with the same sign in V depending on H is obtained for all Pt strip locations and tip combinations. The magnitude of V_{sat} is reduced for smaller tip contact areas and decreases as expected when the temperature difference between the tip and the sample gets smaller. This decrease happens especially when the Pt strip is located on the cold side of the NFO compared to the setting where it is on the hot side.

In the next step, we wanted to investigate the behaviour of the antisymmetric effect when the out-of-plane heat flow is influenced intentionally. Therefore, the ends of the Pt strip were contacted with heatable Au tips and without an in-plane temperature gradient and intentional heating of one of the Au tips, respectively. The measurements in Fig. 50 (a) and 50 (b) were carried out with Pt strip on the hot sample side. Without any tem-

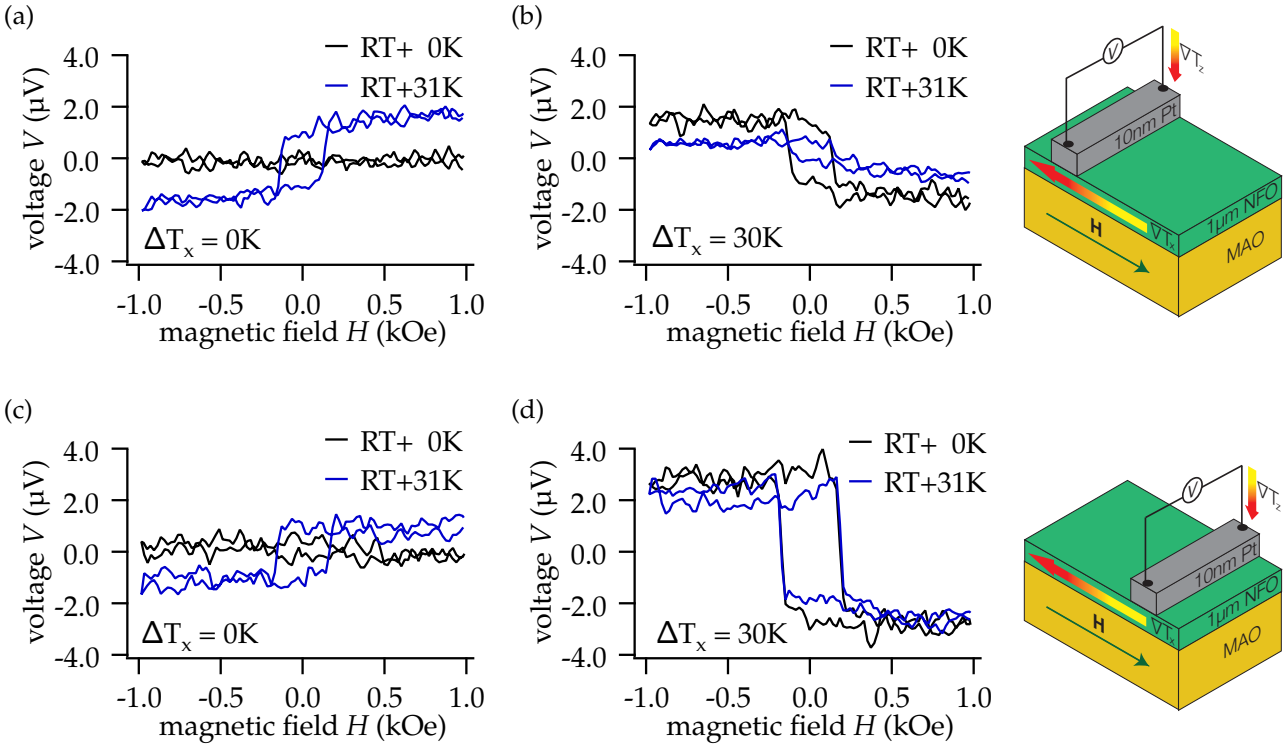

Figure 50: Transverse voltage V as a function of the external magnetic field H measured with Au tips on the hot sample side with (a) ΔT_x = 0 K and (b) 30 K. Measurements with Au tips on the cold sample side with (c) ΔT_x = 0 K and (d) 30 K. For each ΔT_x one Au tip on the Pt strip was heated up to a temperature T_{needle} = RT + 31 K.

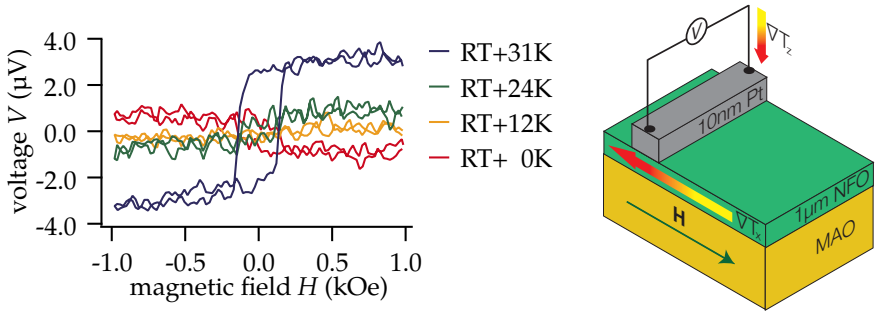

Figure 51: Transverse voltage V as a function of the external magnetic field H measured with Au tips located on the hot side with $\Delta T_x = 12\,\mathrm{K}$ and different Au tip temperatures.

perature gradients ($\Delta T_x = 0\,\mathrm{K}$) and no Au tip heating (RT + 0 K) there is no observable effect as expected. When the Au tip is heated at RT + 31 K and an out-of-plane temperature gradient is generated we can observe an LSSE with a magnitude V_{sat} of about 1.8 μV. When we switch off the Au tip heating and apply an in-plane temperature gradient with $\Delta T_x = 30\,\mathrm{K}$ we obtain a magnitude of $V_{\mathrm{sat}} = -1.6\,\mu\mathrm{V}$ (Fig. 50 (b), RT + 0 K). The sign of V_{sat} has changed, which is caused by a reversal of the out-of-plane heat flow driven through the Au tip. When the tip is heated ($T_{\mathrm{needle}} = \mathrm{RT} + 31\,\mathrm{K}$) we can observe a decreasing of the absolute value of the magnitude to $V_{\mathrm{sat}} = -0.65\,\mu\mathrm{V}$.

When the Pt strip is located on the other side of the NFO film we can observe the same behaviour when there is no in-plane temperature gradient and no tip heating (Fig. 50 (c)). There is no observable effect as expected. A magnitude of $V_{\mathrm{sat}} = 1.1\,\mu\mathrm{V}$ is obtained when the Au tip is heated up to $T_{\mathrm{needle}} = \mathrm{RT} + 31\,\mathrm{K}$. On both sides of the NFO film we get the same sign of magnitude when only the Au tip is heated. This indicates a good controllability of the tip heating and the generation of an out-of-plane heat flow.

In the next step, the in-plane temperature gradient is turned on ($\Delta T_x = 30\,\mathrm{K}$, Fig. 50 (d)). Now we achieve an LSSE with a magnitude of about $V_{\mathrm{sat}} = 2.8\,\mu\mathrm{V}$ which can be decreased to $V_{\mathrm{sat}} = 2.4\,\mu\mathrm{V}$ when the Au tip is again set to a temperature $T_{\mathrm{needle}} = \mathrm{RT} + 31\,\mathrm{K}$. Compared to Fig. 50 (b) we get a larger magnitude on the cold sample side when the same in-plane temperature gradient is applied. We have to take into account that the contact area of the Au tip on the sample can slightly differ when the sample is contacted again. The contact area seems to be larger for the Pt strip on the cold side. However, the magnitude can be decreased by heating the Au tip. We cannot find any evidence

for a possible TSSE which would cause this behaviour, since no TSSE was observed when very thin tips were used.

To support the previous argument we applied a smaller in-plane temperature gradient ∇T_x and heated up the Au tip again in order to change the heat flow direction of the out-of-plane temperature gradient and change the sign of V_{sat}. This behaviour is shown in Fig. 51. Without Au tip heating the antisymmetric effect has the same sign compared to previous measurements where the heat flows from the sample into the tip. For $T_{\mathrm{needle}} = \mathrm{RT} + 12\,\mathrm{K}$ the effect almost vanishes. When the needle temperature is further increased to $T_{\mathrm{needle}} = \mathrm{RT} + 24\,\mathrm{K}$ we obtain an antisymmetric effect with a reversed sign which is further increased for a needle temperature $T_{\mathrm{needle}} = \mathrm{RT} + 31\,\mathrm{K}$.

LSSE measurements on NFO/Pt

In 2013, we showed the presence of the LSSE in semiconducting NFO which will be presented in this section.[158] In the same year Ramos et al.[159] presented LSSE measurements in Fe_3O_4 above and below the Verwey transition.[160] In both materials, NFO and Fe_3O_4, there are unintended side effects, like the ANE. However, the ANE and the LSSE contribution could be separated in both materials by measuring with and without Pt on top at room temperature and low temperatures. The ANE could be switched on and off with the conducting behaviour of the semiconducting materials, controlled by different temperatures.

[158] D. Meier et al. Physical Review B **87** (2013) 054421

[159] R. Ramos et al. Applied Physics Letters **102** (2013) 072413

[160] F. Walz. Journal of Physics: Condensed Matter **14** (2002) R285

LSSE investigations on NFO films were done at room temperature and at low temperatures. The advantage of the films used was the opportunity to switch on and off the electrical conductivity by changing the temperature and, therefore, the contribution of the unintended ANE.

For a characterization of the magnetization properties of the NFO used we performed vibrating sample magnetometry (VSM). In the first measurements, an NFO film of 1 µm thickness with a 10 nm thick Pt film on top was investigated. The film was deposited on $8 \times 5\,\mathrm{mm}^2$ $MgAl_2O_4$ (1) substrates by DLI-CVD. In Fig. 52 (a) the magnetic moment μ is presented and was normalized to the saturation value μ_{sat}. A coercive field of about (165 ± 25) Oe could be achieved which is the same switching field of the observed ISHE voltage on the Pt strip. In Fig. 52 (b) the coercive field and the squareness of the NFO/Pt sample is plotted as a function of the angle α which lies in the sample plane. Both graphs indicate a fourfold magnetic anisotropy caused by the cu-

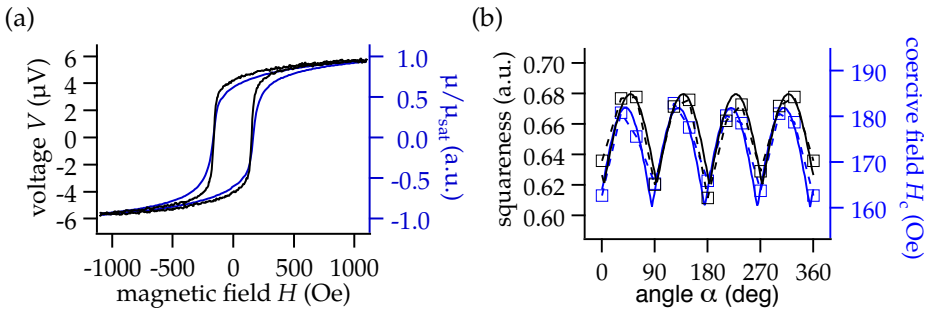

Figure 52: (a) Normalized magnetic moment μ/μ_{sat} of NFO compared to the ISHE voltage V in the LSSE configuration which shows the same switching behaviour with respect to the external magnetic field H. (b) The squareness and the coercive field H_c as a function of the angle α of the sample alignment.

bic inverse spinel structure of the NFO. Two easy axes are found for $\alpha = 45°/225°$ and $\alpha = 135°/315°$. This is in correspondence to the crystallographic structure of the NFO in ⟨110⟩ direction.

For the LSSE investigations, the NFO/Pt system was clamped between two copper blocks with a 500 µm thick sapphire substrate for electrical insulation. A small amount of thermal grease between the sample, the sapphire substrate and the copper blocks supported the thermal conduction between the layers and compensated missing contact due to the materials' roughness. The bottom copper block was heated and cooled by a Peltier element. We measured the temperature difference between the copper blocks by means of two T-type thermocouples. First, we applied a temperature difference ΔT_z in a range of −10 K to 10 K between the two copper blocks. The voltage V was measured on the Pt film transversely to the external magnetic field H up to 1 kOe which was applied in the sample-plane. In Fig. 53 the voltage V

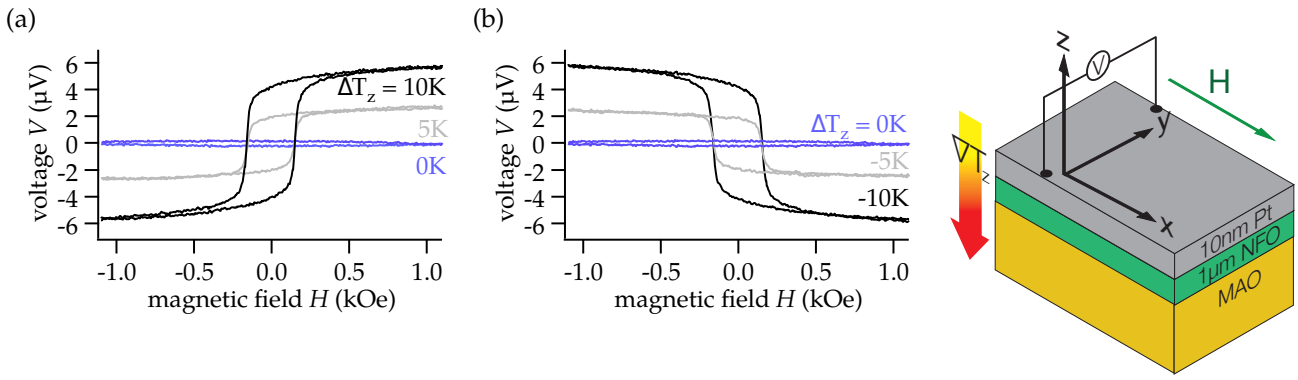

Figure 53: Transverse voltage V as a function of the external magnetic field H for various out-of-plane temperature gradients ∇T_z (a) with the hot side on top and (b) the hot side at the bottom of the sample.

is shown as a function of H for various ΔT_z. The graphs show hysteretical behaviour antisymmetric with respect to H for each ΔT_z. For $\Delta T_z = 0\,\mathrm{K}$ the voltage signal disappears. The voltage in saturation V_{sat} changes its sign depending on the temperature gradient direction. This is shown in Fig. 55 (a) as well as the proportionality between V_{sat} and ΔT_z. Furthermore, the angle dependency of H in the sample plane was investigated, which is shown in Fig. 54 for various angles α with respect to the x-direction (cf. sketch in Fig. 54). In Fig. 55 (b) V_{sat} is plotted as a function of α. The individual measurements for a certain angle show a decrease of V_{sat}. However, even for $\alpha = 90°$ a voltage signal with two minima around the coercive field can be found which is symmetric with respect to H.

Fig. 53 to Fig. 55 describe the characteristics of the LSSE, e.g., the proportionality of the ISHE voltage with ΔT_z and therefore the magnitude of the driven spin current as well as the sign reversal depending on the temperature gradient direction. The dependence of H describes the direction of the spin polarization vector which also changes the sign of V. Furthermore, the angle dependency is given by the cross product of Eq. 24 which shows a sin curve for the defined angle α (Fig. 55 (b)).

We investigated the conductivity of the pure NFO film without Pt on top to estimate the possibility of an ANE contribution in the LSSE measurements. For this reason, two contact lines consisting of 5 nm Ta and 5 nm Au with a width of 100 µm were deposited on a NFO film of 1 µm in thickness. By contacting the ends of each Ta/Au strip we were able to measure the resistance of the NFO film in a four-point-geometry. This was done for different temperatures from room temperature down to 50 K

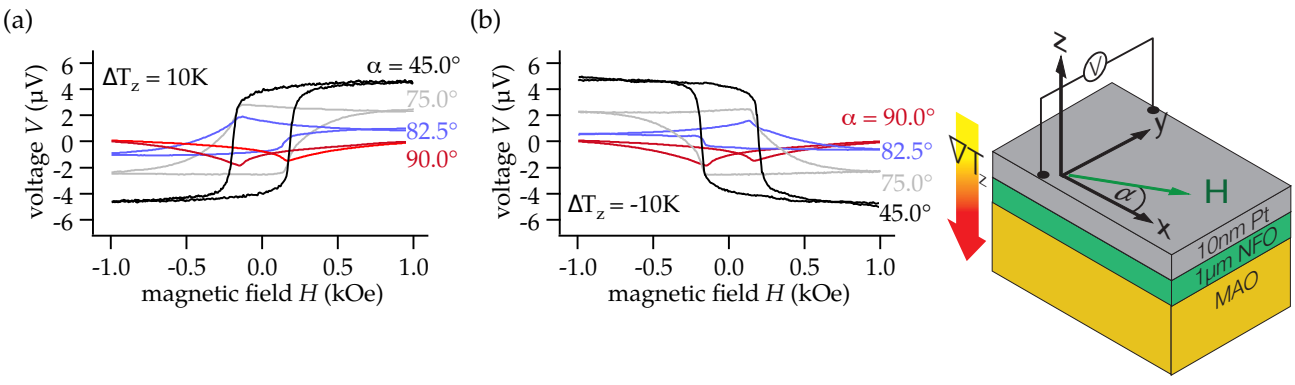

Figure 54: Transverse voltage V as a function of the external magnetic field H for different angles α with respect to the electrical contacts in the y-direction. (a) For an out-of-plane temperature difference $\Delta T_z = 10\,\mathrm{K}$ and (b) for a reversed temperature gradient with $\Delta T_z = -10\,\mathrm{K}$.

inside a closed-cycled helium cryostat. The resistance R was measured with a Keithley 2000 providing a range up to 120 GΩ. At room temperature a resistance of about (336.7 ± 0.6) kΩ was obtained. For lower temperatures the resistance increased to a value of about (83.3 ± 6.9) GΩ at 50 K. These values correspond to conductivities σ of about (4.7529 ± 0.0085) $\Omega^{-1}\,m^{-1}$ at room temperature and (19.2 ± 1.7) × 10^{-6} $\Omega^{-1}\,m^{-1}$ at 50 K. In Fig. 56 the conductivity σ is plotted against the inverse temperature $1/T_0$ to prove an extrinsic semiconducting behaviour. The equation $\sigma \propto \exp(\frac{E_a^{ext}}{k_B T})$ leads to a linear fit function in the region between the corresponding temperatures of 100 K to 300 K regarding a logarithmic scale for σ. The slope of this linear function is equal to the exponent of the exponential function which allows us to determine the thermal activation energy E_a^{ext} for charge transport in the NFO. We get a value of $E_a^{ext} = 0.09$ eV. Therefore, we took into account that the previously measured ISHE voltage (Fig. 53 to Fig. 55) includes a contribution of the ANE due to thermally activated charge carriers.

In the next step, the NFO/Pt sample was kept at low temperatures to suppress the ANE contribution. Figure 57 shows LSSE measurements for the base temperatures $T_0 = 50$ K and $T_0 = 100$ K for various out-of-plane temperature differences ΔT_z. All curves show a hysteretical behaviour of the voltage V which is antisymmetric with respect to the external magnetic field H. The magnitude increases with larger ΔT_z for both base temperatures. However, the voltage in saturation does not seem to be proportional to ΔT_z. A reason for this contradiction compared to previous measurements is the issue of proper adjustment of the heating on top of the sample. The sample was clamped between the cooling head of the cryostat and an upper copper plate with

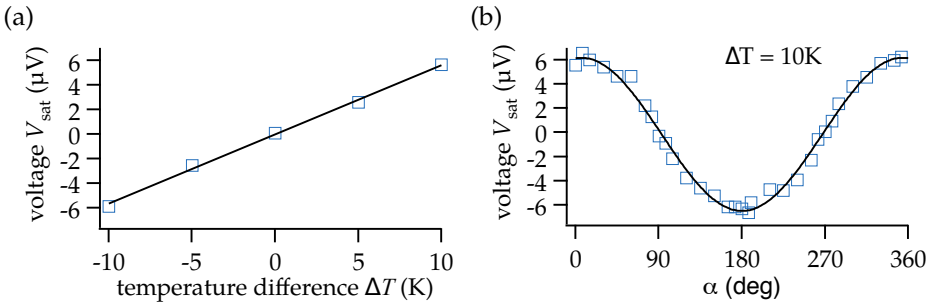

Figure 55: (a) The voltage in saturation V_{sat} as a function of the out-of-plane temperature difference ΔT (squares) shows proportional dependence (linear fit). (b) Angular dependency of V_{sat} from the angle α with respect to the x-direction.

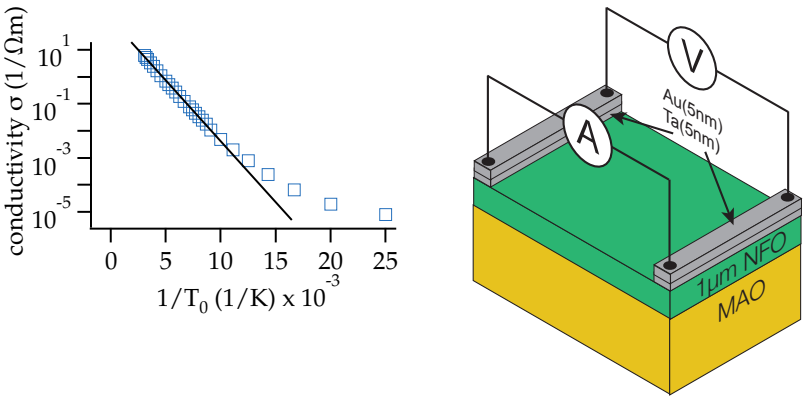

Figure 56: The NFO conductivity σ obtained in a 4-point-measurement geometry shown as a function of the inverse temperature T_0 (circles). A linear function is fitted in the extrinsic region of semiconducting behaviour to calculate the thermal activation energy.

a glued resistive heater. This upper copper plate was separated by a piece of sapphire substrate for electrical insulation. The cooling head of the cryostat has a 27 Ω rhodium iron resistance thermometer for low temperatures down to 1.5 K. The upper copper plate was instead equipped with a thermocouple during the measurements. The thermocouple voltage was calibrated by a temperature measurement on top of the cooling head in order to estimate the temperature on top of the sample in all further measurements. Simultaneously, the resistance of a pure NFO film without Pt was recorded. Figure 56 makes it possible to calculate the temperature of the sample surface to compare it to the temperature obtained with the thermocouple on top of the upper copper plate. However, one can assume a large experimental error for ΔT_z in order to explain the major derivation from the proportionality of the saturated voltage in Fig. 57 with the out-

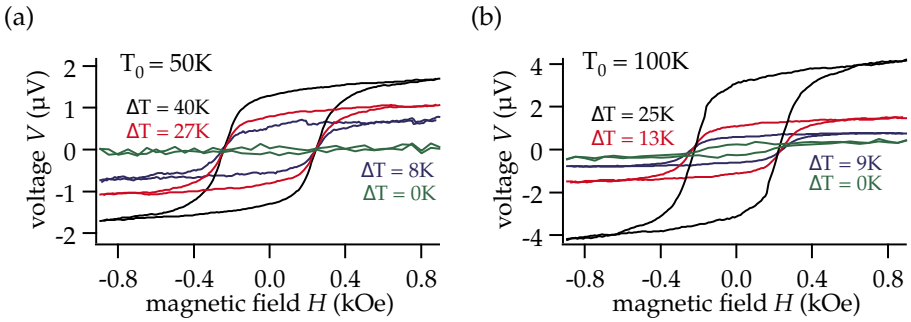

Figure 57: Transverse voltage V as a function of the external magnetic field H for different out-of-plane temperature gradients ∇T_z for the base temperature (a) $T_0 = 50$ K and (b) $T_0 = 100$ K.

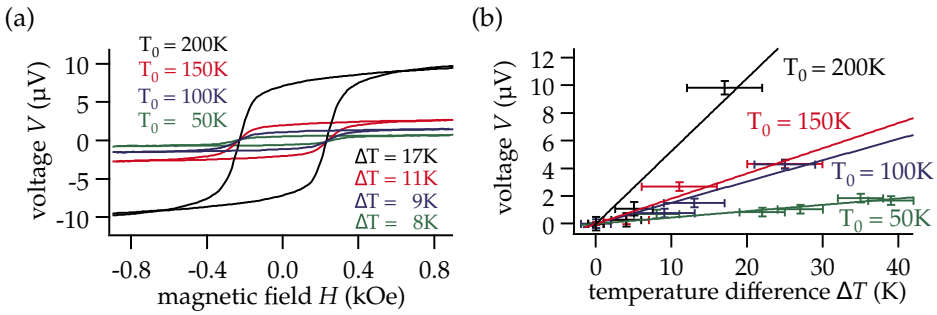

Figure 58: (a) Transverse voltage V as a function of the external magnetic field H for different out-of-plane temperature gradients ∇T_z and base temperatures T_0. (b) The voltage in saturation V_{sat} as a function of the out-of-plane temperature difference ΔT_z for different base temperatures T_0. The slopes of the linear fits are equivalent to the spin Seebeck coefficient for each T_0.

of-plane temperature difference. For this reason, we assumed a sufficient experimental error of $\Delta\Delta T_z = \pm 5\,\mathrm{K}$. A further evidence of a derivation of the estimated ΔT_z is a non-vanishing magnitude for $\Delta T_z = 0\,\mathrm{K}$ in Fig. 57 (b). Nevertheless, a clear signal is still observed at low base temperatures when the conductivity of the NFO is decreased. However, it is obvious that the magnitude for $\Delta T_0 = 50\,\mathrm{K}$ is generally smaller compared to $\Delta T_0 = 100\,\mathrm{K}$ despite similar or even higher temperature differences. We can assume a temperature dependent behaviour which we want to consider in more detail. In Fig. 58 (a) representative measurements with certain temperature differences ΔT_z for various base temperatures are plotted. Due to a difficult adjustment of ΔT_z we obtain a range of 8 K to 17 K in the temperature difference between the lowest base temperature $T_0 = 50\,\mathrm{K}$ and $T_0 = 200\,\mathrm{K}$, respectively. In spite of a double in the temperature difference an increase of at

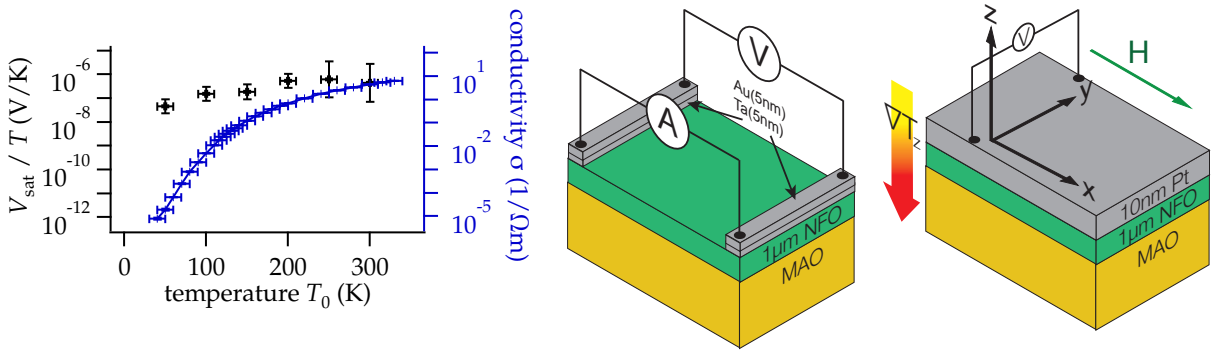

Figure 59: NFO conductivity σ obtained in a 4-point-measurement geometry shown as a function of T_0 compared to the spin Seebeck coefficient $V_{sat}/\Delta T_z$ against T_0. σ decreases over six orders of magnitude and $V_{sat}/\Delta T_z$ decreases only one order of magnitude.

least an order of magnitude in the voltage arises. This supports the assumption that the effort of a more detailed investigation of the temperature dependency would be worthwhile. However, regarding the large experimental error in ΔT_x we applied various temperature differences for each base temperature T_0 in order to obtain a proportionality factor for each T_0. This proportionality factor can be called the *spin Seebeck coefficient* with the assumption of neglecting any contributions of, e.g., an ANE or other unintended side effects. Figure 58 (b) shows the voltage in saturation for at least three varied temperature differences at distinctive base temperatures T_0. The error bars denote the experimental error of the estimated temperature difference as well as the accuracy of the voltage measurement. Considering the fact that the effects vanish for $\Delta T_x = 0\,\mathrm{K}$ we used a linear fit function in the form $y = ax$ to calculate the spin Seebeck coefficient for each T_0.

The calculated spin Seebeck coefficients $V_{\mathrm{sat}}/\Delta T_x$ of the NFO/Pt sample are plotted together with the conductivity σ of the pure NFO film against the base temperature T_0 (Fig. 59). The logarithmic scale was used to show the drastic decrease of σ of about six orders of magnitude compared to the slower decrease of the spin Seebeck coefficient of about one order of magnitude. This proves the fact that the spin Seebeck coefficient is independent of the charge transport in the NFO at least for low temperatures. Consequently, the ANE is not the dominant contribution in the voltage measured. Moreover, we can attribute the main contribution to the LSSE considering that magnetic proximity effects at the interface and therefore proximity ANE in spin polarized Pt can be neglected, which was shown by Kuschel et al.[161] in XRMR measurements. This argumentation can be supported by

[161] T. Kuschel et al. Physical Review Letters **115** (2015) 097401

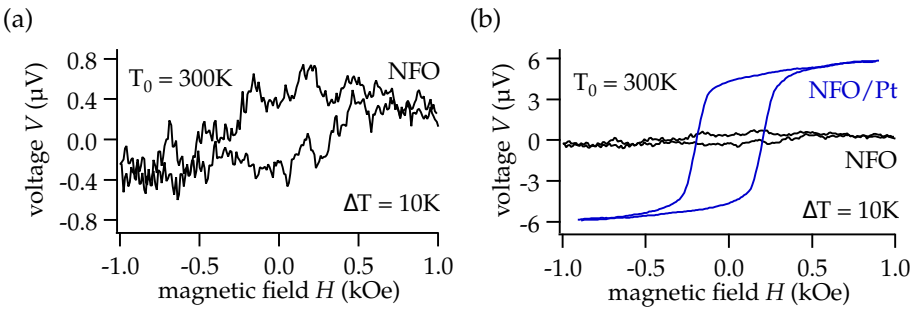

Figure 60: (a) Transverse voltage V measured at a pure NFO film without Pt on top as a function of the external magnetic field H with $\Delta T_z = 10\,\mathrm{K}$. (b) V measured on a pure NFO film compared to V measured on an NFO/Pt bilayer system with an out-of-plane temperature difference of $\Delta T_z = 10\,\mathrm{K}$.

a direct measurement of the ANE on the pure NFO film without any spin detector material on top. This measurement was done at room temperature and plotted in Fig. 60. The voltage V was measured at two points on top of the NFO film transverse to the external magnetic field H applied along the film plane driven by an out-of-plane temperature gradient with a temperature difference $\Delta T_z = 10\,\mathrm{K}$ between the copper blocks. Figure 60 (a) shows the ANE of pure NFO with a saturated voltage of about 400 nV. A poor signal-to-noise ratio due to a temperature sensitive resistance of the NFO made it necessary to take an average of about 40 measurements. In Fig. 60 (b) the ANE is compared to the ISHE voltage of NFO/Pt obtained with the same temperature gradient applied. Here, the saturated voltage reaches a value above 4 µV. This leads to the conclusion that an ANE contribution, if there is any, is below 10 % of the achieved voltage in NFO/Pt at room temperature. This fraction should decrease rapidly regarding the temperature dependent conductivity of NFO (Fig. 59).

Discussion

Measurements on NFO films with an in-plane temperature gradient showed no evidence of the TSSE. The first measurements in TSSE configuration were done under very careful conditions, e.g., using very thin contact wires and measuring in vacuum to prevent thermal convection. There was no characteristic sign change in the observed voltage when the temperature gradient was reversed. For the previously used materials (Py - metal, YIG - insulator) we saw that unintended side effects due to out-of-plane temperature gradients are present. However, even when side effects are observed a TSSE contribution could still be present and hidden under the obtained voltage. In Fig. 50 on both sides (hot and cold) the same sign of V_{sat} was obtained, but with different magnitudes. As sketched in Fig. 14, there are four possible effects, ANE, proximity ANE, LSSE and TSSE which are antisymmetric with respect to H. Effects which are symmetric with respect to H could not be detected due to either absence of magnetic anisotropy, parallel alignment of magnetic easy axis and H or vanishing PNE coefficient. For the first two cases, the angle between the magnetization and the temperature gradient does not change and the voltage remains at the same value. The PNE as well as the proximity PNE only change voltage when the angle between the magnetization and the temperature gradient changes.

However, proximity effects in NFO/Pt can be neglected by XRMR measurements presented by Kuschel et al.[162] If we focus on the saturation voltages V_{sat}, we can ignore possible PNE contributions anyway, since the PNE contributes in the form of an offset voltage which is cancelled out in the V_{sat} determination.[163]

Therefore, we can reduce the number of possible effects to the intended TSSE and to an unintended ANE and LSSE. Further measurements were necessary to distinguish between these different effects. However, Fig. 50 shows that there is no TSSE without any side effects. The dominant effect has to come from an unintended out-of-plane temperature gradient when these measurements are compared to the observations for very thin Au bonding wires. In Fig. 50 we presented measurements performed in the same way as for YIG films. For YIG we have seen that the observed effects are driven by an out-of-plane temperature gradient. This was proved by changing the Au tip temperature and turning on and off the in-plane temperature gradient. We could observe a sign change in the voltage when only in-plane ∇T_x or only Au tip heating were applied. This was proof of the reversal of the out-of-plane ∇T_z. When a fixed in-plane ∇T_x was applied we could change the magnitude of V_{sat} by changing the Au tip temperature. No sign change was observed as a result of changing the Pt strip position. The only inconsistency is the larger magnitude of V_{sat} for Pt strip on the cold side compared to Pt strip on the hot side with an in-plane temperature gradient. For YIG films we have shown that the magnitude decreases when the Pt strip moves from the hot to the cold side. On the cold side the heat flow through the contact tips is much smaller and the magnitude decreases. For the NFO films it can be explained by a larger contact area due to new contacting of the sample when it is rotated in the sample holder to move the Pt strip. The contact area changes when the contact tips are touching the sample at a different angle. Furthermore, the pressure of the micro probing system may differ, which also changes the contact area when the tip is bent on the sample.

When the TSSE can be neglected as well as magnetic proximity induced Nernst effects, there are only two possible remaining effects, the ANE and the LSSE. By measuring in the LSSE configuration (out-of-plane temperature gradient applied) we again achieve a purely antisymmetric voltage with respect to the external magnetic field (Fig. 53). The magnitude is proportional to the temperature difference between the top and the bottom and the sign of voltage changes when the temperature gradient direction

[162] T. Kuschel et al. Physical Review Letters **115** (2015) 097401

[163] M. Schmid et al. Physical Review Letters **111** (2013) 187201

is reversed (Fig. 55 (a)). Furthermore, the magnetic field rotation in the sample plane proves the cross product of the ISHE which converts the thermally driven spin current into electrical voltage (Fig. 55 (b)). The separation between the ANE and the LSSE could be implemented by using the semiconductive behaviour of the NFO. The cooling of the sample down to 50 K has shown a rapid drop of the conductivity of about 6 orders of magnitude ($(19.20 \pm 0.17) \times 10^{-6}\,\Omega^{-1}\,\mathrm{m}^{-1}$), whereas the saturated ISHE voltage divided by ΔT_z, which we define as the LSSE coefficient only decreases by one order of magnitude. Therefore, we can attribute the main contribution of the voltage to the LSSE.

In 2013 Ramos et al.[164] investigated the LSSE in magnetite thin films with Pt on top (Fe_3O_4/Pt). This material shows a transition from metallic to an insulator at around 120 K called the *Verwey transition*.[165] This transition can distinguish between a pure LSSE and a mixture of LSSE and ANE according to the temperature below or above the Verwey transition, respectively. Their investigation included measurements in the LSSE configuration with and without Pt on top of the magnetite film with an increased magnitude with a factor of 4 when Pt is on top. Furthermore, when the mean temperature is decreased to 105 K below the Verwey transition the observed voltage is an order of magnitude smaller. In contrast to our work on NFO they managed to also switch the ANE on and off by cooling the sample to temperatures where the Fe_3O_4 is insulating accompanied by a reduction of the LSSE.

Even in 2010 Uchida et al. reported an LSSE in Mn-Zn ferrite ($(Mn,Zn)Fe_2O_4$)[166] a material comparable to NFO. They did measurements at room temperature and used Pt on top as a spin detector for the ISHE. They claimed that the given antisymmetric $V - H$ dependency is generated by the LSSE. An ANE or proximity ANE were not taken into account, they only claimed that the Mn-Zn ferrite is an insulator. In our work on NFO we could show that side effects like the ANE or proximity ANE have to be regarded and neglected in reference measurements until an LSSE can be definitely found to be the dominant effect.

We have also shown the ANE contribution in an NFO film without Pt on top (Fig. 60) which is below 10 % of magnitude compared to the ISHE voltage obtained with Pt on top. Uchida et al.[167] have shown that for single-crystalline YIG/Pt an enhanced magnitude of $V_{\mathrm{sat}}/\Delta T$ around $T_0 = 50\,\mathrm{K}$ appears but is absent for polycrystalline YIG/Pt. They claimed the reason for this enhancement is a phonon mediated process due to an increase of

[164] R. Ramos et al. Applied Physics Letters **102** (2013) 072413

[165] F. Walz. Journal of Physics: Condensed Matter **14** (2002) R285

[166] K. Uchida et al. Applied Physics Letters **97** (2010) 262504

[167] K. Uchida et al. Journal of Applied Physics **111** (2012) 103903

the phonon lifetime around this temperature.[168] An enhanced magnitude could not be observed for NFO/Pt from room temperature down to 50 K using temperature steps of 50 K. The step size was relatively large. Therefore an enhancement of the magnitude could be hidden in the gap of the observed temperatures or below 50 K.

[168] G. A. Slack and D. W. Oliver. Physical Review B **4** (1971) 592

The angle dependent behaviour for the LSSE was shown in Fig. 54 for a fixed temperature difference of $\Delta T_z = 10\,\mathrm{K}$ and various angles α between the magnetic field $\vec{H}$ and the x-direction. The typical LSSE behaviour was produced by the saturated voltage V_{sat} which vanished for a magnetic field parallel to the electrical contacts. However, a symmetric effect with respect to H could be seen for angles α around 90° when H is aligned along the electrical contacts (Fig. 54). This is similar to the observed symmetric effect in YIG/Pt in equal experiments. This symmetric effect is no PNE but a consequence of the magnetization reversal process of the NFO. During this process the voltage measurement is sensitive to the LSSE caused by the projection of the magnetization on the x-axis which fulfils the ISHE configuration.

For NFO we could demonstrate by angle dependent VSM measurements (Fig. 52 (b)) two magnetic easy axes induced by the fourfold magnetic anisotropy of the cubic inverse spinel structure. Hence, for $\alpha = 0°$ the voltage signal for small external magnetic fields H receives a symmetric contribution when the magnetic moment of the NFO change its in-plane orientation and flips into the direction of the next magnetic easy axis. When a small ANE contribution exists in our NFO/Pt films a PNE contribution would be expected even for angles around $\alpha = 0°$ when the magnetization vector $\vec{M}$ rotates into these easy axes. Nevertheless, no PNE could be observed. From this one can infer that unintended Nernst effects such as the PNE are negligibly small in the NFO/Pt films used and that the PNE coefficient for NFO regarding Eq. 17 is too small for this effect to be observed within the measured ISHE voltage.

In conclusion of this chapter, we can summarize our results as follows: we found similar behaviour of NFO/Pt compared to YIG/Pt in comparable TSSE and LSSE experiments. In the longitudinal configuration we have been able to prove the existence of the LSSE resulting in a thermally driven spin current which could be detected. The LSSE was the dominant effect accompanied by a small contribution of the ANE due to thermally activated charge carriers in the NFO. Other side effects due to magnetic proximity effects could be neglected by XRMR measurements.

This knowledge can be used for the experiments in the transverse configuration. Here, the behaviour was in agreement with YIG/Pt. No TSSE could be detected within the same measurement sensitivity limit. The obtained voltage which was antisymmetric with respect to the external magnetic field can be attributed to the LSSE as the dominant effect accompanied by a small contribution of the ANE. Both effects are also driven by an unintended out-of-plane temperature gradient caused by the electrical contacts.

The ferromagnet NFO as well as other spinels are promising candidates as good alternatives to the well established magnetic insulator YIG. Depending on the application, NFO exhibits a few noticeable advantages. For example, with their high Curie temperatures, NFO and other spinels can be used as spin filter materials for applications at room temperature and higher temperatures. In contrast to conventional FM/IN/FM stacks in TMR measurements a magnetic insulator can be placed between an NM and an FM layer. The magnetic insulator acts as a spin valve and a tunnel barrier at the same time. Magnetic insulators are a rising material class in spintronics. Most material systems, especially ferrites and garnets, have already been known for decades. However, their advantages for the investigation of spin currents, spin waves and magnons, at least in magnetic insulators, cannot be denied. Therefore, garnets like YIG and ferrites like NFO will stay in the focus of future research in spintronics and spin caloritronics.

Summary

In conclusion, we can sum up our work as follows: we investigated the spin Seebeck effect in different material systems, i.e., metal, semiconductor and insulator. During these investigations we were confronted with different side effects we had to identify and to disentangle from the intended phenomena of the thermally driven spin current.

In the beginning, Py/Pt bilayers were used and measured in the transverse configuration of the spin Seebeck effect (TSSE). In accordance with other reports presented in Tab. 1 and discussed in the corresponding chapter it can be concluded that there is no detectable TSSE within the measurement sensitivity limit. A previous project showed no improvement by using different interface treatments of the Py/Pt bilayer or different deposition techniques.[169] The dominant and solely appearing voltage contribution was produced by a planar Nernst effect (PNE). The voltage on the spin detector material (Pt) measured as a function of the external magnetic field shows symmetric behaviour which is contrary to the antisymmetric occurrence of the TSSE. The PNE was investigated in more detail; this is the thermally driven counterpart of the AMR, a spin-dependent phenomenon. Therefore, the PNE is a spincaloric effect and a significant element of our work.

[169] D. Meier. MA thesis. Bielefeld University, 2012

Furthermore, the occurrence of spurious out-of-plane temperature gradients was investigated. These contributions of heat flow, which can emerge due to the electrical contacts, the surroundings and the heating conditions, can influence the voltage and can cause an antisymmetric effect with respect to the external magnetic field. This antisymmetric voltage can be misinterpreted as a TSSE. Therefore, we investigated the impact of an intended out-of-plane heat flow by influence over the electrical contacts. We have seen that an antisymmetric voltage contribution can be added to the symmetric part of the PNE only by using thicker contact needles. The larger contact area between Pt and needles

creates a second heat sink for the heat produced. The in-plane heat flow from one sample side to the other generates the PNE. The out-of-plane heat flow from the sample into the needles is the origin of an anomalous Nernst effect (ANE). This effect is also a spin-dependent phenomenon and, therefore, of considerable interest for spincalorics. Furthermore, the ANE is important to understand in terms of SSE experiments, since it can occur as an unintended effect. We were able to identify and disentangle an ANE in our measurements when intentional (or unintentional) out-of-plane heat flows were involved.

In the next step, we investigated the SSE in the magnetic insulator YIG. In this material class we expected to be able to neglect spurious Nernst effects due to the lack of charge carriers. However, due to the spin detector material of Pt on top of the YIG, a magnetic proximity effect was assumed. A spin-polarized region in the Pt at the interface of the bilayer system could lead to proximity induced Nernst effects. This issue was investigated by XRMR, an interface sensitive method for measuring magnetic moments. This method showed no magnetic moment in the Pt within the limit of sensitivity. A controversial discussion with contrary XMCD results reported by other groups does not eliminate this issue completely. However, it could also be shown numerically and experimentally by groups like Schreier et al.[170] and Kikkawa et al.[171] that possible proximity Nernst effects are negligibly small in SSE measurements. Therefore, the expected effects in our measurements in the transverse SSE configuration were the TSSE itself and an LSSE due to spurious out-of-plane heat flow contributions.

[170] M. Schreier et al. Physical Review B **88** (2013) 094410

[171] T. Kikkawa et al. Physical Review Letters **110** (2013) 067207

In the TSSE configuration we were able to show that there is no evidence of any TSSE contribution within the sensitivity limit of the voltage measurement. However, we could again influence the electrical contacts to evoke an antisymmetric voltage with respect to the external magnetic field. This antisymmetric effect could be attributed to the LSSE. A misinterpretation of the observed ISHE voltage as a TSSE is possible when a disentanglement of both effects is not implemented in the investigations. We have shown a detailed procedure of this disentanglement.

Furthermore, the LSSE was investigated in more detail in YIG/Pt bilayers. The results were discussed in the context of the current literature. In conclusion, the LSSE in YIG/Pt is a well established effect which can be used for the investigation of magnetization directions, thermally induced spin currents and, in future, for the investigation of magnetic sublattices in

more complex systems, such as antiferromagnets or compensated ferrimagnets.

In the last experimental chapter we set the focus on NFO/Pt bilayers. The NFO films investigated in this part of our work have shown a semiconducting character. The conductivity which was dominated by thermally activated charge carriers could be reduced drastically by measuring at low temperatures. This gave us the opportunity to investigate the LSSE and ANE in more detail. The ANE could be switched on and off by varying the base temperature. It was shown that the conductivity of the NFO decreases much faster than the LSSE when the temperature drops. The contribution of the ANE in our LSSE measurements at room temperature could be estimated by measurements with and without Pt on top of the NFO. The ANE which was measured on a pure NFO film is in the order of 10 % of the ISHE voltage in an NFO/Pt bilayer. In the TSSE configuration, instead, we could observe the same behaviour compared to YIG/Pt. No TSSE could be found. However, we could influence the measurements via the electrical contacts and obtained an LSSE/ANE combination as was expected after the previous investigations on all material systems.

In sum, our work has shown that there is no evidence for a TSSE in all investigated material classes. Instead, we have shown that spurious contributions of an out-of-plane temperature gradient can result in unintended side effects which are easily misinterpreted as a TSSE. Our investigations have shown that experiments of this kind should be performed in a more careful way, as reported before. Our contributions in this field provide a better insight in the opposing point of view to the very few TSSE reports. Furthermore, the investigation of Nernst effects in ferromagnetic conductors have also contributed to a better understanding of thermally driven charge currents by adding some results of publications in this branch. The investigations of the LSSE in magnetic insulators and semiconductors have led to a better understanding of the characteristics of the effect which leads to a reliable disentanglement of this effect and unintentional side effects.

The LSSE is a well established and powerful tool for the investigation of thermally driven spin currents. Future investigations will focus on magnetic sublattices in, e.g., antiferromagnets or more complex ferrimagnets. At the moment, magnetic insulators or at least semiconductors are the kind of material classes where the LSSE is the dominant effect and the data interpretation is

straightforward. For the investigated NFO films a further important question is still left unanswered which concerns the spin transport. Is the spin transport accomplished by spin polarized charge transport or by magnons? In further work, NFO can be investigated by techniques which can uncover this issue.

The proof of the LSSE in ferromagnetic conductors will be more challenging due to difficult disentanglement of the dominant side effects. The profit of this attempt will benefit material systems like Heusler compounds or multilayer systems which exhibit a bunch of interesting properties for spintronics. This will be part of future investigations.

Bibliography

Agrawal, M., V. I. Vasyuchka, A. A. Serga, A. Kirihara, P. Pirro, T. Langner, M. B. Jungfleisch, A. V. Chumak, E. T. Papaioannou, and B. Hillebrands. *Role of bulk-magnon transport in the temporal evolution of the longitudinal spin-Seebeck effect*. Physical Review B **89** (2014) 224414.

Althammer, M., S. Meyer, H. Nakayama, M. Schreier, S. Altmannshofer, M. Weiler, H. Huebl, S. Geprägs, M. Opel, R. Gross, D. Meier, C. Klewe, T. Kuschel, J.-M. Schmalhorst, G. Reiss, L. Shen, A. Gupta, Y.-T. Chen, G. E. W. Bauer, E. Saitoh, and S. T. B. Goennenwein. *Quantitative study of the spin Hall magnetoresistance in ferromagnetic insulator/normal metal hybrids*. Physical Review B **87** (2013) 224401.

Ando, K., S. Fujita, J. Ito, S. Yuasa, Y. Suzuki, Y. Nakatani, T. Miyazaki, and H. Yoda. *Spin-transfer torque magnetoresistive random-access memory technologies for normally off computing (invited)*. Journal of Applied Physics **115** (2014) 172607.

Antel, W. J., M. M. Schwickert, T. Lin, W. L. O'Brien, and G. R. Harp. *Induced ferromagnetism and anisotropy of Pt layers in Fe/Pt* (001) *multilayers*. Physical Review B **60** (1999) 12933.

Avery, A., M. Pufall, and B. Zink. *Observation of the Planar Nernst Effect in Permalloy and Nickel Thin Films with In-Plane Thermal Gradients*. Physical Review Letters **109** (2012) 196602.

Bader, S. D. and S. S. P. Parkin. *Spintronics*. Annual Review of Condensed Matter Physics **1** (2010) 71.

Baibich, M. N., J. M. Broto, A. Fert, F. Nguyen van Dau, F. Petroff, P. Etienne, G. Creuzet, A. Friederich, and J. Chazelas. *Giant magnetoresistance of (*001*)Fe/(*001*)Cr magnetic superlattices*. Physical Review Letters **61** (1988) 2472.

Balaji, S., R. Kalai Selvan, L. John Berchmans, S. Angappan, K. Subramanian, and C. O. Augustin. *Combustion synthesis and characterization of Sn^{4+} substituted nanocrystalline $NiFe_2O_4$*. Materials Science and Engineering: B **119** (2005) 119.

Bauer, G. E. W., E. Saitoh, and B. J. van Wees. *Spin caloritronics*. Nature Materials **11** (2012) 391.

Berger, L. *Side-jump mechanism for the Hall effect of ferromagnets*. Physical Review B **2** (1970) 4559.

Binasch, G., P. Grunberg, F. Saurenbach, and W. Zinn. *Enhanced Magnetoresistance in Layered Magnetic-Structures with Antiferromagnetic Interlayer Exchange*. Physical Review B **39** (1989) 4828.

Bosu, S., Y. Sakuraba, K. Uchida, K. Saito, T. Ota, E. Saitoh, and K. Takanashi. *Spin Seebeck effect in thin films of the Heusler compound Co_2MnSi*. Physical Review B **83** (2011) 224401.

Brataas, A., Y. Tserkovnyak, G. E. W. Bauer, and P. J. Kelly. *Spin Pumping and Spin Transfer*. arXiv.org (2011). arXiv: 1108.0385.

Chang, H., P. Li, W. Zhang, T. Liu, A. Hoffmann, L. Deng, and M. Wu. *Nanometer-Thick Yttrium Iron Garnet Films With Extremely Low Damping*. IEEE Magnetics Letters **5** (2014) 6700104.

Chikazumi, S. *Study of Magnetic Annealing on Ni_3Fe Single Crystal*. Journal of the Physical Society of Japan **11** (1956) 551.

Chumak, A. V., A. A. Serga, and B. Hillebrands. *Magnon transistor for all-magnon data processing*. Nature Communications **5** (2014) 4700.

Costache, M. V., M. Sladkov, S. M. Watts, C. H. van der Wal, and B. J. van Wees. *Electrical Detection of Spin Pumping due to the Precessing Magnetization of a Single Ferromagnet*. Physical Review Letters **97** (2006) 216603.

De Groot, F. M. F. *X-ray absorption and dichroism of transition metals and their compounds*. Journal of electron spectroscopy and related phenomena **67** (1994) 94.

Della Coletta, F., M. Opel, S. Geprägs, C. Klewe, and T. Kuschel. *ESRF annual report*. ESRF annual report, HC-1500, 2014.

Dillinger, Joy F. and R. M. Bozorth. *Heat Treatment of Magnetic Materials in a Magnetic Field I. Survey of Iron-Cobalt-Nickel Alloys*. Physics **6** (1935) 279.

Dionne, Gerald F. *Molecular-field coefficients of $MnFe_2O_4$ and $NiFe_2O_4$ spinel ferrite systems*. Journal of Applied Physics **63** (1988) 3777.

Dolia, S. N., R. Sharma, M. P. Sharma, and N. S. Saxena. *Synthesis, X-ray diffraction and optical band gap study of nanoparticles of $NiFe_2O_4$*. Indian Journal of Pure and Applied Physics **44** (2006) 774.

Dyakonov, M. I. and V. I. Perel. *Current-Induced Spin Orientation of Electrons in Semiconductors*. Physics Letters A **A 35** (1971) 459.

— *Possibility of Orienting Electron Spins with Current*. JETP Letters **13** (1971) 467.

Ettingshausen, A. von and W. Nernst. *Ueber das Auftreten electromotorischer Kraefte in Metallplatten, welche von einem Waermestrome durchflossen werden und sich im magnetischen Felde befinden*. Annalen der Physik **265** (1886) 343.

Feng, Z., J. Hu, L. Sun, B. You, D. Wu, J. Du, W. Zhang, A. Hu, Y. Yang, D. M. Tang, B. S. Zhang, and H. F. Ding. *Spin Hall angle quantification from spin pumping and microwave photoresistance*. Physical Review B **85** (2012) 214423.

Flipse, J., F. L. Bakker, A. Slachter, F. K. Dejene, and B. J. van Wees. *Direct observation of the spin-dependent Peltier effect*. Nature Nanotechnology **7** (2012) 166.

Fritsch, D. and C. Ederer. *Epitaxial strain effects in the spinel ferrites $CoFe_2O_4$ and $NiFe_2O_4$ from first principles*. Physical Review B **82** (2010) 104117.

Geissler, J., E. Goering, M. Justen, F. Weigand, G. Schütz, J. Langer, D. Schmitz, H. Maletta, and R. Mattheis. *Pt magnetization profile in a Pt/Co bilayer studied by resonant magnetic x-ray reflectometry*. Physical Review B **65** (2001) 020405.

Geprägs, S., A. Kehlberger, T. Schulz, C. Mix, F. Della Coletta, S. Meyer, A. Kamra, M. Althammer, G. Jakob, H. Huebl, R. Gross, S. T. B. Goennenwein, and M. Kläui. *Origin of the spin Seebeck effect probed by temperature dependent measurements in $Gd_3Fe_5O_{12}$*. arXiv.org (2014). arXiv: 1405.4971v1.

Geprägs, S., S. Meyer, S. Altmannshofer, M. Opel, F. Wilhelm, A. Rogalev, R. Gross, and S. T. B. Goennenwein. *Investigation of induced Pt magnetic polarization in $Pt/Y_3Fe_5O_{12}$ bilayers*. Applied Physics Letters **101** (2012) 262407.

Gilbert, T. L. *Classics in Magnetics A Phenomenological Theory of Damping in Ferromagnetic Materials*. Magnetics, IEEE Transactions on **40** (2004) 3443.

GmbH, CrysTec. *MgO data sheet*. http://www.crystec.de/daten/mgo.pdf. [Online; accessed 03-February-2015]. 2015.

— *Sapphire data sheet*. http://www.crystec.de/daten/al2o3.pdf. [Online; accessed 03-February-2015]. 2015.

Gu, M., X. Li, and Y. Cao. *Optical storage arrays: a perspective for future big data storage*. Light: Science & Applications **3** (2014) e177.

Guo, G. Y., Q. Niu, and N. Nagaosa. *Anomalous Nernst and Hall effects in magnetized platinum and palladium*. Physical Review B **89** (2014) 214406.

Haetge, J., C. Suchomski, and T. Brezesinski. *Ordered Mesoporous MFe_2O_4 (M = Co, Cu, Mg, Ni, Zn) Thin Tilms with Nanocrystalline Walls, Uniform* 16 *nm Diameter Pores and High Thermal*

Stability: Template-Directed Synthesis and Characterization of Redox Active Trevorite. Inorganic chemistry **49** (2010) 11619.

Hall, E. H. *On a new action of the magnet on electric currents*. American Journal of Mathematics **2** (1879) 287.

— *XXXVIII. On the new action of magnetism on a permanent electric current*. The London, Edinburgh, and Dublin Philosophical Magazine and Journal of Science **10** (1880) 301.

Heinrich, B., Y. Tserkovnyak, G. Woltersdorf, A. Brataas, R. Urban, and G. E. W. Bauer. *Dynamic exchange coupling in magnetic bilayers*. Physical Review Letters **90** (2003) 187601.

Hirsch, J. E. *Spin hall effect*. Physical Review Letters **83** (1999) 1834.

Ho, C. Y., M. W. Ackerman, K. Y. Wu, S. G. Oh, and T. N. Havill. *Thermal conductivity of ten selected binary alloy systems*. Journal of Physical and Chemical Reference Data **7** (1978) 959.

Hoffmann, A. *Spin Hall Effects in Metals*. Magnetics, IEEE Transactions on **49** (2013) 5172.

Huang, S. Y., W. G. Wang, S. F. Lee, J. Kwo, and C. L. Chien. *Intrinsic spin-dependent thermal transport*. Physical Review Letters **107** (2011) 216604.

Ikeda, S., J. Hayakawa, Y. Ashizawa, Y. M. Lee, K. Miura, H. Hasegawa, M. Tsunoda, F. Matsukura, and H. Ohno. *Tunnel magnetoresistance of* 604 *at* 300*K by suppression of Ta diffusion in CoFeB/MgO/CoFeB pseudo-spin-valves annealed at high temperature*. Applied Physics Letters **93** (2008) 082508.

Inoue, H. Y., K. Harii, K. Ando, K. Sasage, and E. Saitoh. *Detection of pure inverse spin-Hall effect induced by spin pumping at various excitation*. Journal of Applied Physics **102** (2007) 083915.

Jaworski, C. M., J. Yang, S. Mack, D. D. Awschalom, J. P. Heremans, and R. C. Myers. *Observation of the spin-Seebeck effect in a ferromagnetic semiconductor*. Nature Materials **9** (2010) 898.

Jiles, D. C. *Introduction to Magnetism and Magnetic Materials, Second Edition*. Introduction to Magnetism and Magnetic Materials, Second Edition, CRC Press, 1998.

Julliere, M. *Tunneling Between Ferromagnetic-Films*. Physics Letters A **54** (1975) 225.

Jungwirth, T., Q. Niu, and A. H. MacDonald. *Anomalous Hall effect in ferromagnetic semiconductors*. Physical Review Letters (2001) 207208.

Kajiwara, Y., K. Harii, S. Takahashi, J. Ohe, K. Uchida, M. Mizuguchi, H. Umezawa, H. Kawai, K. Ando, K. Takanashi, S Maekawa, and E.. Saitoh. *Transmission of electrical signals by spin-wave interconversion in a magnetic insulator*. Nature **464** (2010) 262.

Kato, Y. K., R. C. Myers, A. C. Gossard, and D. D. Awschalom. *Observation of the Spin Hall Effect in Semiconductors*. Science **306** (2004) 1910.

Kehlberger, A., G. Jakob, M. C. Onbasli, D. H. Kim, C. A. Ross, and M. Kläui. *Investigation of the magnetic properties of insulating thin films using the longitudinal spin Seebeck effect*. Journal of Applied Physics **115** (2014) 17C731.

Kehlberger, A., R. Röser, G. Jakob, U. Ritzmann, D. Hinzke, U. Nowak, M. C. Onbasli, D. H. Kim, C. A. Ross, M. B. Jungfleisch, B. Hillebrands, and M. Kläui. *Determination of the origin of the spin Seebeck effect - bulk vs. interface effects*. arXiv.org (2013). arXiv: 1306.0784v1.

Kikkawa, T., K. Uchida, Y. Shiomi, Z. Qiu, D. Hou, D. Tian, H. Nakayama, X. F. Jin, and E. Saitoh. *Longitudinal spin Seebeck effect free from the proximity Nernst effect*. Physical Review Letters **110** (2013) 067207.

Klewe, C., M. Meinert, A. Boehnke, K. Kuepper, E. Arenholz, A. Gupta, J. M. Schmalhorst, T. Kuschel, and G. Reiss. *Physical characteristics and cation distribution of $NiFe_2O_4$ thin films with high resistivity prepared by reactive co-sputtering*. Journal of Applied Physics **115** (2014) 123903.

Kuschel, T., C. Klewe, J.-M. Schmalhorst, F. Bertram, O. Kuschel, T. Schemme, J. Wollschläger, S. Francoual, J. Strempfer, A. Gupta, M. Meinert, G. Götz, D. Meier, and G. Reiss. *Static Magnetic Proximity Effect in Pt/$NiFe_2O_4$ and Pt/Fe Bilayers Investigated by X-Ray Resonant Magnetic Reflectivity*. Physical Review Letters **115** (2015) 097401.

Ky, V. D. *The Planar Nernst Effect in Permalloy Films*. physica status solidi (b) **17** (1966) K207.

Landau, L. D. and E. Lifshitz. *On the theory of the dispersion of magnetic permeability in ferromagnetic bodies*. Phys. Z. Sowjet. **8** (1935) 153.

Leven, B., A. V. Chumak, and B. Hillebrands. *Magnonen für den Computer von Übermorgen*. Physik in unserer Zeit **46** (2015) 34.

Li, N., Y.-H. A. Wang, M. N. Iliev, T. M. Klein, and A. Gupta. *Growth of Atomically Smooth Epitaxial Nickel Ferrite Films by Direct Liquid Injection CVD*. Chemical Vapor Deposition **17** (2011) 261.

Liu, H., Y. Honda, T. Taira, K. Matsuda, M. Arita, T. Uemura, and M. Yamamoto. *Giant tunneling magnetoresistance in epitaxial Co2MnSi/MgO/Co2MnSi magnetic tunnel junctions by half-metallicity of Co2MnSi and coherent tunneling*. Applied Physics Letters **101** (2012) 132418.

Liu, L., C. F. Pai, Y. Li, H. W. Tseng, D. C. Ralph, and R. A. Buhrman. *Spin-Torque Switching with the Giant Spin Hall Effect of Tantalum*. Science **336** (2012) 555.

Liu, T., H. Chang, V. Vlaminck, Y. Sun, M. Kabatek, A. Hoffmann, L. Deng, and M. Wu. *Ferromagnetic resonance of sputtered yttrium iron garnet nanometer films*. Journal of Applied Physics **115** (2014) 17A501.

Lu, Y. M., Y. Choi, C. M. Ortega, X. M. Cheng, J. W. Cai, S. Y. Huang, L. Sun, and C. L. Chien. *Pt Magnetic Polarization on $Y_3Fe_5O_{12}$ and Magnetotransport Characteristics*. Physical Review Letters **110** (2013) 147207.

Macke, S. and E. Goering. *Magnetic reflectometry of heterostructures*. Journal of Physics: Condensed Matter **26** (2014) 363201.

Meier, D. *Erste Untersuchungen zum spin Seebeck effect in Dünnschichtsystemen*. MA thesis. Bielefeld University, 2012.

Meier, D., T. Kuschel, L. Shen, A. Gupta, T. Kikkawa, K. Uchida, E. Saitoh, J. M. Schmalhorst, and G. Reiss. *Thermally driven spin and charge currents in thin $NiFe_2O_4$/Pt films*. Physical Review B **87** (2013) 054421.

Meier, D., D. Reinhardt, M. Schmid, C. H. Back, J.-M. Schmalhorst, T. Kuschel, and G. Reiss. *Influence of heat flow directions on Nernst effects in Py/Pt bilayers*. Physical Review B **88** (2013) 184425.

Meier, D., D. Reinhardt, M. van Straaten, C. Klewe, M. Althammer, M. Schreier, S. T. B. Goennenwein, A. Gupta, M. Schmid, C. H. Back, J.-M. Schmalhorst, T. Kuschel, and G. Reiss. *Longitudinal spin Seebeck effect contribution in transverse spin Seebeck effect experiments in Pt/YIG and Pt/NFO*. Nature Communications **6** (2015) 8211.

Mosendz, O., J. E. Pearson, F. Y. Fradin, G. E. W. Bauer, S. D. Bader, and A. Hoffmann. *Quantifying Spin Hall Angles from Spin Pumping: Experiments and Theory*. Physical Review Letters **104** (2010) 046601.

Mosendz, O., V. Vlaminck, J. E. Pearson, F. Y. Fradin, G. E. W. Bauer, S. D. Bader, and A. Hoffmann. *Detection and quantification of inverse spin Hall effect from spin pumping in permalloy/normal metal bilayers*. Physical Review B **82** (2010) 214403.

Mott, N. F. *The Electrical Conductivity of Transition Metals*. In: *Proceedings of the Royal Society of London. Series A*. Vol. 153. 1936 699.

Murakami, S. *Spin Hall Effect in p-type Semiconductors*. arXiv.org (2004). arXiv: 0405003v1.

Nagaosa, N., J. Sinova, S. Onoda, A. H. MacDonald, and N. P. Ong. *Anomalous Hall effect*. Reviews of Modern Physics **82** (2010) 1539.

Nakayama, H., M. Althammer, Y. T. Chen, K. Uchida, Y. Kajiwara, D. Kikuchi, T. Ohtani, S. Geprägs, M. Opel, S. Takahashi, R. Gross, G. E. W. Bauer, S. T. B. Goennenwein, and E. Saitoh. *Spin Hall Magnetoresistance Induced by a Nonequilibrium Proximity Effect*. Physical Review Letters **110** (2013) 206601.

Obstbaum, M., M. Härtinger, H. G. Bauer, T. Meier, F. Swientek, C. H. Back, and G. Woltersdorf. *Inverse spin Hall effect in Ni81Fe19/normal-metal bilayers*. Physical Review B **89** (2014) 060407.

Ohnuma, Y., H. Adachi, E. Saitoh, and S. Maekawa. *Spin Seebeck effect in antiferromagnets and compensated ferrimagnets*. Physical Review B **87** (2013) 014423.

Onsager, L. *Reciprocal relations in irreversible processes. I.* Physical Review **37** (1931) 405.

Paoletti, A. *Physics of Magnetic Garnets: Proceedings of the International School of Physics "Enrico Fermi", Course 70, Varenna on Lake Como, 27th June - 9th July 1977*. Physics of Magnetic Garnets (1978).

Parkin, S. and S.-H. Yang. *Memory on the racetrack*. Nature Nanotechnology **10** (2015) 195.

Popova, E., N. Keller, F. Jomard, L. Thomas, M. C. Brianso, F. Gendron, M. Guyot, and M. Tessier. *Exchange coupling in ultrathin epitaxial yttrium iron garnet films*. The European Physical Journal B **31** (2003) 69.

Rai, R. C., S. Wilser, M. Guminiak, B. Cai, and M. L. Nakarmi. *Optical and electronic properties of $NiFe_2O_4$ and $CoFe_2O_4$ thin films*. Applied Physics A **106** (2012) 207.

Ralph, D. C. and M. D. Stiles. *Spin transfer torques*. Journal of magnetism and magnetic materials **320** (2008) 1190.

Ramos, R., T. Kikkawa, K. Uchida, H. Adachi, I. Lucas, M. H. Aguirre, P. Algarabel, L. Morellon, S. Maekawa, E. Saitoh, and M. R. Ibarra. *Observation of the spin Seebeck effect in epitaxial Fe_3O_4 thin films*. Applied Physics Letters **102** (2013) 072413.

Ramsey, T. H. *Summary of Some Properties of Yttrium Iron Garnet and Study of Dislocations Observed in an Yttrium Iron Garnet Crystal*. Journal of the American Ceramic Society **42** (1959) 645.

Roschewsky, N., M. Schreier, A. Kamra, F. Schade, K. Ganzhorn, S. Meyer, H. Huebl, S. Geprägs, R. Gross, and S. T. B. Goen-

nenwein. *Time resolved spin Seebeck effect experiments*. Applied Physics Letters **104** (2014) 202410.

Saitoh, E., M. Ueda, H. Miyajima, and G. Tatara. *Conversion of spin current into charge current at room temperature: Inverse spin-Hall effect*. Applied Physics Letters **88** (2006) 182509.

Sanders, D. and D. Walton. *Effect of magnon-phonon thermal relaxation on heat transport by magnons*. Physical Review B **15** (1977) 1489.

Schmid, M., S. Srichandan, D. Meier, T. Kuschel, J.-M. Schmalhorst, M. Vogel, G. Reiss, C. Strunk, and C. H. Back. *Transverse Spin Seebeck Effect versus Anomalous and Planar Nernst Effects in Permalloy Thin Films*. Physical Review Letters **111** (2013) 187201.

Schreier, M., G. E. W. Bauer, V. I. Vasyuchka, J. Flipse, K. Uchida, J. Lotze, V. Lauer, A. V. Chumak, A. A. Serga, S. Daimon, T. Kikkawa, E. Saitoh, B. J. van Wees, B. Hillebrands, R. Gross, and S. T. B. Goennenwein. *Sign of inverse spin Hall voltages generated by ferromagnetic resonance and temperature gradients in yttrium iron garnet platinum bilayers*. Journal of Physics D: Applied Physics (2014) 025001.

Schreier, M., A. Kamra, M. Weiler, J. Xiao, G. E. W. Bauer, R. Gross, and S. T. B. Goennenwein. *Magnon, phonon, and electron temperature profiles and the spin Seebeck effect in magnetic insulator/normal metal hybrid structures*. Physical Review B **88** (2013) 094410.

Schreier, M., N. Roschewsky, E. Dobler, S. Meyer, H. Huebl, R. Gross, and S. T. B. Goennenwein. *Current heating induced spin Seebeck effect*. Applied Physics Letters **103** (2013) 242404.

Schütz, G., W. Wagner, W. Wilhelm, P. Kienle, R. Zeller, R. Frahm, and G. Materlik. *Absorption of circularly polarized x rays in iron*. Physical Review Letters **58** (1987) 737.

Seebeck, T. J. *Magnetische Polarisation der Metalle und Erze durch Temperatur-Differenz*. Abh. Akad. Wiss. Berlin **1822** (1820-21) 189.

Serga, A. A., A. V. Chumak, and B. Hillebrands. *YIG magnonics*. J. Phys. D: Appl. Phys. **43** (2010) 264002.

Siegel, G., M. C. Prestgard, S. Teng, and A. Tiwari. *Robust longitudinal spin-Seebeck effect in Bi-YIG thin films*. Scientific Reports **4** (2014) 4429.

Sinova, J., D. Culcer, Q. Niu, N. A. Sinitsyn, T. Jungwirth, and A. H. MacDonald. *Universal intrinsic spin Hall effect*. Physical Review Letters **92** (2004) 126603.

Slack, G. A. and D. W. Oliver. *Thermal conductivity of garnets and phonon scattering by rare-earth ions*. Physical Review B **4** (1971) 592.

Slaughter, J. M. *Materials for Magnetoresistive Random Access Memory*. Annual Review of Materials Research **39** (2009) 277.

Slonczewski, J. C. *Current-driven excitation of magnetic multilayers*. Journal of magnetism and magnetic materials **159** (1995) L1.

Smit, J. *The Spontaneous Hall Effect in Ferromagnetics II*. Physica **24** (1958) 39.

Soldatov, I. V., N. Panarina, C. Hess, L. Schultz, and R. Schäfer. *Thermoelectric effects and magnetic anisotropy of GaMnAs thin films*. Physical Review B **90** (2014) 104423.

Stoner, E. C. *Collective Electron Ferromagnetism*. In: *Proceedings of the Royal Society of London. Series A*. 1938 372.

Sun, Q.-C., H. Sims, D. Mazumdar, J. X. Ma, B. S. Holinsworth, K. R. O'Neal, G. Kim, W. H. Butler, A. Gupta, and J. L. Musfeldt. *Optical band gap hierarchy in a magnetic oxide: Electronic structure of $NiFe_2O_4$*. Physical Review B **86** (2012) 205106.

Thompson, D. A., L. T. Romankiw, and A. Mayadas. *Thin film magnetoresistors in memory, storage, and related applications*. Magnetics, IEEE Transactions on **11** (1975) 1039.

Tserkovnyak, Y., A. Brataas, and G. E. W. Bauer. *Enhanced gilbert damping in thin ferromagnetic films*. Physical Review Letters **88** (2002) 117601.

Uchida, K., H. Adachi, T. Ota, H. Nakayama, S. Maekawa, and E. Saitoh. *Observation of longitudinal spin-Seebeck effect in magnetic insulators*. Applied Physics Letters **97** (2010) 172505.

Uchida, K., T. Nonaka, T. Kikkawa, Y. Kajiwara, and E. Saitoh. *Longitudinal spin Seebeck effect in various garnet ferrites*. Physical Review B **87** (2013) 104412.

Uchida, K., T. Nonaka, T. Ota, and E. Saitoh. *Longitudinal spin-Seebeck effect in sintered polycrystalline (Mn,Zn)Fe_2O_4*. Applied Physics Letters **97** (2010) 262504.

Uchida, K., T. Ota, H. Adachi, J. Xiao, T. Nonaka, Y. Kajiwara, G. E. W. Bauer, S. Maekawa, and E. Saitoh. *Thermal spin pumping and magnon-phonon-mediated spin-Seebeck effect*. Journal of Applied Physics **111** (2012) 103903.

Uchida, K., T. Ota, K. Harii, K. Ando, H. Nakayama, and E. Saitoh. *Electric detection of the spin-Seebeck effect in ferromagnetic metals (invited)*. Journal of Applied Physics **107** (2010) 09A951.

Uchida, K., S. Takahashi, K. Harii, J. Ieda, W. Koshibae, K. Ando, S. Maekawa, and E. Saitoh. *Observation of the spin Seebeck effect*. Nature **455** (2008) 778.

Uchida, K., J. Xiao, H. Adachi, J. Ohe, S. Takahashi, J. Ieda, T. Ota, Y. Kajiwara, H. Umezawa, H. Kawai, G. E. W. Bauer, S. Maekawa, and E. Saitoh. *Spin Seebeck insulator*. Nature Materials **9** (2010) 894.

Waldron, R. D. *Infrared spectra of ferrites*. Physical Review **99** (1955) 1727.

Walz, F. *The Verwey transition - a topical review*. Journal of Physics: Condensed Matter **14** (2002) R285.

Wang, S. H., L. K. Zou, J. W. Cai, B. G. Shen, and J. R. Sun. *Transverse thermoelectric effects in platinum strips on permalloy films*. Physical Review B **88** (2013) 214304.

Wegrowe, J. E., H. J. Drouhin, and D. Lacour. *Anisotropic magnetothermal transport and spin Seebeck effect*. Physical Review B **89** (2014) 094409.

Wei, D., M. Obstbaum, M. Ribow, C. H. Back, and G. Woltersdorf. *Spin Hall voltages from a.c. and d.c. spin currents*. Nature Communications **5** (2014) 3768.

Weiler, M., M. Althammer, F. Czeschka, H. Huebl, M. Wagner, M. Opel, I.-M. Imort, G. Reiss, A. Thomas, R. Gross, and S. T. B. Goennenwein. *Local Charge and Spin Currents in Magnetothermal Landscapes*. Physical Review Letters **108** (2012) 106602.

Wilhelm, F., P. Poulopoulos, G. Ceballos, H. Wende, K. Baberschke, P. Srivastava, D. Benea, H. Ebert, M. Angelakeris, N. K. Flevaris, D. Niarchos, A. Rogalev, and N. B. Brookes. *Layer-resolved magnetic moments in Ni/Pt multilayers*. Physical Review Letters **85** (2000) 413.

Wunderlich, J., B. Kaestner, J. Sinova, and T. Jungwirth. *Experimental Observation of the Spin-Hall Effect in a Two-Dimensional Spin-Orbit Coupled Semiconductor System*. Physical Review Letters **94** (2005) 047204.

Xiao, J., G. E. W. Bauer, K. Uchida, E. Saitoh, and S. Maekawa. *Theory of magnon-driven spin Seebeck effect*. Physical Review B **81** (2010) 214418.

Yager, W. A., J. K. Galt, F. R. Merritt, and E. A. Wood. *Ferromagnetic Resonance in Nickel Ferrite*. Physical Review **80** (1950) 744.

Zhang, Q., S. Hikino, and S. Yunoki. *First-principles study of the spin-mixing conductance in Pt/$Ni_{81}Fe_{19}$ junctions*. Applied Physics Letters **99** (2011) 172105.

Publications and conferences

Publications

1. **D. Meier**, T. Kuschel, L. Shen, A. Gupta, T. Kikkawa, K. Uchida, E. Saitoh, J.-M. Schmalhorst, G. Reiss: *Thermally driven spin and charge currents in thin $NiFe_2O_4$/Pt films*, Physical Review B **88**, 054421 (2013)

2. M. Althammer, S. Meyer, H. Nakayama, M. Schreier, S. Altmannshofer, M. Weiler, H. Huebl, S. Geprags, M. Opel, R. Gross, **D. Meier**, C. Klewe, T. Kuschel, J.-M. Schmalhorst, G. Reiss, L. Shen, A. Gupta, Y. T. Chen, G. E. W. Bauer, E. Saitoh, S. T. B. Goennenwein: *Quantitative study of the spin Hall magnetoresistance in ferromagnetic insulator/normal metal hybrids*, Physical Review B **87**, 224401 (2013)

3. M. Schmid, S. Srichandan, **D. Meier**, T. Kuschel, J.-M. Schmalhorst, M. Vogel, G. Reiss, C. Strunk, C. H. Back: *Transverse Spin Seebeck Effect versus Anomalous and Planar Nernst Effects in Permalloy Thin Films*, Physical Review Letters **111**, 187201 (2013)

4. **D. Meier**, D. Reinhardt, M. Schmid, C. H. Back, J.-M. Schmalhorst, T. Kuschel, G. Reiss: *Influence of heat flow directions on Nernst effects in Py/Pt bilayers*, Physical Review B **88**, 184425 (2013)

5. L. Marnitz, K. Rott, S. Niehörster, C. Klewe, **D. Meier**, S. Fabretti, M. Witziok, A. Krampf, O. Kuschel, T. Schemme, K. Kuepper, J. Wollschläger, A. Thomas, G. Reiss, T. Kuschel: *Sign change in the tunnel magnetoresistance of Fe_3O_4/MgO/Co-Fe-B magnetic tunnel junctions depending on the annealing temperature and the interface treatment*, AIP Advances **5**, 047103 (2015)

6. T. Kuschel, C. Klewe, J.-M. Schmalhorst, F. Bertram, O. Kuschel, T. Schemme, J. Wollschläger, S. Francoual, J. Strempfer, A. Gupta, M. Meinert, G. Götz, **D. Meier**, G. Reiss: *Static Magnetic Proximity Effect in Pt/$NiFe_2O_4$ and Pt/Fe Bilayers Investigated by X-Ray Resonant Magnetic Reflectivity*, Physical Review Letters **115**, 097401 (2015)

7. **D. Meier**, D. Reinhardt, M. van Straaten, C. Klewe, M. Althammer, S. T. B. Goennenwein, A. Gupta, M. Schmid, C. H. Back, J.-M. Schmalhorst, T. Kuschel, G. Reiss: *Longitudinal spin Seebeck effect contribution in transverse spin Seebeck effect experiments in Pt/YIG and Pt/NFO*, Nature Communications **6**, 8211 (2015)

Conferences

2012

1. D. Meier, T. Kuschel, H. Meyer zu Theenhausen, J.-M. Schmalhorst, G. Reiss: *Realization of an experimental setup for temperature dependent measurements of the Spin Seebeck Effect*, DPG spring meeting, Berlin (2012), Poster MA 52.61

2. D. Meier, T. Kuschel, H. Meyer zu Theenhausen, J.-M. Schmalhorst, G. Reiss: *Realization of an experimental setup for temperature dependent measurements of the Spin Seebeck Effect*, 1st SpinCaT PhD Workshop, Regensburg (2012), Poster

3. D. Meier, T. Kuschel, T. Kikkawa, K. Uchida, E. Saitoh, J.-M. Schmalhorst, G. Reiss: *Recent results of permalloy thin films obtained in a setup for transverse spin Seebeck effect measurements*, Spin Caloritronics 4, Sendai (2012), Poster

4. D. Meier, T. Kuschel, L. Shen, A. Gupta, T. Kikkawa, K. Uchida, E. Saitoh, J.-M. Schmalhorst, G. Reiss: *Investigations of the longitudinal spin Seebeck effect in $NiFe_2O_4$/Pt films*, International Workshop on Spin Phenomena in Reduced Dimensions, Regensburg (2012), Poster

5. D. Meier, T. Kuschel, L. Shen, A. Gupta, T. Kikkawa, K. Uchida, E. Saitoh, J.-M. Schmalhorst, G. Reiss: *Recent results of longitudinal spin Seebeck effect measurements on $NiFe_2O_4$/Pt films*, 2nd SpinCaT PhD Workshop, Göttingen (2012), Talk

2013

6. D. Meier, T. Kuschel, L. Shen, A. Gupta, T. Kikkawa, K. Uchida, E. Saitoh, J.-M. Schmalhorst, G. Reiss: *Longitudinal spin Seebeck effect and anomalous Nernst effect in $NiFe_2O_4$/Pt films*, 510. WE-Heraeus-Seminar, Non-Magnetic Control of Spin, Bad Honnef (2013), Poster

7. D. Meier, T. Kuschel, L. Shen, A. Gupta, T. Kikkawa, K. Uchida, E. Saitoh, J.-M. Schmalhorst, G. Reiss: *Longitudinal spin Seebeck effect and anomalous Nernst effect in $NiFe_2O_4$/Pt films*, DPG spring meeting, Regensburg (2013), Talk MA 9.4

8. D. Meier, D. Reinhardt, M. Schmid, L. Shen, A. Gupta, T. Kikkawa, K. Uchida, E. Saitoh, C. H. Back, J.-M. Schmalhorst, T. Kuschel, G. Reiss: *The influence of the anomalous*

Nernst effect in spin Seebeck effect measurements, 3rd SpinCaT PhD Workshop, Dresden (2013), Talk

9. D. Meier, D. Reinhardt, T. Matalla-Wagner, C. Klewe, J.-M. Schmalhorst, T. Kuschel, G. Reiss: *Influence of heat flow directions on Nernst effects in magnetic thin films*, Workshop: Spin caloritronics in insulators, Mainz (2013), Poster

2014

10. D. Meier, D. Reinhardt, M. Schmid, C. H. Back, J.-M. Schmalhorst, T. Kuschel, G. Reiss: *Influence of heat flow directions on Nernst effects in Py/Pt bilayers*, DPG spring meeting, Dresden (2014), Talk MA 36.10

11. D. Meier, D. Reinhardt, M. Schmid, C. H. Back, J.-M. Schmalhorst, T. Kuschel, G. Reiss: *Influence of heat flow directions on Nernst effects in Py/Pt bilayers*, IEEE International Magnetics Conference, INTERMAG, Dresden (2014), Poster AS-11

12. D. Meier, D. Reinhardt, M. van Straaten, C. Klewe, M. Schmid, C. H. Back, M. Althammer, S. T. B. Goennenwein, A. Gupta, J.-M. Schmalhorst, T. Kuschel, G. Reiss: *LSSE and Nernst effects in TSSE measurements on YIG/Pt, NFO/Pt and Py/Pt bilayers*, Spin Caloritronics 6, Bad Irsee (2014), Poster

13. D. Meier, D. Reinhardt, M. van Straaten, C. Klewe, M. Althammer, S. T. B. Goennenwein, A. Gupta, M. Schmid, C. H. Back, J.-M. Schmalhorst, T. Kuschel, G. Reiss: *Contributing longitudinal spin Seebeck effect in transverse spin Seebeck effect experiments in YIG/Pt and NFO/Pt*, 59th Annual Magnetism & Magnetic Materials Conference, Honolulu (2014), Talk HB-10

2015

14. D. Meier, D. Reinhardt, M. van Straaten, C. Klewe, J.-M. Schmalhorst, T. Kuschel, G. Reiss, M. Althammer, M. Schreier, S.T.B. Goennenwein, M. Schmid. C.H. Back, A. Gupta: *Longitudinal spin Seebeck effect contribution in transverse spin Seebeck effect experiments in YIG/Pt and NFO/Pt*, DPG spring meeting, Berlin (2015), Talk MA 29.6

Danksagung

Ich möchte hier allen Menschen danken, die mich bei der Erstellung dieser Arbeit unterstützt haben. Allen voran möchte ich mich bei meinem Doktorvater Prof. Dr. Günter Reiss und bei Dr. Jan Schmalhorst bedanken, für die sehr spannende Aufgabenstellung, die hervorragende Betreuung und die aufschlußreichen wissenschaftlichen Diskussionen.

Ich danke Dr. Timo Kuschel für seine exzellente Betreuung, für sehr gutes Teamwork und für seine hilfreiche Unterstützung während der gesamten Zeit. Für das sehr gute Teamwork danke ich ebenfalls Christoph Klewe und Alexander Böhnke, mit denen zusammen ich das Thema Spinkalorik als Doktoranden geteilt habe.

Für die Betreuung und Instandhaltung nahezu aller Laborgeräte und den damit verbundenen Hilfestellungen danke ich Dr. Karsten Rott. Für jegliche Arbeit mit der Verwaltung, Bestellungen und Formalien danke ich Aggi Windmann. Für alle meine Fragen bezüglich des Layouts dieser Arbeit danke ich Dr. Andy Thomas.

Ich bedanke mich bei all den tollen Kollegen, die mir in den letzten Jahren durch Rat und Tat und der einen oder anderen netten Unterhaltung ein super Arbeitsklima in der Arbeitsgruppe geboten haben. Im speziellen danke ich Dr. Daniel Ebke, Dr. Savio Fabretti, Dr. Oliver Schebaum, Christian Sterwerf, Daniel Reinhardt und Tristan Matalla-Wagner. Ganz besonders danke ich meinen Bürokollegen Manuel Glas, Alessia Niesen, Stefan Niehörster und Michael van Straaten für ihre Hilfe, all die wissenschaftlichen und auch nichtwissenschaftlichen Gespräche und der tollen Atmosphäre.

Ich bedanke mich bei Prof. Dr. Eiji Saitoh für die Möglichkeit eines kurzen Forschungsaufenthaltes an der Tohoku Universität, Sendai, Japan. Durch meinen Aufenthalt in seiner Arbeitsgruppe erhielt ich interessante Einblicke in die Messungen des Spin Seebeck Effektes und die Möglichkeit einer ersten wissenschaftlichen

Kollaboration. Dr. Ken-ichi Uchida und Takashi Kikkawa danke ich für ihre Unterstützung und Betreuung bei unseren Messungen an der Tohoku Universität.

Für eine hervorragende Zusammenarbeit im Rahmen des DFG Schwerpunktsprogramms SPP 1538 Spin Caloric Transport bedanke ich mich bei Prof. Dr. Christian H. Back und bei Dr. Maximilian Schmid von der Universität Regensburg und bei Dr. Sebastian T. B. Goennenwein, Dr. Matthias Althammer und Michael Schreier vom Walther Meissner Institut in Garching, sowohl für die sehr hilfreichen Diskussionen, als auch für den Probenaustausch.

Außerdem bedanken möchte ich mich bei Prof. Dr. Arunava Gupta und Dr. Liming Shen vom MINT Center der Universität von Alabama, USA, für die gute Zusammenarbeit und der Probenherstellung.

Der Deutschen Forschungsgemeinschaft danke ich für das oben genannte SPP 1538 und die damit verbundene finanzielle Unterstützung, welches ein außergewöhnlich gutes Umfeld für alle darin befindlichen Doktoranden aufwies und damit eine gute Grundlage für wissenschaftlichen Austausch bot.

Mein größter Dank gilt meiner Familie und meinem privaten Umfeld. Meinen Eltern danke ich für all ihre Unterstützung und Zeit. Besonders danke ich Andrea, für ihre liebevolle Unterstützung und all ihr Verständnis, die sie mir beim Anfertigen dieser Arbeit entgegen brachte.